

# Invitation to Elementary Particles

M. Bombara, M. Gintner, I. Melo

October 2012



# Preface

In this text we hope to give the reader not familiar with the Quantum Field Theory a picture and a certain level of true understanding of today's particle physics through a direct experience with real experimental data.

To achieve this goal we present a non-orthodox approach to the topic. Usually, theoretical concepts and tools required are subject of university courses on Quantum Field Theory (QFT), designed for specialists. In our approach we try to build a consistent framework of knowledge, skills and experience that would make sense for a novice without getting a grip on the QFT.

First, we introduce necessary basic notions and build a minimal language required. For this, only a rudimentary knowledge of Special Theory of Relativity and Quantum Mechanics is assumed. Then, we use the language to formulate and explain the rules of the micro-world and how we explore it experimentally. Of course, the scope of our discussion is rather limited in its extent as well as in its depth. Nevertheless, whenever possible we try to provide the reasoning supporting stated assertions as well as the derivations of the presented formulas.

The cornerstone of our approach is the introduction of the software tools that can enable the reader to explore elementary particle physics even at the pre-QFT level. The software we are talking about is routinely used in particle physics research and is freely available. Where applicable, we provide a basic guidance to its installation and usage.

First of all, we introduce the CompHEP package for the calculation of cross sections. With the help of this package the reader can numerically calculate cross sections of various collision processes or generate events produced in such collisions. Secondly, we introduce the Minerva and Hypatia packages developed by the LHC collaborations for displaying and analysis of LHC events. Finally, there is the SKALTA web interface that enables the

reader to analyze real cosmic ray data. The reader will learn how to use these tools. Our goal has been to make these tools a part of the learning process in order to provide the reader with a direct experience from the real research environment.

The inspiration for writing of this text in this manner is twofold. First, all three of us share a long experience with organizing the international activity for high school students called International Masterclasses in Particle Physics. We have been participating in the Masterclasses as local Slovak organizers and lecturers for several years now. Thanks to Masterclasses we had to cope with the challenge of bringing high-school students to the level where they are able to understand and analyze real events from particle collisions. All this in half a day. What had seemed impossible at first, now has become a yearly successful routine. Masterclasses also convinced us how much an added value in terms of the excitement and motivation of students represents their direct contact with the world of real scientific research. In the process, we realized that all this experience could and should be applied to designing courses for the university students of various carrier perspectives.

Secondly, teaching of engineering students combined with our own research interests in particle physics and our familiarity with the CERN research environment and infrastructure has resulted in the idea of designing a course of particle physics for future engineers who are interested in engineering jobs either at big accelerator research centers or in companies with accelerator related products. CERN, in particular, frequently offers very interesting and prestigious jobs for engineers of various specialties. We believe that taking a properly designed university course of particle physics can prepare engineering students for challenges associated with seeking such opportunities.

Perhaps, this text could also serve as a supplement to a course on the QFT or to some particle phenomenology courses.

As far as the authorship of the text is concerned, chapters 1 and 2 were written by M. Gintner, chapters 3 - 7 by I. Melo and chapter 8 by M. Bombara.

We would like to give thanks to members of the International Particle Physics Outreach Group for stimulating discussions, in particular to Michael Kobel and Konrad Jende from Dresden Technical University, authors of the W boson analysis measurement. We also benefited from the work of Farid Ould-Saada and Maiken Pedersen from the University of Oslo, authors of the Z boson analysis exercise. We would also like to appreciate valuable com-

ments of Boris Tomášik from the Matej Bel University in Banská Bystrica which helped to improve the text.

Invitation to Elementary Particles was written with the financial support of the APVV Grant Agency, Grant LPP-0059-09.

Žilina and Košice,  
October 2012

*Authors*



# Contents

<b>Preface</b>	<b>iii</b>
<b>1 Peeking into the micro-world</b>	<b>1</b>
1.1 Small and fast . . . . .	1
1.2 Two important numbers . . . . .	3
1.3 Natural units for “small” and “fast” . . . . .	5
1.4 A math detour: the scalar product . . . . .	8
1.5 The Lorentz transformations ... . . . .	10
1.6 The kinematics of particle decays ... . . . .	14
1.7 The quantum interactions . . . . .	20
1.8 The cross section: experimentalist’s view . . . . .	31
<b>2 A particle zoo</b>	<b>39</b>
2.1 Particles and anti-particles . . . . .	39
2.2 Fermions and bosons . . . . .	40
2.3 Forces . . . . .	42
2.4 Leptons . . . . .	47
2.5 Quarks . . . . .	49
2.6 Families . . . . .	52
2.7 Higgs boson . . . . .	53
<b>3 CompHEP</b>	<b>59</b>
3.1 Total and differential cross sections . . . . .	60
3.2 Simulation chain . . . . .	61
3.3 CompHEP and the simulation chain . . . . .	63
3.4 CompHEP download and installation instructions . . . . .	64
3.5 Compton scattering - CompHEP calculation . . . . .	64

<b>4</b>	<b>ATLAS detector and particle ID</b>	<b>77</b>
4.1	ATLAS detector at LHC . . . . .	77
4.2	Particle identification . . . . .	82
4.3	Important kinematic variables . . . . .	85
4.3.1	Rapidity and pseudorapidity . . . . .	85
4.3.2	Transverse momentum . . . . .	86
4.3.3	Missing transverse momentum and missing transverse energy . . . . .	87
4.3.4	Invariant mass . . . . .	88
<b>5</b>	<b>Proton structure</b>	<b>95</b>
5.1	Scattering of electrons off protons . . . . .	95
5.2	Parton Distribution Functions . . . . .	99
5.3	Proton-proton collisions . . . . .	101
<b>6</b>	<b><math>W</math> bosons at LHC</b>	<b>107</b>
6.1	$W$ boson production cross sections . . . . .	107
6.2	Charge asymmetry . . . . .	110
6.3	$W$ boson decay . . . . .	111
6.4	Signals vs Backgrounds . . . . .	114
6.5	$W$ boson events in Minerva . . . . .	118
6.5.1	Tips for event analysis . . . . .	119
6.5.2	Typical $W \rightarrow e^- \bar{\nu}_e$ event . . . . .	120
6.5.3	Typical $W \rightarrow \mu^+ \nu_\mu$ event . . . . .	121
6.6	Higgs boson in $H \rightarrow W^+ W^-$ channel . . . . .	121
6.6.1	Higgs production and decay . . . . .	121
6.6.2	Discovery of a new particle consistent with the Higgs .	122
6.7	Exercises and measurements . . . . .	123
6.7.1	Charge asymmetry dependence on the collision energy	123
6.7.2	Search for $W$ bosons in the ATLAS data . . . . .	124
6.7.3	Search for the Higgs in $W^+ W^-$ channel. . . . .	125
<b>7</b>	<b><math>Z</math> bosons at LHC</b>	<b>137</b>
7.1	$Z$ boson production . . . . .	137
7.2	$Z$ production cross sections . . . . .	138
7.2.1	Distributions in $m_{e^+ e^-}$ and $p_T(e^+)$ . $Z$ boson signatures in the electron and muon decay modes at LHC . . . . .	140
7.3	$Z$ boson events in Hypatia . . . . .	142

7.3.1	Typical $Z \rightarrow e^+e^-$ event . . . . .	143
7.3.2	Typical $Z \rightarrow \mu^+\mu^-$ event . . . . .	144
7.4	Search for Z bosons in the ATLAS data . . . . .	145
<b>8</b>	<b>Cosmic Rays at SKALTA</b>	<b>153</b>
8.1	Introduction to Cosmic Rays . . . . .	153
8.1.1	Primary cosmic rays . . . . .	153
8.1.2	Secondary cosmic rays . . . . .	159
8.2	SKALTA experiment . . . . .	162
8.3	Data analysis . . . . .	166
8.3.1	How to use the web interface . . . . .	166
8.3.2	Analysis with raw data . . . . .	171
8.3.3	Caveats during analysis . . . . .	173
8.4	Exercises with SKALTA . . . . .	176
8.4.1	Exercise n. 1: Are the cosmic rays measured by SKALTA affected by the Sun? . . . . .	176
8.4.2	Exercise n. 2: What is the relation between secondary cosmic ray flux and atmospheric conditions (such as air temperature and density)? . . . . .	177
<b>A</b>	<b>Physical constants</b>	<b>179</b>



# Chapter 1

## Peeking into the micro-world

In this chapter we will talk about the theoretical formalism behind our understanding of the world of elementary particles. We will introduce the natural units used in particle physics. We will learn how to calculate kinematics of the collisions and decays of relativistic particles. Eventually, the notion of the cross section will be introduced and discussed.

### 1.1 Small and fast

In the study of the micro-world we are trying to understand the smallest parts of the Universe and discover the laws the structure is governed by.

One of the most important findings of the humankind is that the matter has a discrete structure. Speculations about this possibility have a long history (Dēmokritos of Abdera, ca. 460 BC – ca. 370 BC). However, in science, this knowledge started to form some two hundred years ago (Antoine-Laurent Lavoisier, 1743 – 1794) and it took more than a century to become widely accepted.

The classical view of the discrete structure was based on the mechanistic idea of small indivisible particles the whole matter is made of. Then, the main task was to find out what was the size and other physical properties of such particles and what kinds of forces act among them. In attempts to resolve these questions, scientists kept descending deeper and deeper into the structure of matter. They kept breaking “indivisible” particles into smaller parts: molecules to atoms, atoms to nuclei and electrons, nuclei to protons and neutrons, protons and neutrons to quarks, ... . For each of the objects

in the list there was always a period in time when they were held indivisible. And, for the moment, they were called “elementary” or “fundamental”.

In the process, physicists learned about the properties of the particles and formulated the laws binding their behavior. And, to a big surprise of everybody involved, the observed behavior of these tiny particles began to depart from the expectations of the Newtonian mechanics. This resulted in the formulation of a completely new theory of the micro-world known as Quantum Mechanics (QM) [1], [2].

The fact best known to the general public about the QM is that its rules look strange from the point of view of our everyday experience. Nevertheless, at the same time, the familiar laws of classical physics presumably follow from the quantum laws. How does it happen? Well, the macroscopic objects consist of the huge multitude of bound together tiny particles each obeying the strange quantum laws. We believe that in the systems of the large numbers of interacting particles the microscopic quantum phenomena get “averaged out”. Hence, classical physics is the effective manifestation of the quantum laws in the big world.

When valued against our everyday experience the objects of the micro-world, for which we will frequently use the term “particles”, whether elementary from today’s point of view or not, are extremely light. Very often, the processes particles participate in can provide energies comparable or much higher than the particle’s rest energy,  $mc^2$ . Consequently, velocities close to the speed of light are no exceptions in the micro-world. Hence, when describing the behavior of particles the laws of the QM must be accompanied by the laws of Einstein’s Special Relativity [3].

The QM was originally formulated for systems consisting of a single non-relativistic point particle experiencing external forces. Attempts to generalize this for relativistic particles resulted in the formulation of Quantum Field Theory (QFT) [4], [5], [6], [7]. How do these theories differ? As far as the “quantum nature” is concerned, the QFT follows exactly the same postulates as the non-relativistic QM. The two theories differ in the physical systems they describe. While the non-relativistic QM describes a fixed number of the non-relativistic point particles, the physical system described by the QFT is a physical field. There are different types of the physical fields. Every type of particles has its own physical field spread throughout the Universe. The particle types are distinguished by the values of certain physical quantities: mass, spin, electric charge, etc. Therefore, these quantities are considered as fundamental characteristics of particle fields.

Special Relativity dethroned the mass conservation law. The energy stored in the form of mass can be transformed into kinetic energy and *vice versa*. This is in accordance with the observed phenomenon that the identities and the quantities of particles can be changed in their mutual interactions. This is the phenomenon which the “particle” QM fails to account for, while the QFT succeeds.

What we picture in our minds as point particles are, in the QFT, demonstrations of specific states of physical fields. In this context, the particles are often called “field disturbances” or “field excitations”. When we think about the forces acting among the particles, we should rather think about the field disturbances influencing each other. Nevertheless, when we describe field disturbances which are sufficiently small in their space extent we can picture them, with a proper caution, as point particles<sup>1</sup>.

In what follows we are not going to present the course of the QFT, neither use the QFT formalism. It is difficult subject which Ph.D. students of particle theoretical physics usually learn over many years. However, we cannot avoid mentioning and using certain notions, rules, and facts which are inherent to the QFT. We will try to do it in a coherent way to maintain the inner logic and understandability of the whole text.

## 1.2 Two important numbers

For all physical phenomena there are certain quantities and constants which are important, and other ones which do not play any recognizable role.

The historical progress of physics relied heavily on the fact that the number of the important quantities in any problem physics addressed was very small. For example, a single gravitational constant governs all gravitational phenomena: from the free fall of the apple to the planetary motion. We do not need to know either the electric charge of the electron, or the number of protons in an apple. Thus, Sir Isaac Newton was able to formulate the law with a minimal knowledge of the surrounding Universe and no real information about the structure of matter.

The value of the gravitational constant defines how strong the gravitational effects are: where they dominate (e.g. the motion of the planets of the Solar system) and where they are negligible (e.g. the motion of electrons

---

<sup>1</sup>The important part of this reasoning is also the fact that QFT interactions are local.

bound in atoms). Analogically, the electrical phenomena are governed by the value of the elementary electric charge<sup>2</sup>.

In the same spirit, there is a single constant which governs the emergence of the quantum effects. It is the Planck constant,

$$h = 6.626\,069\,57(29) \times 10^{-34} \text{ J} \cdot \text{s}. \quad (1.1)$$

The number is very small when expressed in terms of the SI units. Since the sizes of the SI units are tuned to the macroscopic world, the smallness of (1.1) suggests that the quantum effect will be negligible at the macroscopic size scale.

For practical reasons, people often use the so-called reduced Planck constant defined as

$$\hbar = \frac{h}{2\pi} \approx 1.0546 \times 10^{-34} \text{ J} \cdot \text{s}. \quad (1.2)$$

To get an idea how tiny the quantum effects are, let us calculate how much energy a quantum of blue light of the wavelength of 400 nm carries. It can be calculated as follows

$$E = \frac{hc}{\lambda} \approx 5 \times 10^{-19} \text{ J}. \quad (1.3)$$

As is well known, the relativistic effects cannot be ignored when the velocity of an object approaches the speed of light,

$$c = 299\,792\,458 \text{ m} \cdot \text{s}^{-1}. \quad (1.4)$$

Exactly this number tells us when the explanation of an observed phenomenon could originate in the Special Relativity. Opposite to the smallness of the Planck constant, the speed of light expressed in the SI units is quite a large number. That is why the time dilatation and the length contraction do not make a part of our experience.

An alternative way how to judge whether an object is relativistic is to compare its kinetic energy to its mass-related energy. When big objects of ordinary world are considered their mass-related energy is huge. For example,

---

<sup>2</sup>The size of the electron's electric charge is equal to the elementary electric charge,  $e \approx 1.6 \times 10^{-19} \text{ C}$ .

if a body weighs 1 kg, its mass<sup>3</sup> energy is

$$E = m \cdot c^2 = 1 \text{ kg} \cdot (3 \times 10^8 \text{ m s}^{-1})^2 = 9 \times 10^{16} \text{ J}.$$

It would take about 7 years to produce this amount of electric energy in the 400MW unit of a power plant.

Let us find what speed the body must reach in order that its kinetic energy equals to its mass energy. The total energy of the moving body is

$$E = \sqrt{m^2 c^4 + \vec{p}^2 c^2}, \quad (1.5)$$

where its momentum reads

$$\vec{p} = \frac{m\vec{v}}{\sqrt{1 - v^2/c^2}}. \quad (1.6)$$

The kinetic energy can be obtained from

$$E_{\text{kin}} = E - mc^2. \quad (1.7)$$

Now, the requirement  $E_{\text{kin}} = mc^2$  results in

$$v = \frac{\sqrt{3}}{2} c \approx 0.866 c \approx 2.6 \times 10^8 \text{ m s}^{-1}.$$

Thus, indeed, when the kinetic energy of a moving object is comparable with its mass energy the Special Relativity laws must be used to describe the motion.

Since particles of the micro-world are both quantum and relativistic there are two fundamental constants setting scales for the micro-world phenomena: the Planck constant,  $h$ , along with the speed of light,  $c$ .

### 1.3 Natural units for “small” and “fast”

Students in all countries of the world are learning to use the metric or some other system of units to measure length, weight, time, etc. The units they are

---

<sup>3</sup>Whenever we are talking about the mass we are considering what in some literature is called the “rest mass”. Throughout the text, we are never using the notion of the mass in the sense of the “relativistic mass”, the one which depends on the speed of the object.

What we call here as the *mass-related energy*, or the *mass energy*, is often called the “rest energy” in the literature.

told about, whether *meter*, *kilogram*, *second*, or *pound*, *foot*, *Fahrenheit*, are designed to be practical when used in the “usual” world. They are supposed to be useful when building houses and cars, sewing clothes, tanking gas, cooking.

These units become impractical, though, when used in areas which significantly differ from the “sizes” of our everyday world. Therefore, different areas of physics dealing with phenomena taking places at unusual scales tend to introduce and utilize system of units that would be more natural from their perspectives.

The natural choice for physics of elementary particles is the system where

$$\hbar = c = 1. \quad (1.8)$$

In this system the units for the length, time, and mass are related through a single basic unit. Should it be a meter then the transformation relations for a second and a kilogram can be found by solving the equations (1.8). They can be rewritten in the form

$$c_{\text{SI}} \cdot \frac{\text{m}}{\text{s}} = 1, \quad (1.9)$$

and

$$\hbar_{\text{SI}} \cdot \text{J} \cdot \text{s} = \hbar_{\text{SI}} \cdot \frac{\text{kg} \cdot \text{m}^2}{\text{s}} = 1, \quad (1.10)$$

where  $c_{\text{SI}} \approx 3.00 \times 10^8$  and  $\hbar_{\text{SI}} \approx 1.05 \times 10^{-34}$  are the dimensionless values of  $c$  and  $\hbar$ , respectively, in the SI system of units. The Eq. (1.9) implies

$$1 \text{ s} = c_{\text{SI}} \cdot \text{m} \approx 3.00 \times 10^8 \text{ m}. \quad (1.11)$$

Combining Eqs. (1.10) and (1.11) we can express kilograms through meters

$$1 \text{ kg} = \frac{c_{\text{SI}}}{\hbar_{\text{SI}}} \text{ m}^{-1} \approx 2.83 \times 10^{42} \text{ m}^{-1} \quad (1.12)$$

Clearly, in the meter-based natural system of units we can write

$$[L] = [T] = [M]^{-1} = \text{m} \quad (1.13)$$

Instead of the meter, we could have chosen seconds or kilograms as the common units for the length, time and mass. However, neither of these three choices is natural from the point of view of the micro-world.

A more suitable common unit for all three quantities can be chosen in such a way that typical micro-world energies become human-friendly numbers. We could make a choice where the mass energy of an elementary particle, the electron, for example, would be equal to one. Or, where the energy of the ground state of the hydrogen atom would equal to one. These choices look natural. In reality, however, probably for historical reasons, a more technical choice prevailed: *electronvolt*, eV. *An electronvolt is the energy equal to the kinetic energy of an electron accelerated from the rest by the electric potential difference of 1 Volt.*

The kinetic energy of such an electron in the SI units has a value

$$E_{\text{kin}} = e \cdot U \approx 1.60 \times 10^{-19} \text{ C} \cdot 1 \text{ V} = 1.60 \times 10^{-19} \text{ J} \quad (1.14)$$

Thus, 1 eV is related to joules in the following way

$$1 \text{ eV} = e_{\text{SI}} \text{ J} \approx 1.60 \times 10^{-19} \text{ J}, \quad (1.15)$$

where  $e_{\text{SI}}$  is the absolute value of the electron charge in the SI units. What is the relation of 1 eV to the  $\hbar = c = 1$  natural units? It is not difficult to find that in the meter-based natural units

$$1 \text{ J} = \frac{1}{\hbar_{\text{SI}} \cdot c_{\text{SI}}} \text{ m}^{-1}. \quad (1.16)$$

Then, (1.15) and (1.16) imply

$$1 \text{ eV} = \frac{e_{\text{SI}}}{\hbar_{\text{SI}} \cdot c_{\text{SI}}} \text{ m}^{-1} \approx 5.03 \times 10^6 \text{ m}^{-1}, \quad (1.17)$$

or, the other way around,

$$1 \text{ m} = \frac{e_{\text{SI}}}{\hbar_{\text{SI}} \cdot c_{\text{SI}}} \text{ eV}^{-1} \approx 5.03 \times 10^6 \text{ eV}^{-1}. \quad (1.18)$$

Using the transformation relation (1.18) along with (1.11) and (1.12) we can choose eV as the common unit of the length-time-mass triad

$$[L]^{-1} = [T]^{-1} = [M] = \text{eV} \quad (1.19)$$

$$1 \text{ s} = \frac{e_{\text{SI}}}{\hbar_{\text{SI}}} \text{ eV}^{-1} \approx 1.51 \times 10^{15} \text{ eV}^{-1} \quad (1.20)$$

$$1 \text{ kg} = \frac{c_{\text{SI}}^2}{e_{\text{SI}}} \text{ eV} \approx 5.63 \times 10^{35} \text{ eV} \quad (1.21)$$

To give the reader some feeling about the electronvolts we can mention that the mass energy of the electron equals to 0.511 MeV and the energy of the hydrogen atom ground state is  $-13.6$  eV. It is also very useful to remember that the mass energy of the proton is roughly about 1 GeV.

In the natural units, all relativistic and quantum relations can be written in simpler forms: since  $\hbar = c = 1$  we can cease writing these constants explicitly. Thus, for example, the relativistic mass-energy-momentum relation (1.5) can be written in the following form

$$E^2 = m^2 + \vec{p}^2. \quad (1.22)$$

Looking at this relation, it is natural to think about the energy, mass and momentum as different forms of the same essence. Of course, if the energy is measured in the electronvolts then the mass and momentum possess the electronvolt units as well

$$[E] = [M] = [\vec{p}] = \text{eV}.$$

When presenting the values of the mass and momentum, particle experimentalists are accustomed to properly include the speed of light into the quantities' units. Thus, the mass of the electron would be written as  $0.511 \text{ MeV}/c^2$ . The electron's momentum unit would be written as  $\text{eV}/c$ . This custom helps to avoid any confusion regarding the nature of the quoted value when it is not explicitly stated whether the number is the mass, energy or momentum.

As an example of the simplification of relations due to the dropping off the reduced Planck constant we can write the energy of the light quantum as

$$E = \omega = 2\pi f, \quad (1.23)$$

where  $\omega$  is the angular frequency, and  $f$  is the regular frequency.

## 1.4 A math detour: the scalar product

Here, before we proceed further, it might be a proper place for a little math detour. This detour will pay off by enabling us to introduce the formalism of *four-vectors*. Through the four-vectors the space and time can be viewed in a unified manner. Further, it can simplify the calculations of the relativistic collisions and decays.

The four-vectors are elements of a special four-dimensional vector space called the *Minkowski space*. The Minkowski space represents our space-time as the Special Relativity understands it. To introduce the Minkowski space we need to deepen our understanding of the scalar product. That is what this detour is about.

The scalar product is not a necessary part of the vector space definition. It is an additional structure a vector space can be enriched with. Moreover, the implementation of the scalar product is not unique. The scalar product is any binary mapping from the real vector space  $V$  to the real numbers  $\mathcal{R}$ ,  $V \times V \mapsto \mathcal{R}$ , which fulfills the following three criteria:

$\forall \vec{a}, \vec{b}, \vec{c} \in V, \forall \alpha, \beta \in \mathcal{R}$ :

- (i) the positive definiteness:  $(\vec{a}, \vec{a}) \geq 0 \quad \wedge \quad (\vec{a}, \vec{a}) = 0 \Leftrightarrow \vec{a} = 0$ ;
- (ii) the linearity:  $(\vec{c}, \alpha \vec{a} + \beta \vec{b}) = \alpha (\vec{c}, \vec{a}) + \beta (\vec{c}, \vec{b})$ ;
- (iii) the symmetry:  $(\vec{a}, \vec{b}) = (\vec{b}, \vec{a})$ ;

where  $(\vec{a}, \vec{b})$  is an alternative notation for the scalar product  $\vec{a} \cdot \vec{b}$ .

In a particular basis the scalar product can be expressed in terms of the vector's coordinates  $a^i$  and  $b^i$  and a matrix  $G$  called the *metric tensor*

$$(\vec{a}, \vec{b}) = a^i g_{ij} b^j, \quad (1.24)$$

where  $g_{ij}$  are the metric tensor's elements and  $i, j$  run through all coordinates. In writing the relation (1.24) we have used the Einstein's summation convention: it should be summed over indices which repeat twice in the product expression and which are placed in the opposite up-down position. At the same time we agree to write the indices of vector coordinates as superscripts while the indices of the metric tensor as subscripts.

Using this formalism the metric tensor defining usual scalar product through coordinates in the orthonormal basis is the unit matrix,  $g_{ij} = \delta_{ij}$ . Then, we obtain our usual relation for the scalar product

$$(\vec{a}, \vec{b}) = a^i g_{ij} b^j = \sum_i a^i b^i. \quad (1.25)$$

The vector space with this usual kind of the scalar product is called *Euclidean*.

If we defined a new quantity,  $b_i \equiv g_{ij}b^j$  the scalar product could be written as

$$(\vec{a}, \vec{b}) = a^i b_i,$$

where the Einstein summation rule has been used. The superscripted coordinates are called *contravariant*, while the subscripted ones are called *covariant*. Of course, in the case of the Euclidean vector space and working in the orthonormal basis there is no difference between the values of a contravariant coordinate and its covariant conjugate,  $b_i = b^i$ . However, once we use a non-orthonormal basis or define the scalar product differently the metric tensor can differ from the unit matrix and the simple relation (1.25) would alter to something more complex.

## 1.5 The Lorentz transformations and the four-vectors

Let us recall that, relativistically speaking, space and time are interconnected, forming a four-dimensional space, or the *space-time* if you wish. The position of any event occurring at a single space point and at a single time moment can be described in the space-time by four coordinates,  $t, x, y, z$ . Of course, it presumes a reference frame with a coordinate system has been chosen. A different reference frame would result in different values of the four coordinates for the same event.

The transformation of coordinates of the same event between mutually moving inertial frames includes a counter-intuitive mixing of the space and time coordinates. For example, let us have two inertial frames,  $S$  and  $S'$ , all their axes parallel to each other:  $x \parallel x'$ ,  $y \parallel y'$ ,  $z \parallel z'$ . Let their origins coincide at  $t = t' = 0$ , where  $t$  and  $t'$  are times measured<sup>4</sup> in  $S$  and  $S'$ . Let  $S'$  move with respect to  $S$  at the constant velocity  $v$  along the  $x$ -axis as is shown in Fig. 1.1. If the event space-time coordinates in  $S$  read  $t, x, y, z$ , then the coordinates of the same event in  $S'$  are

$$t' = \gamma(t - \beta x/c), \quad x' = \gamma(x - \beta ct), \quad y' = y, \quad z' = z, \quad (1.26)$$

where  $\beta = v/c$  and  $\gamma = (1 - \beta^2)^{-1/2}$ . The Eqs. (1.26) are the *Lorentz transformations* under the assumption stated above. The Lorentz transfor-

---

<sup>4</sup>Time in each frame is measured by the clock which is at rest with respect to the frame.

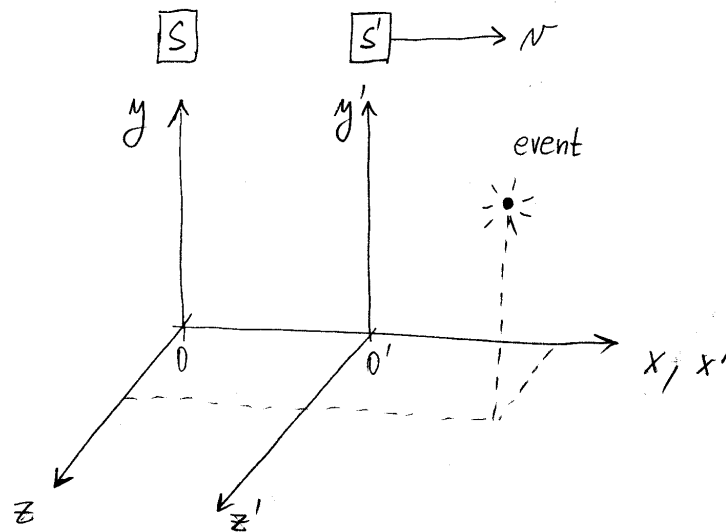


Figure 1.1: Mutually moving inertial frames with Cartesian coordinates. The frame  $S'(x', y', z')$  moves along the axis  $x$  at the speed  $v$  with respect to  $S(x, y, z)$ .

mations related to the transition between two mutually moving frames are often referred to as *boosts*.

In classical Newtonian physics, the transition between two inertial frames would not influence the time coordinate; in other words, Newton assumed that *time was absolute*. Of course, this assertion was based on the everyday human experience which was limited to velocities very far below the speed of light.

When we imagine the rotations in the three dimensional space its coordinates transform as the coordinates of the three-dimensional vectors. It is confirmed by the fact that the quantity  $x^2 + y^2 + z^2$  does not change under the space rotations. Thus, the  $(x, y, z)$  triplet of the Cartesian coordinates forms a vector (usually called the *position vector*)

$$\vec{r} = (x, y, z). \quad (1.27)$$

Note that the invariant quantity  $x^2 + y^2 + z^2$  can be expressed as the Euclidean scalar product  $\vec{r} \cdot \vec{r}$ . In addition, the rotations do not change the scalar

product of any two position vectors,  $\vec{r}_1 \cdot \vec{r}_2$ , either. All these statements are true independently of the dimensionality of the Euclidean vector space.

Can we introduce a space-time position vectors for the space-time events? Can we classify  $(t, x, y, z)$  as coordinates of such a vector? Can the Lorentz transformations be understood as some kind of rotations in the space-time? The quantity which does not change under the Lorentz transformations reads

$$s^2 \equiv (ct)^2 - x^2 - y^2 - z^2, \quad (1.28)$$

or, more generally,  $(ct)^2 - \vec{r}^2$ . It is often called the quadrature of the *space-time interval*. Obviously, due to the minus signs in (1.28) it is not positive definite. Since  $s^2$  cannot fulfill the first of the three scalar product properties, the positive definiteness, it cannot be related to any scalar product.

Nevertheless, we can still utilize the formalism of the metric tensor and co(ntra)variant vectors developed in Section 1.4. Note that

$$(ct)^2 - \vec{r}^2 = (ct, \vec{r}) \cdot \begin{pmatrix} 1 & 0 \\ 0 & -\mathbf{I}^{(3)} \end{pmatrix} \cdot \begin{pmatrix} ct \\ \vec{r} \end{pmatrix},$$

where  $\mathbf{I}^{(3)}$  is the  $3 \times 3$  unit matrix,  $\mathbf{I}^{(3)} = \text{diag}(1, 1, 1)$ . Thus, if we define the metric tensor  $G = \text{diag}(1, -1, -1, -1)$  and  $r \equiv (r^0, r^1, r^2, r^3) = (ct, x, y, z)$  the quadrature of the space-time interval can be written as

$$(ct)^2 - \vec{r}^2 = r^\mu g_{\mu\nu} r^\nu. \quad (1.29)$$

Note that we have adopted a couple of conventions here. The index of the time component of  $r$  is zero. To distinguish  $r$  from Euclidean vectors we use the Greek alphabet for  $r$ 's indices and do not use the arrow symbol. The arrow is retained for the space three-vectors.

It can be shown that the Lorentz transformations also preserve the expression  $r'^\mu g_{\mu\nu} r'^\nu$ , where  $r'_i = (ct', x', y', z')$  is the space-time position of some other event. At this point it is hard to resist to define the *pseudo-scalar product* in the space-time — the vector space of the position *four-vectors*  $r = (r^0, r^1, r^2, r^3)$ . The pseudo-scalar product reads

$$r' \cdot r = r'^\mu g_{\mu\nu} r^\nu = c^2 t' t - x' x - y' y - z' z, \quad (1.30)$$

where  $g_{00} = 1$ ,  $g_{ii} = -1$  when  $i = 1, 2, 3$ , and  $g_{\mu\nu} = 0$  when  $\mu \neq \nu$ . Note that to distinguish the space components of  $g_{\mu\nu}$  the Latin indices have been used.

Even though the pseudo-scalar product is not positive definite it meets the other two conditions: the linearity and the symmetry. The four-dimensional vector space representing the space-time endowed with the pseudo-scalar product is called the *Minkowski space*. The Lorentz transformations can be viewed as the four-dimensional “rotations” in the Minkowski space, the vector space equipped with a different than usual (Euclidean) scalar product.

The covariant components of a Minkowski four-vector have a nontrivial relationship with their contravariant counterparts. Indeed,

$$r_0 = g_{0\nu}r^\nu = r^0, \quad r_i = g_{i\nu}r^\nu = -r^i, \quad \forall i. \quad (1.31)$$

In the jargon used by physicists, by the action of the metric tensor the four-vector components “lower” their indices; in the process, the space components change their signs while the time component does not.

Since the metric tensor  $G$  is a regular matrix it has its inverse,  $G^{-1}$ , so that  $G \cdot G^{-1} = G^{-1} \cdot G = \mathbf{I}$ . It will prove as a reasonable convention to assign upper indices to the elements of  $G^{-1}$ :  $g^{\mu\nu}$ . Thus, the  $G^{-1} \cdot G = \mathbf{I}$  condition can be written in the terms of the components as

$$g^{\mu\alpha}g_{\alpha\nu} = \delta_\nu^\mu$$

Our convention has led to assigning one upper and one lower index to the Kronecker’s delta  $\delta_\nu^\mu$ . Applying the inverse matrix of the metric tensor we can “raise” indices of covariant components

$$r^0 = g^{0\nu}r_\nu = r_0, \quad r^i = g^{i\nu}r_\nu = -r_i, \quad \forall i. \quad (1.32)$$

It is not difficult to check that  $G = G^{-1}$  or, in other words,  $g_{\mu\nu} = g^{\mu\nu}$ ,  $\forall \mu, \nu$ .

There are also other quantities which transform as the components of Minkowski four-vectors when relating their values in different inertial frames. We will mention the most important four-vector with respect to the following text. They are the energy  $E$  and the momentum  $\vec{p}$  of a particle of a mass  $m$ . When viewing this particle from two different inertial frames,  $S$  and  $S'$ , the primed and unprimed energies and momenta are related by the Lorentz transformations

$$E' = \gamma(E - \beta p_x), \quad p'_x = \gamma(p_x - \beta E), \quad p'_y = p_y, \quad p'_z = p_z, \quad (1.33)$$

where, for simplicity, the relations are written in the natural ( $c = 1$ ) units. We can define a Minkowski four-vectors

$$p = (p^0, p^1, p^2, p^3) = (E, p_x, p_y, p_z), \quad (1.34)$$

and name it the *four-momentum*. As before, the pseudo-scalar<sup>5</sup> product of four-momenta is an invariant of the Lorentz transformations. Therefore,  $p^2 = p \cdot p$  is also invariant and equals to the square of the particle's mass ( $c = 1$ )

$$p^2 = m^2 \quad (1.35)$$

Simply said, the mass is the frame independent characteristics of the particle itself. It is reasonable to require the frame independence from any fundamental characteristic of an elementary particle, be it the electric charge, spin, and so on.

## 1.6 The kinematics of particle decays and collisions

Collisions and decays of particles are the basic experimental tools for the study of the micro-world. As we mentioned above we are talking about quantum-relativistic processes where the quantities and identities of participating particles can change. Thus, it is important to learn what to expect in relativistic collisions and to choose a proper language to describe it.

First of all, all laws governing the particle processes should be the same in all inertial reference frames.

Secondly, there is a very powerful tool which can be used for the prediction of a particle decay/collision even if we do not know all details of the interactions acting on the participating particles. The tool is the *Conservation Laws*.

The conservation laws are direct consequences of the continuous symmetries of the physical world we study. Thus, for example, the *conservation of the energy* can be inferred from the invariance with respect to time translations. The *conservation of the momentum* results from the invariance with respect to translations in space. The *conservation of the angular momentum*

---

<sup>5</sup>In the rest of the text we will drop the prefix “pseudo” from the word “pseudo-scalar” unless there is a risk of misunderstanding.

results from the invariance with respect to rotations in space. Since we believe that these symmetries are possessed by the “empty” space-time what remains is the question about the symmetries of the particular system under the study. If the system does not break the symmetries mentioned above the corresponding conservation laws hold.

Physicists found that there are some other symmetries in the micro-world which are not related to the space-time transformations. They rather follow from the continuous transformations exchanging or altering the quantum fields. The best known conservation law of this type is the *conservation of the electric charge*.

Now, we would like to illustrate how the conservation laws can help to solve the relativistic decay and collision problems.

## Problem 1

Let us consider a particle of the mass  $M$  decaying into two identical particles, each of the mass  $m$ . What are the energies  $\varepsilon_{1,2}$  and momenta  $\vec{p}_{1,2}$  of the daughter particles?

**Solution:** The mother particle has a four-momentum  $P = (E, \vec{P})$ . The conservation of the energy and momentum (or of the four-momentum) implies

$$E = \varepsilon_1 + \varepsilon_2 \quad (1.36)$$

$$\vec{P} = \vec{p}_1 + \vec{p}_2 \quad (1.37)$$

Usually, one tries to choose the reference frame where the problem solving would proceed in the simplest way. In this Problem, the rest frame of the mother particle will serve well. There,  $E = M$  and  $\vec{P} = 0$ , i.e.  $P = (M, \vec{0})$ . Hence, the Eqs. (1.36) and (1.37) imply

$$M = \varepsilon_1 + \varepsilon_2 = \sqrt{m^2 + \vec{p}_1^2} + \sqrt{m^2 + \vec{p}_2^2} \quad (1.38)$$

$$\vec{0} = \vec{p}_1 + \vec{p}_2 \quad (1.39)$$

The Eq. (1.39) implies that the daughter particles will fly back-to-back with the equal sized momenta. Combining (1.38) and (1.39) we find that

$$\varepsilon_1 = \varepsilon_2 = \frac{M}{2} \quad (1.40)$$

Then,

$$|\vec{p}_1| = |\vec{p}_2| = \frac{1}{2}\sqrt{M^2 - 4m^2} \quad (1.41)$$

Note that the conservation of the four-momentum is not providing us with the directions the pair of the daughter particles will fly away.

**Alternative solution:** We will show how the same results can be obtained if we exploit the scalar products of the four-vectors. The four-momentum conservation law,  $P = p_1 + p_2$ , implies

$$p_2 = P - p_1. \quad (1.42)$$

Let us square (in the sense of the scalar product) the equation (1.42)

$$(p_2)^2 = P^2 + (p_1)^2 - 2 p_1 \cdot P.$$

The squares of the four-momenta give the square masses of the corresponding particles,  $(p_1)^2 = (p_2)^2 = m^2$ ,  $P^2 = M^2$ . Hence,

$$0 = M^2 - 2 p_1 \cdot P. \quad (1.43)$$

The Eq. (1.43) is valid in any reference frame. Now, we can choose the frame in which the scalar product  $p_1 \cdot P$  will be expressed in terms of energies and momenta. If we are interested in the results in the mother's rest frame we substitute  $p_1 = (\varepsilon_1, \vec{p}_1)$  and  $P = (M, \vec{0})$ . Then,

$$p_1 \cdot P = \varepsilon_1 M,$$

and, after substituting it into (1.43), we finally obtain

$$\varepsilon_1 = \frac{M}{2}. \quad (1.44)$$

From here, it is pretty straightforward to obtain the second of the Eqs. (1.40) and the Eq. (1.41).

The results (1.40) and (1.41) hold in the rest frame of the mother particle. If we wished to see their forms in any other inertial frame we would have to Lorentz-transform them. That will be the subject of Problem 2.

## Problem 2

What are the energies and momenta of the daughter particles of the Problem 1 in the frame where the four-momentum of the mother particle is  $P = (E, \vec{P})$ ?

**Solution:** Let  $S'$  be the rest reference frame of the mother particle. Let  $S$  be the frame where the mother particle possesses the momentum  $\vec{P}$ . We are free to choose the  $x$ -axis of  $S$  in the same direction as the momentum of the mother particle, i.e.  $\vec{P} = (|\vec{P}|, 0, 0)$ . Let us choose the axes in both frames as in Fig. 1.1 so that we can use the Lorentz transformations (1.33). In our setup they read

$$M = \gamma(E - \beta|\vec{P}|), \quad 0 = \gamma(|\vec{P}| - \beta E). \quad (1.45)$$

By solving these equations we can express the  $\beta$  and  $\gamma$  factors for the Lorentz transformations from the frame where mother particle moves to its rest frame as

$$\beta = \frac{|\vec{P}|}{E}, \quad \gamma = \frac{E}{M}, \quad (1.46)$$

where  $E = \sqrt{M^2 + \vec{P}^2}$ .

Let the momentum of the daughter-1 particle in the mother's rest frame be<sup>6</sup>  $\vec{p}'_1 = (p'_x, p'_y, 0)$ . The angle  $\theta'_1$  between  $\vec{p}'_1$  and the  $x'$ -axis is given by  $\cos \theta'_1 = p'_x/|\vec{p}'_1|$  and  $\sin \theta'_1 = p'_y/|\vec{p}'_1|$ . Let us write down the Lorentz transformations from  $S'$  to  $S$

$$\varepsilon_1 = \gamma(\varepsilon'_1 + \beta|\vec{p}'_1| \cos \theta'_1), \quad (1.47)$$

$$p_x = \gamma(|\vec{p}'_1| \cos \theta'_1 + \beta\varepsilon'_1), \quad (1.48)$$

$$p_y = p'_y = |\vec{p}'_1| \sin \theta'_1 \quad (1.49)$$

$$p_z = p'_z = 0 \quad (1.50)$$

After substituting the results obtained in the Problem 1,  $\varepsilon_1 = M/2$ ,  $|\vec{p}'_1| =$

---

<sup>6</sup>Without the loss of generality, we can always choose the coordinate frame so that  $p'_z = 0$ .

$\sqrt{M^2 - 4m^2}/2$ , and the Eq. (1.46) into the Eqs. (1.47) — (1.49) we get

$$\varepsilon_1 = \frac{1}{2} \left( E + b |\vec{P}| \cos \theta'_1 \right), \quad (1.51)$$

$$p_x = \frac{1}{2} \left( b E \cos \theta'_1 + |\vec{P}| \right), \quad (1.52)$$

$$p_y = \frac{1}{2} b M \sin \theta'_1, \quad (1.53)$$

where  $b = \sqrt{1 - 4m^2/M^2}$ . We can also calculate the angle  $\theta_1$  between the momentum  $\vec{p}_1 = (p_x, p_y, 0)$  of the daughter-1 particle and the momentum  $\vec{P}$  of the mother particle in the  $S$  frame as  $\tan \theta_1 = p_x/p_y$ .

The  $S$  frame energy  $\varepsilon_2$  and momentum  $\vec{p}_2$  of the second daughter particle can be calculated easily when we realize that  $\varepsilon'_2 = \varepsilon'_1$  and  $\vec{p}'_2 = (-p'_x, -p'_y, 0)$ .

### Problem 3

We collide two identical particles, each of the mass  $m$ . One is moving with the overall energy  $\varepsilon_1$ , the other is at rest. In the collision, the two particles annihilate and a new real<sup>7</sup> particle of the mass  $M$  emerges. What is the mass created in this collision? Think of dis/advantages of the particle accelerator with the fixed target *vs.* the accelerator colliding two opposite beams of particles with the same-sized momenta<sup>8</sup>.

**Solution:** The four-momentum conservation reads

$$p_1 + p_2 = P, \quad (1.54)$$

where  $p_1 = (\varepsilon_1, \vec{p}_1)$  is the four-momentum of the colliding particle 1,  $p_2 = (m, 0)$  is the four-momentum of the colliding particle 2, and  $P = (E, \vec{P})$  is the four-momentum of the created particle. Then, (1.54) implies

$$E = \varepsilon_1 + m, \quad \vec{P} = \vec{p}_1. \quad (1.55)$$

When we rearrange (1.54) into  $p_1 = P - p_2$  and square the equation we obtain the frame independent relation

$$2 p_2 \cdot P = M^2, \quad (1.56)$$

---

<sup>7</sup>The “real” particle fulfills the relation  $E^2 - \vec{p}^2 = M^2$ . As we will see in Section 1.7 there are also “virtual” particles for which the relation does not hold.

<sup>8</sup>This type of an accelerator is referred to as a collider.

which in our fixed-target frame turns into

$$2mE = M^2. \quad (1.57)$$

The substitution of the first of the Eqs. (1.55) into (1.57) results in

$$M = \sqrt{2m(\varepsilon_1 + m)}. \quad (1.58)$$

Thus, we can see that the mass of the created particles grows as the square root of the energy the accelerator delivers to the collision.

Let us see what happens when the same energy is delivered by a collider. That means we have the same particles as before, each carrying the energy  $\varepsilon_1/2$ . In this case, the four-momenta of the colliding particles read  $p_1 = (\varepsilon_1/2, \vec{k}_1)$ ,  $p_2 = (\varepsilon_1/2, -\vec{k}_1)$ . Therefore,  $P = (\varepsilon_1, \vec{0})$ . When we substitute these four-momenta into the frame-independent relation (1.56) we obtain

$$M = \varepsilon_1. \quad (1.59)$$

Thus, in the collider case, the whole energy delivered by the accelerator,  $\varepsilon_1$ , can turn into the mass of a new particle. This is the advantage of the collider over the fixed-target accelerator. On the other hand, to make a collider one needs to build two accelerators.

The explanation for the poorer performance of the fixed target accelerator is simple. When one of the colliding particles is at rest, the momentum conservation law implies that the particle created in the collision must move, taking over the momentum of the initial moving particle. Thus, a part of the energy of the moving initial particle must be invested into the kinetic energy of the newly emerged particle. On the other hand, in the collider case, since the collision occurs in the collision's center of mass frame, the new particle is created at rest. Therefore, all energy delivered to the collision can be used to create a mass.

At the end of this Section we would like to turn the reader's attention to the fact that the Special Relativity accommodates the existence of particles of zero mass. The particle of this kind has to move at the speed of light. Even if it does not have a mass it has the energy and momentum interconnected by the relation

$$E = |\vec{p}|, \quad (1.60)$$

which follows from the general  $E^2 = m^2 + \vec{p}^2$  equation. The example of such a particle is the *photon*.

## 1.7 The quantum interactions

In Section 1.6, we learned how the conservations of energy and momentum can be used to constrain the kinematics of the particles produced in decays and collisions. Nevertheless, while these conservation laws can help us to restrict how a particle will move if created they cannot predict whether and when it will be created.

What will happen in a particular collision? When the given particle will decay? And into what? These are the questions for answering of which we have to understand the dynamics of the processes. That means, we have to know what forces act between particular sorts of particles and how they act.

### Classical *vs.* quantum-relativistic force

Before we start talking about what types of forces we know today in the micro-world and what properties they have, we will first discuss general features of forces in the world that is quantum and relativistic. We will see that forces in the micro-world exhibit certain effects not observed in the macroscopic world. This difference has lead into a shift in terminology. Rather than the “force”, particle physicists prefer to use the word “interaction”.

The classical Newtonian force has only a single effect: it changes the velocity (momentum) of the object it is acting upon. This is condensed in the Newton’s equation of motion

$$\vec{F} = m\vec{a}.$$

The very same effect has also the force-interaction in the micro-world: it can change the momentum of the particle it is acting upon. And it can do it even with the particle of zero mass which is the situation that could not be handled by Newton’s physics.

The strength of an interaction is proportional to the *charge* associated with the interaction. Well-known examples of such charges, even in classical physics, are the electric charge and the gravitational mass.

The interactions between quantum particles, however, can produce effects that have no match in the classical world. They can change the number and identity of particles. For example, the electromagnetic and weak interactions are responsible for the processes in which the electron and the positron annihilate each other and create either the massless photon or the very massive  $Z$

boson<sup>9</sup>. The same interactions can cause the  $Z$  boson to decay into various particle+antiparticle pairs: neutrino + anti-neutrino, quark + anti-quark, muon + anti-muon, and some others. The  $W^-$  boson can decay to the electron + anti-neutrino pair. Particles can radiate off or absorb other particles as they move on. All these phenomena are caused by the quantum-relativistic interactions. By the detection and observation of these phenomena we can study the properties of the interactions.

### Particles and fields

In Section 1.1, we mentioned that “particles” are local excitations of fields. All particles of the given type are excitations of a single field spread throughout the Universe. More types of fundamental particles imply more sorts of quantum fields.

As a matter of fact, there are two kinds of disturbances of a field. First, there are disturbances which we view as particles. These disturbances are special. They are like stable well formed ripples moving across the field. Their most important property is that the energy and momentum they carry are bound together by the relation

$$E^2 = m^2 + \vec{p}^2 \quad (1.61)$$

While  $E$  and  $\vec{p}$  are variables,  $m$  is one of the fundamental Lorentz-invariant characteristics of the given field; thus, a constant. All ripples representing real particles must obey the Eq. (1.61) with  $m$  of the given field.

The Universe is filled with fields of all known fundamental particles. If the disturbances of the same or of different fields can somehow influence each other this can be understood as mutual interactions of particles. As a particle-like ripple, say the electron, moves across the electron field it disturbs the electromagnetic (EM) field. The disturbances of the electromagnetic field carry away parts of the electron’s energy and momentum.

Particle-like ripples in the electromagnetic field are called the photons. However, most of the time the electromagnetic disturbances caused by the passing electron do not possess the qualities of the photons. They do not obey the relation (1.61) and do not form anything reminding us of particles. This is the second type of disturbances found in the quantum fields. Very often, it is referred to by a misleading name “virtual particles”.

---

<sup>9</sup>The  $Z$  and  $W$  bosons are elementary particles associated with the weak force. The reader will learn more about the elementary particle systematics in Chapter 2.

Even though the virtual particles may look like second-class citizens, they play a very important role in physics of quantum fields. The non-particle disturbances can transfer energy and momentum from one particle-like ripple to another one. Effectively, they mediate the classical action of the force between two particles. The force thus mediated can be repulsive as well as attractive, even though the attractive part can be at odds with our intuition.

Beside the force-like action the disturbances participate in all other effects of the quantum interactions described above. Thus, for example, two particle-like ripples of the electron field<sup>10</sup> can completely cancel each other while creating a virtual disturbance in the elmag field. The virtual disturbance would carry away the total energy and momentum of the two ripples. After a while, the very same virtual disturbance can turn into two particle ripples of any of quantum fields possessing the electric charge.

### Feynman diagrams

There is a nice and useful way how to picture the structure of the relations between ripples and disturbances standing behind a particular interaction. It is called the *Feynman diagrams*<sup>11</sup>. Now, we will try to explain how the Feynman diagrams will be used in this text. Let us have a field  $A$  and a field  $B$ . Let the fields  $A$  and  $B$  interact with each other. That means, the particle ripple in the field  $A$  creates disturbances in the field  $B$ . Another particle  $A$  passing by can be affected by the  $B$  field disturbance. In addition, in passing by it also disturbs the field  $B$  which can be “felt” by the former particle  $A$ . This situation is represented in the diagram in Fig. 1.2.

The diagram should be read from left to right<sup>12</sup> like this: two particles  $A$  are passing by and affect each other by the disturbances created in the

---

<sup>10</sup>The two ripples must be in the particle-anti-particle relation. For more on the anti-particles, see Section 2.1.

<sup>11</sup>The main purpose for which Richard Feynman cleverly designed its diagrammatic technique was to graphically represent the structure of very complex mathematical expressions emerging in the perturbative approach of calculating probability amplitudes of scattering processes. This is what the Feynman diagrams have been used for up to these days. Nevertheless, as a byproduct the diagrams also provide a powerful shorthand language in terms of which physicists can think of particle scattering processes. A word of warning: Since the diagrams look simple they often misguide unexperienced persons to incorrect conclusions about particle phenomena.

<sup>12</sup>Some authors draw the Feynman diagrams in the bottom-up direction. It is only a matter of convention. The reader should always make sure she knows what convention is used for the Feynman diagram she is looking at.

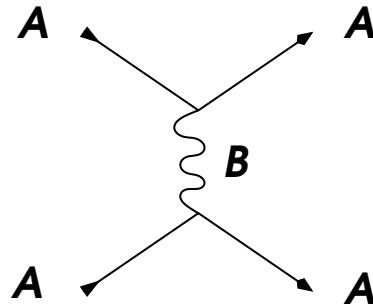


Figure 1.2: The example of the Feynman diagram for the process  $AA \rightarrow AA$  in the toy theory described in the text.

field  $B$ . In more common language, *two real particles  $A$  exchange the virtual particle  $B$* . The diagram does not depict how the particles move in space. It rather shows the topology of the cause-effect relations. The  $B$  line is not necessarily time-oriented because it represents a mutual effect of both  $A$  particles on each other.

Some terminology: the lines with loose ends are called the *external lines*. The lines without the loose ends are called the *internal lines*. The former represent the particle-like ripples — real particles, the latter represent virtual particles. Different types of particles are represented by different line styles. In the diagram above, the  $A$  particles are represented by solid lines, the  $B$  particles by wavy lines. The point where three or more lines meet is called the *vertex*. Actually, this name is used not only for the point itself but it includes also the lines attached to it.

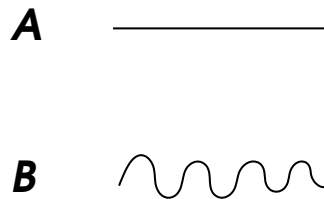


Figure 1.3: Propagators of the  $A$  and  $B$  fields of the toy quantum field theory.

Every QFT has to state what fields it contains. Graphically, this statement is represented by the list of all lines which can be used to build the theory's Feynman diagrams. In our case, the list would contain the lines as in Fig. 1.3 which are usually called *propagators*. In addition, every QFT

has to state which of its fields can influence each other. Graphically, it is represented by the list of vertices. The diagram in Fig. 1.2 would be present in the theory containing at least the vertex depicted in Fig. 1.4.

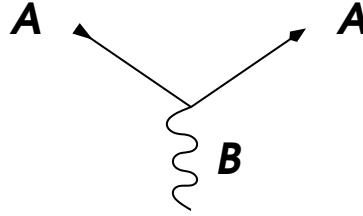


Figure 1.4: The vertex of the toy quantum field theory.

The vertices and propagators are like the LEGO pieces of which we can build diagrams of processes that can take place in the given theory. We can rotate the pieces and attach them to each other. When rotating vertices we have to remember: diagram's loose ends representing particles which change their position from the initial state (the left-hand side of the diagram) to the final state (the right-hand side of the diagram) or *vice versa* will become anti-particles. Thus, when we rotate the vertex in Fig. 1.4 counterclockwise by the right angle we end up with the vertex in Fig. 1.5. Note that the symbol

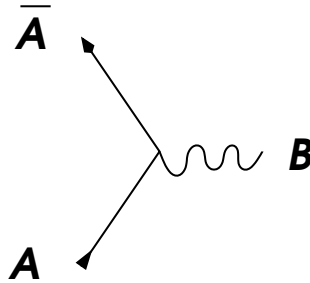


Figure 1.5: The vertex obtained by the counterclockwise rotating of the vertex in Fig. 1.4.

for the anti-particle of  $A$  is obtained by adding the bar over the letter,  $\bar{A}$ . Another indication for the anti-particle is the arrow exiting the initial state or entering the final state.

The lines in the Feynman diagrams are associated with the flows of the momenta and the energies between the initial and final states of the given process. Of course, the total four-momentum of the initial state must be

the same as the total momentum of the final state. But the four-momentum must also be conserved anywhere inside the diagram. In particular, the sum of the four-momenta flowing in any given vertex must be the same as the sum of the four-momenta flowing out of the vertex.

Now, we are in the position to construct diagrams of all processes possible in our toy theory. They must be constructed using the lines and vertex of Figs. 1.3 and 1.4 (1.5) only. We will depict a couple of possible processes. In Fig. 1.6, the particle  $A$  and anti-particle  $\bar{A}$  annihilate each other and create a disturbance in the field  $B$  which, in turn, creates the  $A\bar{A}$  pair, again.

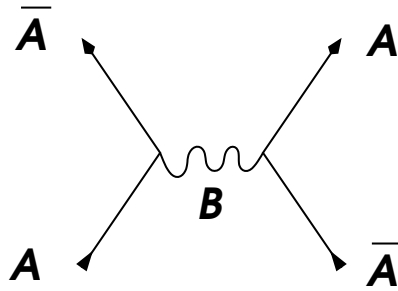


Figure 1.6: The example of the Feynman diagram for the process  $A\bar{A} \rightarrow A\bar{A}$ .

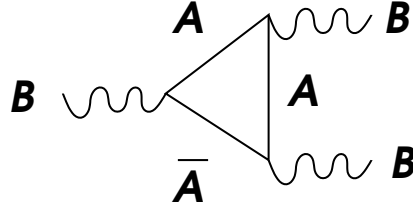


Figure 1.7: The example of the Feynman diagram for the process  $B \rightarrow BB$ .

Another Feynman diagram that can be built in our toy theory is shown in Fig. 1.7 where  $B$  turns into two  $B$  particles. But, is the process represented by the diagram possible? If a single particle of non-zero mass  $m_B$  could replicate itself in two pieces we would earn extra energy  $m_B c^2$  for free. Such a self-multiplication would break the conservation of energy! A simple algebra of four-vectors we learned in Section 1.6 can also get us to the same conclusion. Let  $p$  be a four-momentum of the initial  $B$  particle and  $p_{1,2}$  the four-momenta of the final  $B$  particles. The conservation of the four-momentum reads

$$p = p_1 + p_2. \quad (1.62)$$

Squaring the equation and working in the CM frame implies

$$m_B^2 = (E_1 + E_2)^2 > (2m_B)^2, \quad (1.63)$$

where  $E_{1,2}$  are the energies of the final state particles. As we can see in (1.63) it is impossible to conserve energy in the process suggested by the Feynman diagram in Fig. 1.7. Thus, the process cannot proceed if  $m_B \neq 0$ .

Yet, the double-check of how the Feynman diagram in Fig. 1.7 has been built out of the pieces in Figs. 1.3 and 1.4 (1.5) does not reveal any mistakes. The moral of this last diagram is that not all possible Feynman diagrams represent viable processes. Some can be forbidden by the conservation laws.

Some readers has probably already realized that an initial state can proceed to a given final state in different ways. In other words, there are different Feynman diagrams with the same particles at their both — left and right — ends. An example of two such Feynman diagrams representing the process  $A\bar{A} \rightarrow A\bar{A}$  is shown in Fig. 1.8. So how to deal with the ambiguity? Which

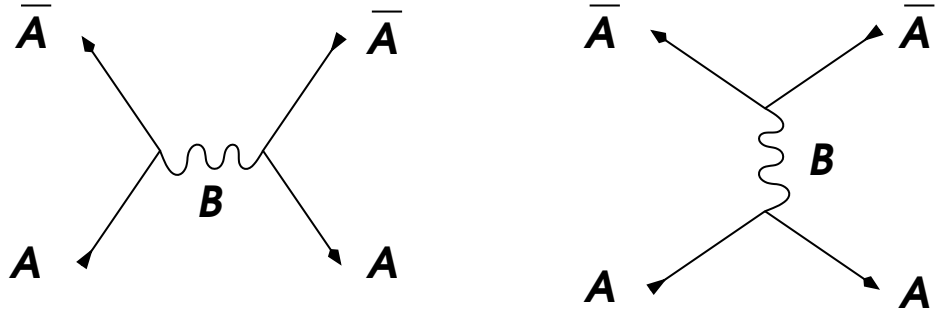


Figure 1.8: Two Feynman diagrams for the process  $A\bar{A} \rightarrow A\bar{A}$ .

of the two diagrams represents the way the interaction of  $A$  with  $\bar{A}$  really proceeds?

In addition,  $A\bar{A}$  is not the only final state that can occur in the  $A\bar{A}$  collision. The  $B\bar{B}$  pair can be produced as well<sup>13</sup>. A Feynman diagram for this process is shown in Fig. 1.9. And, in the  $A\bar{A}$  collision, there are infinitely more final states possible even in our toy QFT.

Remember, all these phenomena take place in the quantum world. Feynman diagrams are just graphical representations of the mathematical expressions which enable us to calculate the probability that in a given collision a

<sup>13</sup>If  $m_A < m_B$  the  $B\bar{B}$  pair in the final state is produced only if the collision provides enough kinetic energy.

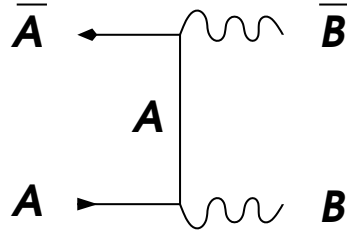


Figure 1.9: A Feynman diagram for the process  $A\bar{A} \rightarrow B\bar{B}$ .

given final state is observed<sup>14</sup>. The basic rule reads: *To calculate the probability for the given process we have to sum up contributions of all Feynman diagrams which take the given initial state to the given final state.* Hence, both diagrams of Fig. 1.8, at least, have to be considered when calculating the probability of the  $A\bar{A} \rightarrow A\bar{A}$  process.

The rule looks simple and clear. Well, till the moment the reader realizes a very unpleasant fact: the number of Feynman diagrams connecting a given initial state to a given final state is infinite! The two diagrams of Fig. 1.8 do not complete the story of the  $A\bar{A} \rightarrow A\bar{A}$  process. In Fig. 1.10 we display the example of a more complicated Feynman diagram that connects the initial state  $A\bar{A}$  with the final state  $A\bar{A}$ . No doubt, the reader will be able to come up with more examples!

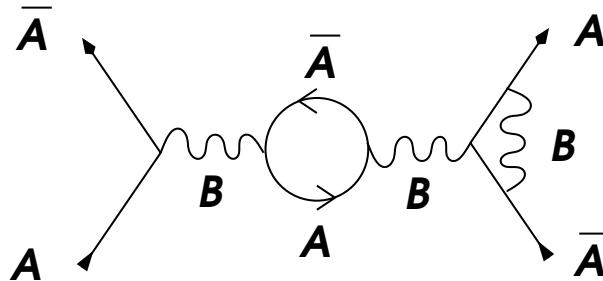


Figure 1.10: A Feynman diagram for the process  $A\bar{A} \rightarrow A\bar{A}$  with more vertices.

Is there a way how to deal with the infinite number of Feynman diagrams contributing to the given process? Fortunately, there is, even though it does

<sup>14</sup>The “given initial/final state” means that not only the particle contents of the states is fixed but also the energies and momenta of the initial and final particles. The probability of the process observation depends also on these quantities.

not apply to all kinds of QFT's.

The probability of observing a process in the given collision depends on the strengths of interactions involved in Feynman diagrams of the process. If the interactions are not too strong<sup>15</sup> then the contributions of particular Feynman diagrams to the probability decrease with the number of their vertices. Thus, the dominant contributions to the overall sum originate from diagrams with the least number of vertices. Obviously, the overall sum should be a finite number in order to match the experiment. Therefore, to calculate a probability prediction up to a chosen finite precision it is sufficient to consider a finite number of Feynman diagrams only.

As an illustration, consider the case of  $A\bar{A} \rightarrow A\bar{A}$ . The related Feynman diagrams in Fig. 1.8 contain two vertices each. The Feynman diagram of the same process shown in Fig. 1.10 contains four vertices. If the interaction involved is weak enough then the contributions of the diagrams in Fig. 1.8 dominate the contribution of the diagram of Fig. 1.10.

### From theory to experiment

Even though, for particle collisions, the probability of the observation of a unique process is the fundamental prediction of any quantum theory, it is not this quantity that is supplied to experimentalists. When designing a theory output that would be useful for experimentalists one has to take into account specific attributes of particle collision experiments.

First of all, the detectors in collision experiments do not distinguish full information needed to pin down a single final state in terms of a unique energy, momentum, position, and time of every particle<sup>16</sup>. Thus, there are always several process candidates that would be detected as the same collision event.

In order to calculate the probability of observing a collision event we have to sum up probabilities of all candidates that are not distinguishable by the detector. The number of the candidates is related to the “granularity” of

---

<sup>15</sup>It is beyond the scope of this text to quantify what is meant by “not too strong”. Nevertheless, the criterion holds for the electromagnetic and weak interactions at the energies we have encountered so far in experiments. It also holds for the strong interactions (Quantum Chromodynamics, see Section 2.3) between quarks when the momenta of interacting particles are high enough. We say that QFT's for which the criterion holds are solvable *perturbatively*.

<sup>16</sup>Neither colliding particles of the initial state are in a sharply defined states.

detectors, i.e. how fine the differences in the values of measured quantities can be recognized, and to the “density” of the final states.

So, how many process candidates are behind a detected event? The QM laws imply that the number of quantum states of a particle living in the space volume  $dx dy dz$  and the momentum volume  $dp_x dp_y dp_z$  is

$$dN_{\text{qs}} = \frac{dx dy dz dp_x dp_y dp_z}{(2\pi\hbar)^3}, \quad (1.64)$$

where  $h = 2\pi\hbar$  is the Planck constant. If there are more particles in the final state each particle contributes by the same factor  $dN_{\text{qs}}$ ,

$$dN_{\text{qs}}^{\text{tot}} = dN_{\text{qs}}^{(1)} \cdot \dots \cdot dN_{\text{qs}}^{(n)}, \quad (1.65)$$

where  $dN_{\text{qs}}^{(i)}$  is given by (1.64), and  $n$  is the number of particle in the final state. On the other hand, since the particles emerge from a single interaction their energies and momenta are related by the energy-momentum conservation law. This restriction decreases the overall number of the quantum states  $dN_{\text{qs}}^{\text{tot}}$ .

If we had a detector that would distinguish infinitely small differences in positions and momenta then any detected event would consist of the infinitely close process candidates with the same probabilities  $P_{\text{cand}}$  only. Therefore, the probability of such an infinitesimal event would read

$$dP_{\text{event}} = P_{\text{cand}} dN_{\text{qs}}^{\text{tot}}. \quad (1.66)$$

The probability  $P_{\text{cand}}$  is a function of the external particle momenta and positions. Thus, to obtain the probability of an event detected by a realistic detector with a finite resolution we have to integrate over  $dN_{\text{qs}}$  to sum up contributions of the process candidates which are not distinguished. Of course, the obtained probability would depend on the technical parameters of the given detector.

While the probability (1.66) refers to a single collision of two particles, in the real accelerator experiment particle beams of certain intensity<sup>17</sup> are brought into collision with a target or with another beam. Of course, the flux is another accelerator dependent technical parameter. The quantity we are looking for should be useful for all accelerators colliding the same particles

---

<sup>17</sup>It is the number of particles crossing a unit perpendicular area per a unit time. It is also called the *flux*.

independently of their beam intensities. It should also be independent of time the collisions last. Such a quantity can be obtained by dividing the probability (1.66) by the flux of the beam of a single particle,  $\phi$ , and by the time of the collision,  $T$ ,

$$d\sigma \propto \frac{dP_{\text{event}}}{\phi \cdot T} \quad (1.67)$$

The quantity thus constructed is called the *cross section*  $\sigma$ . This is the quantity that provides a useful information about theory for all experiments. It can be used to derive predictions for measurements at different detectors and accelerators. How it is done will be explained in Section 1.8.

It is beyond the scope of this text to learn how to calculate the cross section of a specific process by hand starting from its Feynman diagrams. Nevertheless, in Chapter 3 we introduce a free software tool for automatic calculation of cross sections. Thus, upon achieving an understanding of the software, the reader will be able to perform numerical calculations of the cross sections for various processes.

### Mass peaks

Earlier in this Section we said that the inner lines of the Feynman diagrams correspond to virtual particles that are basically non-particle disturbances of quantum fields. These disturbances transfer energy and momentum between particles but they do not have to fulfill the relation  $E^2 - \vec{p}^2 = m^2$ . However, whenever the four-momentum flowing along the inner line of the diagram approaches the condition, the cross section of the process rises. When a virtual particle's four-momentum respects this condition we say that the virtual particle is *on-shell*.

As an illustration of the rising cross section effect, let us consider the process  $A\bar{A} \rightarrow B \rightarrow A\bar{A}$  represented by the diagram in Fig. 6. Let  $p_{1,2}$  be the four-momenta of the initial particles, while  $p_{3,4}$  be the four-momenta of the final particles. Let  $q$  be the four-momentum flowing along the internal line representing the virtual particle  $B$  of the mass  $m_B$ . While  $p_1^2 = p_2^2 = p_3^2 = p_4^2 = m_A^2$ , the  $B$  particle does not have to be on-shell. The conservation of the four-momentum requires

$$p_1 + p_2 = q = p_3 + p_4. \quad (1.68)$$

If we collide the particles at the collider, i.e.  $\vec{p}_1 = -\vec{p}_2$  and  $E_1 = E_2 \equiv E$ ,

then<sup>18</sup>

$$s \equiv (p_1 + p_2)^2 = 4E^2. \quad (1.69)$$

The total energy of the collision is  $\sqrt{s} = 2E$ . At the same time,  $q^2 = s$ . Therefore, if we use the collision energy  $\sqrt{s} = m_B$ , the  $B$  particle will be on-shell. When  $\sqrt{s} \neq m_B$ , the  $B$  particle is *off-shell*. If we measured the cross section as a function of the energy of the collision we should observe a peak at the value  $m_B$  as it is sketched in Fig. 1.11. Thus, by observing the peak we could actually learn about the existence of the particle  $B$  and from the position of the peak on the  $\sqrt{s}$  axis we can determine its mass.

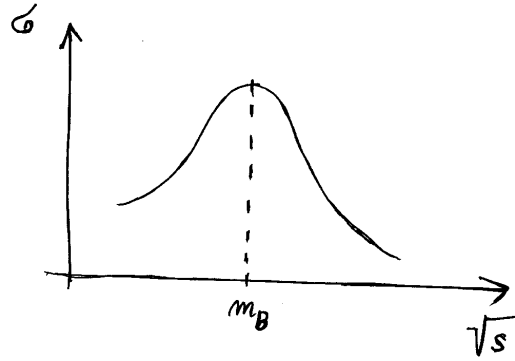


Figure 1.11: The mass peak in the graph of the cross section as a function of the collision energy.

## 1.8 The cross section: experimentalist's view

### Quantum measurements

It is important to keep in mind the quantum character of the particle systems. In Quantum Mechanics, each observable quantity has a spectrum of its eigenstates and corresponding eigenvalues. If a system is in one of an observable's eigenstates then the measurement of the observable will produce the corresponding eigenvalue.

---

<sup>18</sup>Note that it is customary to denote the square of the total four-momenta of two colliding particles as  $s$ .

However, a physical system can also be in a state which is not an eigenstate of an observable. Yet, any possible state of the system can be written as a linear superposition of the eigenstates of an observable. The quantum states are represented by vectors and the eigenstates of any observable form a basis of the corresponding vector space.

What happens if we measure an observable on a quantum system in an arbitrary state? In the process of the measurement, the state collapses to one of the eigenstates of the observable and the measurement will yield its eigenvalue. In other words, the measurement of an observable can always produce only one of the observable's eigenvalues.

Closely related to this behavior is another fact: the result of an individual measurement is not predictable unless the system is in an eigenstate of the measured observable. Nevertheless, we can predict the frequency of the occurrences of the particular eigenvalues in repeated measurements. The frequency is related to the coefficients of the state decomposition into the eigenstates of the measured observable.

If we wish to determine experimentally the state of a quantum system we have to prepare the same system in (infinitely) many copies and perform the same set of measurements<sup>19</sup> on every copy.

### Accelerator experiments

The basic idea of the accelerator experiments is to prepare and investigate the physical system consisting of two colliding particles. The system is prepared in a defined initial state. The state evolves with time. The evolution depends on the interaction between the particles. The collision point is surrounded by detectors the role of which is to determine the state of the system after the collision. Then, backwards, from the information about the system's final state physicists are trying to determine the properties of the interaction.

Typically, the detectors identifying particles emerging from the collision measure particle's energies and momenta. Recall that in the process of measurement the measured state collapses into an unpredictable eigenstate of the measured observable. Hence, if the measured final state is not an eigenstate of the "detector's observable" the result of every detected collision will look

---

<sup>19</sup>Usually the measurements of more than one observable are needed to obtain the full information about the state of the system. For the expert readers we recall that the operators of the chosen set of measured observables should commute with each other.

differently. The information from many collisions are needed to reconstruct the original state after the collision.

In order to test a theorist's hypothesis about the interaction one has to calculate the probabilities of various results in the form of the cross section mentioned in Section 1.7. To (in)validate the hypothesis, the experimentalists try to compare the predictions with actual outputs from detectors. However, particle detectors do not measure cross sections. They count the events while measuring some associated quantities, like energies and momenta of individual detected particles. Therefore, we have to figure out how to predict the number of events from the theoretical prediction of the cross section. As we will see, the number depends not only on physics of the process but also on the technical parameters of the accelerator.

An important technical parameter of every accelerator is the intensity of its beam(s) along with the properties of its target if there is any. For simplicity, let us assume the steady homogeneous flow of the beam particles. The intensity  $I$  of the beam tells us how many particles of the beam cross a perpendicular unit area per a unit time

$$I = \frac{N_B}{S_B T} = n_B v_B, \quad (1.70)$$

where  $n_B$  is the volume density of particles in the beam and  $v_B$  is their speed. If we placed an impenetrable wall of the area  $\sigma < S_B$  in the way of the beam, perpendicular to the beam, the wall would be hit by  $I\sigma$  beam particles per second; or by  $I\sigma T$  beam particles over the time period  $T$ . The situation is outlined in Fig. 1.12.

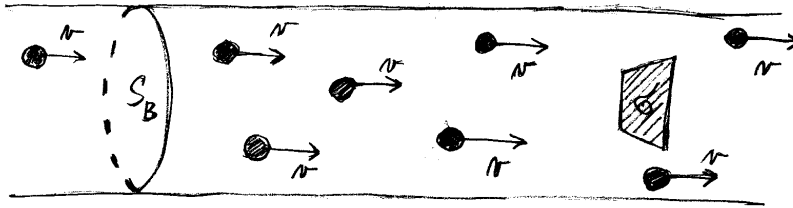


Figure 1.12: A particle beam of the cross section  $S_B$  hitting a perpendicular wall of the area  $\sigma$ .

Let us consider the accelerator experiment with a fixed target where we

detect a specific type of events<sup>20</sup>. Let the particle beam have the intensity  $I$  and the cross section  $S_B$ . Let the target have the thickness  $h_t \ll v_B T$  in the place where the beam hits it. Let the volume density of particles in the target be  $n_t$ . The number of particles contained in the projection of the beam through the target — and thus the number of particles that the beam particles can collide with — is  $S_B h_t n_t$  (see Fig. 1.13).

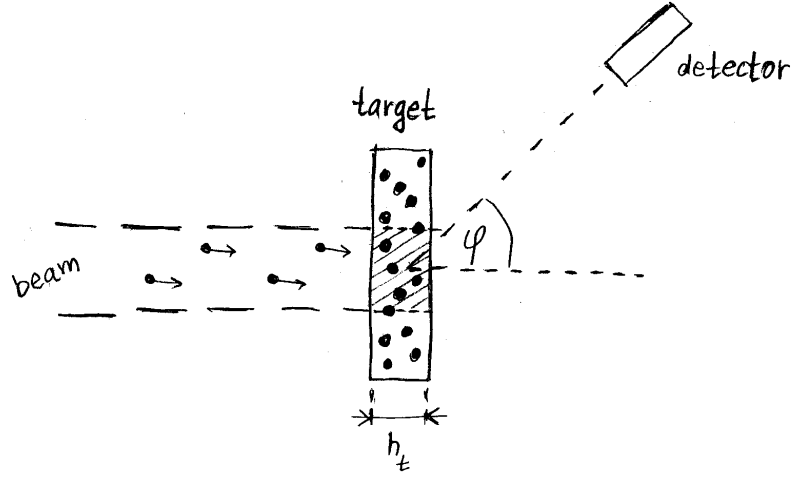


Figure 1.13: The outline of an experiment when a particle beam hits a target and a detector registers particles emerging from the collision at the angle  $\varphi$ .

Let the number of the events detected over the time  $T$  be  $N_E$ . The same number of the beam particles over the same time  $T$  would be intercepted if the fictitious perpendicular wall of the area  $S$ , such that

$$N_E = IST, \quad (1.71)$$

were put in the way of the beam. The wall size effectively represents the ability of the target to intercept beam particles and produce the observed events. The fraction  $\sigma$  of the area  $S$  related to a single particle of the target,

$$\sigma = \frac{S}{N_t} = \frac{N_E}{n_B v_B S_B h_t n_t T}, \quad (1.72)$$

<sup>20</sup>For example, these can be the events when particles emerge from the collision at a certain angle to the beam direction. Or the events with particles of a certain energy. They can be the events with particles of a given kind. There are plenty of possibilities. The choice depends on the information we are trying to extract from the experiment.

is the *cross section* we introduced at the end of Section 1.7. Here,  $N_t = S_B h_t n_t$  is the number of the target particles in the region where the beam passes through the target. The cross section is proportional to the likelihood of observing the specific result in a single collision. It contains the physical information about the process, freed of the dependence on the intensity of the beam and on the parameters of the target.

The cross section (1.72) can be rewritten in the form

$$\sigma = \frac{N_E S_B}{N_B N_t}, \quad (1.73)$$

where  $N_B = n_B S_B v_B T$  is the number of the beam particles crossing the perpendicular beam area  $S_B$  over the time interval  $T$ . In the expression (1.73),  $N_E/N_B$  is the probability that a single beam particle will cause the expected event, while  $S_B/N_t$  is the area of the target per a target particle. Then,  $\sigma$  is the size of the single particle target area which looks impenetrable for the beam.

The dependence of the number of the observed events  $N_E$  on the beam intensity and on the parameters of the target is summed up in the quantity called the *luminosity*

$$\mathcal{L} = n_B n_t v_B S_B h_t. \quad (1.74)$$

Once a theorist calculates the value of  $\sigma$  predicted by a theory, the number of events per a second which should be observed in the experiment with the beam luminosity  $\mathcal{L}$  is

$$\frac{N_E}{T} = \sigma \mathcal{L}. \quad (1.75)$$

The number of events over period  $T$  is  $N_E = \sigma L$ , where  $L = \mathcal{L}T$  is called the *integrated luminosity*.

When in the Eq. (1.74) we use the same substitutions as those used to get the expression (1.73) we obtain

$$\mathcal{L} = \frac{N_B N_t}{S_B T}. \quad (1.76)$$

We can see that  $\mathcal{L}$  is the number of all possible collisions per a unit perpendicular area and per a unit time.

In experimental particle physics, it is customary to define a specific unit for the cross section. The unit is called the *barn* and denoted “b”. Its relation to  $\text{m}^2$  is

$$1 \text{ b} = 10^{-28} \text{ m}^2. \quad (1.77)$$

The area of 1 b is roughly equal to the cross section of a nucleus of the mass number of 100. Using the relations of Section 1.3 we find that

$$1 \text{ b} \approx 2.53 \times 10^3 \text{ GeV}^{-2}. \quad (1.78)$$

For the cross sections encountered in the particle physics it is more convenient to use fractions of barn:  $1 \text{ mb} = 10^{-3} \text{ b}$ ,  $1 \mu\text{b} = 10^{-6} \text{ b}$ ,  $1 \text{ nb} = 10^{-9} \text{ b}$ ,  $1 \text{ pb} = 10^{-12} \text{ b}$ , and so on. If cross sections are given in barns, or in their fractions, then a suitable unit for the integrated luminosity is the inverse barn (or the inverse of its fraction). This way the number of the produced events,  $N_E$ , can be calculated very easily using the relation  $N_E = \sigma L$ .

### Colliders

In Section 1.6 we saw that the accelerator with two colliding beams of particles of the same momenta — the collider — can utilize the invested energy better than the accelerator with the fixed target. Let us revise the notions of the cross section and the luminosity introduced above for the case of the collider.

In a sense, the fixed target accelerator can be viewed as a collider in the rest frame of one of the colliding beams. If the beams of the collider are collinear, the transformation to the rest frame of the beam is the boost along the beams axis. The cross section represents the area perpendicular to the beam. Thus, it is an invariant quantity with respect to the boost. Even though the quantities defining the cross section (1.72) change when boosted, their changes cancel out so that the expression (1.72) remains invariant. The generalized formula for the cross section in the case of two colliding beams reads

$$\sigma = \frac{N_E}{n_1 n_2 |v_1 - v_2| V T} = \frac{N_E S_B}{N_1 N_2}, \quad (1.79)$$

where  $n_{1,2}$  are the particle densities of the beams,  $v_{1,2}$  are the particle velocities in the beams,  $V$  is the volume in which the interactions occur, and  $T$  is the time over which the collisions take place. In the second expression,  $N_{1,2} = n_{1,2} V$ . The luminosity is

$$\mathcal{L} = n_1 n_2 |v_1 - v_2| V = \frac{N_1 N_2}{S_B T}. \quad (1.80)$$

Thus, again,  $N_E = \sigma \mathcal{L} T$ .

### Differential cross section

In order to maximize the experimental information obtained about the process under investigation it is useful to measure the number of events as a function of a single or more kinematical variables. For example, we can follow how the number of events changes with the angle a final-state particle is scattered into. Or, how the number of events depends on the energy of a final-state particle. In practice, the numbers of events fallen into finite-sized intervals — *bins* — of the considered variable are counted. Thus, the obtained dependences are referred to as *distributions*. Graphically, measured distributions are represented by histograms.

Dividing the number of events in each bin by the integrated luminosity the cross section  $\Delta\sigma$  for the bin is obtained. Of course, the cross sections depend on the sizes  $\Delta x$  of the bins. To eliminate this dependence a quantity called the *differential cross section* can be defined as

$$\frac{d\sigma}{dx} \equiv \lim_{\Delta x \rightarrow 0} \frac{\Delta\sigma}{\Delta x}. \quad (1.81)$$

The generalization to the differential cross sections of more variables is obvious.

So far, in order to focus on the essence of physics, we have been talking about the accelerator experiment in an idealized fashion. In practice, however, the technical realization of the idea is much more complex. There are uncertainties about the initial state which have to be taken into account. Inhomogeneous clouds of particles rather than a single particle, or a homogeneous beam, are accelerated and brought into collisions. In addition, the detectors are also not perfect: they have their limits of what they can distinguish, the dead zones where they are not sensitive, their after-detection recovery times when they are not active, false readings, particles coming from the outside, and so on. Eventually, the number of detected events is always finite which might introduce statistical deviations from the prediction based on the infinite number of events idealization. Even the theoretical predictions are burdened by uncertainties of theory's input parameters which are also obtained in experiments. All these factors have to be taken into account when confronting theory with experiment.



# Chapter 2

## A particle zoo

In this chapter we will provide the reader with an overview of our today's knowledge of elementary particles. We will give the list of the known particles and talk about their properties and the roles they play in the micro-world.

### 2.1 Particles and anti-particles

In spite of the aureola that surrounds the anti-particles in the eyes of the general public, there is nothing extraordinary about them. Quite on the contrary, the anti-particles are as ordinary as particles. It is a simple consequence of the quantum field theory formalism that in every quantum field two kinds of the particle ripples<sup>1</sup> can be generated: *particles* and their *anti-particles*. They are like two sides of a single coin. In fact, it is just the matter of a convention which of the two kinds we call particles, and which anti-particles.

The anti-particles have exactly the same mass as their particles. It must be so: the mass is a fundamental characteristic of the field both kinds of the ripples live in.

For the same reason, they have to have the same spin<sup>2</sup>.

For the same reason, they have to share the same kinds of charges. However, with the opposite polarities. If, for example, the electron has the electric charge  $-1$ , its anti-particle — positron — has also the electric charge, but its value is  $+1$ .

---

<sup>1</sup>Recall what was said about field disturbances in Section 1.7.

<sup>2</sup>For more about the spin, see Section 2.2.

Some sorts of particles are indistinguishable from their anti-particles. Or we say that the particles are their own anti-particles. This happens when the field has no characteristics which can assume opposite values. Photons are an example of particles identical with their anti-particles.

Anti-particles enjoy such a celebrity status because when particle meets its anti-particle they both disappear. It looks like magic! This is something that can really ignite your imagination. Contrary to that, the explanation provided by the quantum field theory is quite boring. When the particle ripple meets the anti-particle ripple they can cancel each other. In the process, they disturb some other field their field interacts with. It must be so to conserve the overall energy and momentum brought in by the particle and the anti-particle. For example, when the electron passes by the positron they can annihilate each other creating the photon or the  $Z$  boson instead.

It is very tempting to picture a particle and its anti-particle as two opposite ripples of the same size moving along a string. (See Fig. 2.1a.) When they meet they cancel each other and there is no ripple for the moment, as in Fig. 2.1b. That would correspond to their mutual annihilation. Of course, the next moment the two ripples re-emerge, each leaving the meeting point in its own direction (Fig. 2.1c). That is where the analogy fails. Or, at best, it shows the situation when the particle and the anti-particle pass by each other without interacting in a non-trivial way.

The main message of the “string ripple” analogy is to point out that particles and their anti-particles are phenomena of the same origin, representing the same material basis. Anti-particles are not “from the other world”. At the same time, however, we strongly warn a reader not to use this analogy for making any further reaching conclusions about the properties and behavior of quantum fields.

## 2.2 Fermions and bosons

Beside the mass, another of the fundamental properties of elementary particles (or fields, if you wish) is their spin. Spin is a quantity related to the angular momentum. However, it is not possible to associate it with the image of a spinning little sphere. To the best of our today’s knowledge spin has no mechanistic analogy and we should view it as the inner property of an elementary particle. This property cannot be changed by any known way. It adds with the angular momentum and thus it subjects to the conservation

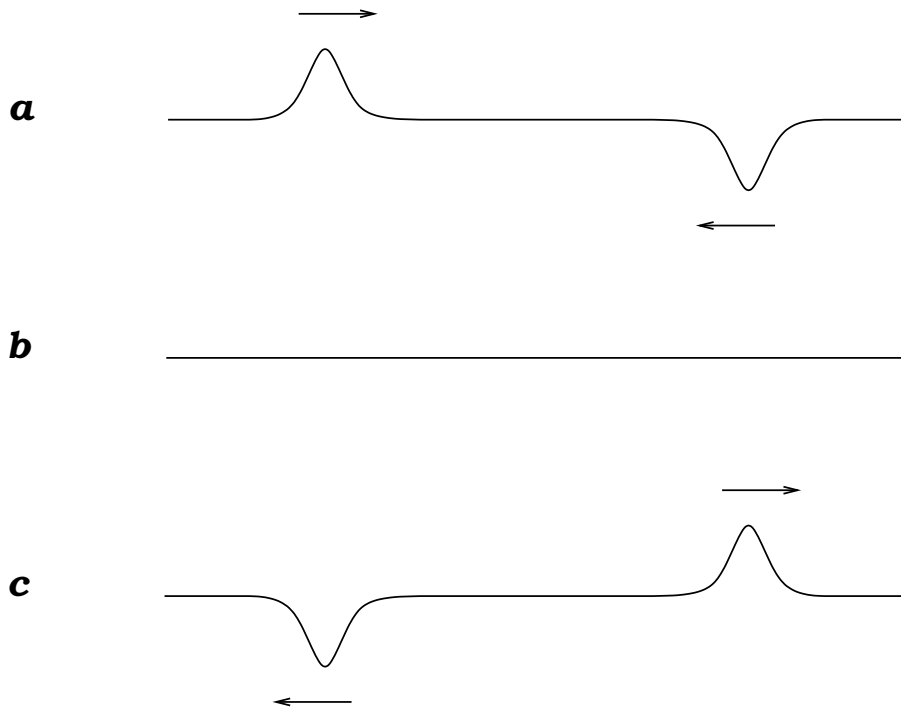


Figure 2.1: Ripples on a string moving in the opposite directions. (a) The ripples approaching each other. (b) The ripples met and canceled each other for the moment. (c) The ripples moving away.

of the angular momentum.

The Quantum Mechanics dictates that spin  $S$  of a particle can assume only the following values

$$S = \hbar \sqrt{s(s+1)}, \quad s = \frac{n}{2}, \quad (2.1)$$

where  $n = 0, 1, 2, \dots$ . In the jargon used by particle physicists, the value of  $s$  is usually referred to as spin of the particle. We will follow this practice here, as well.

Spin has an observable impact on the behavior of elementary particles. Probably the most noticeable effect is associated with the division of particles into two distinct groups, *bosons* and *fermions*. The former are particles with spins equal to the natural numbers,  $s = 0, 1, 2, \dots$ , while the latter possess spins of the values equal to the half-natural numbers,  $s = 1/2, 3/2, 5/2, \dots$

Fermions exercise very interesting phenomenon: there cannot be two fermions in the world occupying the same quantum state. This is called the *Pauli exclusion principle*. As first suggested by Paul Ehrenfest in 1931 the Pauli principle is responsible for the electron shell structure of atoms. Electrons in atoms cannot all occupy the lowest energy state. Therefore atoms occupy a certain space volume and cannot be squeezed too closely together. Consequently, they organize themselves into sustainable structures. Without the Pauli principle the ordinary matter would occupy much smaller volume. The same principle is partly responsible for the fact that solid macroscopic objects cannot penetrate each other. That is why some people say that fermions are particles of matter.

On the other hand, bosons are different. They do not exclude each other from the occupied state. There is no limit on how many bosons can be found in the same quantum state. Briefly, bosons are not subject to the Pauli principle. As a consequence, we do not see around bulk objects composed of, say, photons, which are bosons of spin 1. On the other hand, things like lasers would not work if multiple bosons could not occupy the same state.

To avoid misunderstanding: we are not claiming that photons play no important role in building and sustaining structures of objects. On the contrary. Photons are quanta of the electromagnetic field which holds the whole crystal structure together. From the large scale matter perspective the elementary bosons known today are responsible for the existence of forces acting among fermions. That is why some people say that bosons are particles carrying forces.

All elementary fermions we know today have spin  $1/2$ . All elementary bosons we know today<sup>3</sup> have spin 1.

## 2.3 Forces

According to our knowledge, there are four fundamental forces standing behind all known physical phenomena. The four forces are

- gravitational

---

<sup>3</sup>On July 4, 2012, two LHC experiments, the ATLAS and the CMS, announced the discovery of a new boson of the mass about 125 GeV. We do not know boson's spin except that it is different from 1. At this moment, we also do not know whether the particle is elementary. If yes, we would have the first example of the elementary boson with spin other than 1. To resolve this question further measurements are needed.

- electromagnetic
- strong (nuclear)
- weak

### The gravitational force

The gravitational force was the first fundamental force recognized and described in physics. Therefore, it might seem paradoxical that it is the only force of the four listed above that has no quantum description yet. While physicists have managed to discover quantum forms of electromagnetic, strong, and weak forces, the case of gravity still resists.

The gravitational force is the weakest force of the four, but it extends to infinity. At large space dimensions, we encounter the influence of gravity everywhere. It is because it grows as mass cumulates. The ubiquity of the gravity in the macro-world resulted in formulation of the classical law of gravity as early as in 17th century. On the other hand, the quantum law of gravity is not known even in the beginning of the 21th century. The main reason is that at the smallest observable scales today, its effects are negligible. We do not need to have the quantum gravity theory to successfully describe the observed phenomena in the micro-world. The very same reason leads to a lack of the experimental input which would guide theorists in resolving this problem.

Since we do not have the quantum theory of gravity, we do not know the quantum field — particle — responsible for the quantum gravity interactions in the micro-world. Frankly, it is also possible that the quantum field theory formalism is not the proper language for the gravity. Nevertheless, the hypothetical quantum of the gravity already has its name: *graviton*. It should be massless and it should possess spin 2.

### The electromagnetic force

Beside the gravity, the electromagnetism is the second and the last of the four forces that could not be overlooked in the macro-world. The electromagnetic force, as the gravity, also extends to infinity. Unlike the gravity, there are two opposite polarities of the charge associated with the electromagnetic force. Fields generated by the two polarities cancel each other.

The opposite electric charges attract each other with the great strength — the electric force is some forty orders of magnitude stronger than the gravitational one. The electric force dominates in binding nuclei, electrons, atoms, and molecules into larger structures. Hence, it creates macroscopic objects with well balanced positive and negative electric charges. There is a host of the electric charge inside these bodies, but its fields shield each other on the outside.

Due to the large electric force strength, any small imbalance of the electric charges in the macroscopic bodies results in powerful macroscopic phenomena which could not have been overlooked by physicists in the past. The investigation of these phenomena lead physicists of 19th century to formulation of the classical theory of electromagnetism (J.C. Maxwell, 1831 – 1879).

The formulation of the quantum counterpart of the classical electromagnetic theory was accomplished by the middle of the 20th century (S-I. Tomonaga, J. Schwinger, R. Feynman, F. Dyson). It was the first successful quantum field theory. It is known as the Quantum Electrodynamics (QED). The particle responsible for the electromagnetic force — the quantum of the electromagnetic field — is the photon. It is a zero mass elementary particle with spin 1. The photon has a zero electric charge and it is identical with its anti-particle.

### **The weak force**

The remaining two fundamental forces, the weak one and the strong one, are hardly noticeable in macroscopic phenomena. Or better to say, they are difficult to be recognized as forces in the phenomena observable in the macro-world.

The weak force is responsible for the radioactive beta decay. The radioactive decay was observed in the end of the 19th century (A.H. Becquerel, 1852 – 1908). It had happened long before physicists realized that force can cause the disappearance and creation of particles.

The first semi-successful attempt to build the quantum field description of the weak force was made by E. Fermi (1901 – 1954). He formulated his “four-fermion interaction theory” of the weak interactions in 1934. However, the satisfactory quantum description of the weak interactions have been accomplished by the formulation of the combined theory of the electromagnetic and weak interactions by S. Glashow, S. Weinberg, and A. Salam in the end of 1960s only. The combined electromagnetic and weak interactions are of-

ten referred to as the electroweak (elweak) interactions. The theory of the electroweak interactions is known as the Standard model of the electroweak interactions.

The extension of the weak force is extremely small, about  $10^{-18}$  m. There are three elementary bosons associated with the weak force. Their full names read *vector gauge bosons*  $W^+$ ,  $W^-$ , and  $Z^0$ . The superscripts suggest their electric charges:  $\pm 1$  and 0, in terms of the proton charge. All three have spin 1. These three bosons are the only “force particles” with non-zero masses. And they are pretty heavy, indeed. The masses of  $W^\pm$  and  $Z^0$  are about 80 GeV and 91 GeV, respectively. As many careful readers suspect at this point,  $W^+$  and  $W^-$  enjoy the particle-antiparticle relationship, while  $Z^0$  is its own anti-particle.

Since the weak gauge bosons carry electric and weak charges, they experience a phenomenon not known from the QED. The  $W^\pm$  and  $Z^0$  bosons can interact among themselves and even with the photon. This kind of interactions is called the *self-interactions*.

### The strong force

The strong interactions manifest their existence through the most common and observable phenomenon around us. The phenomenon is the mass of the macroscopic objects, including the masses of our own bodies. If we summed up masses of all elementary particles our body is made of it would account for only about 10% of its mass. The energy of the strong interactions is responsible for the remaining 90% of our body weight. Of course, while it is easy to notice the fact that things around us have masses it is very difficult to figure out its connection to the strong interactions.

The strong interactions are better known for their role in binding protons and neutrons together to form the nucleus<sup>4</sup>. They succeed despite the presence of the repulsive electric forces between protons. This suggests that the strong interactions are stronger than the electric ones. Indeed, the strong forces are about hundred times stronger than the electromagnetic interactions. However, unlike the electromagnetic and gravitational interactions, the strong forces have a very short range not exceeding  $10^{-15}$  m.

Nevertheless, even protons and neutrons are not elementary particles. They are composed of quarks which, we believe, are elementary. The quan-

---

<sup>4</sup>That is why the strong forces are also known as *nuclear* forces.

tum theory of the strong interactions took a long time to build (1950s – 1970s) and it includes a long list of names of known physicists. The name of the theory is the Quantum Chromodynamics (QCD). There are eight bosons responsible for the strong force called *gluons*. They are massless and they have spin 1.

In order to participate in the strong interactions, particles must carry a strong charge. Physicists have playfully named the charge as a color<sup>5</sup>. Actually, there are three kinds of the strong charge, each having two opposite polarities. The three strong charges are called *blue*, *red*, and *green*. Gluons carry neither electric, nor weak charge, but they possess strong charges. Consequently, they experience the strong self-interactions.

## Summary

We summarize the properties of the four fundamental forces in Table 2.1.

Table 2.1: Fundamental forces.

force	particle	mass (GeV)	spin	electric charge
gravity	graviton	0	2	0
EM	photon	0	1	0
weak	$W^\pm, Z^0$	80.4, 91.2	1	$\pm 1, 0$
strong	8 gluons	0	1	0

The QCD and the Glashow-Weinberg-Salam theory are known together under a single name: the *Standard Model* (SM). The SM has been very successful theory in terms of its confrontation with experimental measurements over the period of the last forty years. From the theoretical point of view, the major shortcoming of the model is that it does not include the gravitational interaction.

---

<sup>5</sup>That is where the part *chromo* in the word “chromodynamics” comes from.

## 2.4 Leptons

There is a group of elementary fermions that are not interacting strongly. We call them *leptons*. All leptons interact weakly. This is the list of known leptons (and their anti-particles) along with their usual symbols:

### LEPTONS

- electron,  $e^-$
- muon,  $\mu^-$
- tauon,  $\tau^-$
- electron neutrino,  $\nu_e$
- muon neutrino,  $\nu_\mu$
- tauon neutrino,  $\nu_\tau$

### ANTI-LEPTONS

- positron,  $e^+$
- anti-muon,  $\mu^+$
- anti-tauon,  $\tau^+$
- electron anti-neutrino,  $\bar{\nu}_e$
- muon anti-neutrino,  $\bar{\nu}_\mu$
- tauon anti-neutrino,  $\bar{\nu}_\tau$

The basic physical properties of the leptons are shown in Table 2.2.

Table 2.2: Leptons.

lepton	mass (MeV)	electric charge
$e^-$	0.511	-1
$\mu^-$	105.7	-1
$\tau^-$	1776.8	-1
$\nu_e$	$\leq 2 \times 10^{-6}$	0
$\nu_\mu$	$\leq 0.19$	0
$\nu_\tau$	$\leq 18.2$	0

The electromagnetic interactions of the charged leptons  $\ell^- = e^-, \mu^-, \tau^-$  are represented by the vertex in Fig. 2.2.

Since neutrinos have no electric charge they interact only weakly. The weak interactions deserve their name. They are so weak that the Earth, or

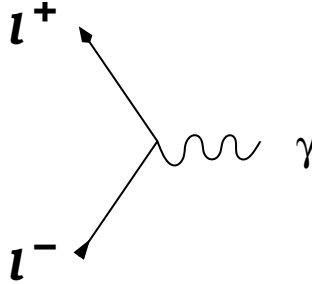


Figure 2.2: The electromagnetic vertex of charged leptons.

even big stars, are transparent for neutrinos. There are about  $10^{11}$  solar neutrinos passing through a person's thumbnail every second; yet, only one or two of them will interact with her body in her lifetime!

Because the neutrinos interact so feebly, it is very difficult to perform experiments with them to measure their properties. For example, even the masses of neutrinos have not been determined yet. There are upper limits for the neutrino masses as it can be seen in Table 2. For some time physicists believed that the masses of all neutrinos can be zero. However, recent experiments proved that at least one of the neutrinos is massive.

The same experiments proved that neutrinos change their identity as they fly from the source to the detector. Thus the electron neutrino becomes the muon neutrino, the muon neutrino becomes the tau neutrino, and so around. Physicists call this phenomenon *neutrino oscillations*. The discovery of the neutrino oscillations helped to solve the longstanding problem of the missing solar electron neutrinos. The problem was that detectors at the Earth detected only about one third of the electron neutrinos that the Sun was supposed to produce. Eventually, experimentalists confirmed that the missing electron neutrinos turned to other two species along their path from the Sun to the Earth.

In Fig. 2.3, we show the vertices representing the weak interactions of leptons with the  $Z$  boson. These interactions are also called the *neutral-current* interactions.

In Fig. 2.4 we show the vertex of the so-called *charged-current* interactions. These are the weak interactions with the participation of the  $W^\pm$  bosons. In Fig 2.4 we show only the vertices with  $W^-$ . We leave it up to the reader to draw the charge conjugated vertices.

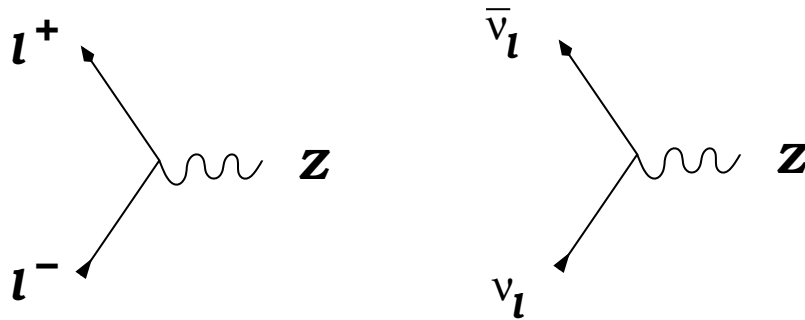


Figure 2.3: The neutral-current vertices of the weak interactions.

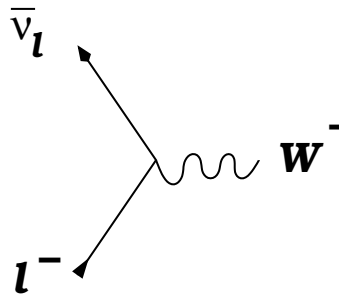


Figure 2.4: The charged-current vertex of the weak interactions.

## 2.5 Quarks

The elementary fermions that interact strongly are called *quarks*. Every elementary fermion we know today is either lepton or quark. Every quark also interacts electromagnetically and weakly. The list of the known quarks (and their anti-particles) reads:

## QUARKS

- up,  $u$
- down,  $d$
- charm,  $c$
- strange,  $s$
- top,  $t$
- bottom,  $b$

## ANTI-QUARKS

- anti-up,  $\bar{u}$
- anti-down,  $\bar{d}$
- anti-charm,  $\bar{c}$
- anti-strange,  $\bar{s}$
- anti-top,  $\bar{t}$
- anti-bottom,  $\bar{b}$

The items shown in the list do not represent the complete breakdown into the individual quark types. The list shows the division of quarks according to their *flavor*. Quarks of different flavors have different masses. However, each flavor still contains three different types of quarks. Each carries different type of the color charge. Thus, for example, we have the blue up quark, the red up quark, and the green up quark, and so on. Except for the color charge, the quarks of the same flavor are identical in all other properties.

The basic physical properties of different quark flavors are shown in Table 2.3.

Table 2.3: Quarks.

quark	mass (GeV)	electric charge
$u$	$2.3 \times 10^{-3}$	$2/3$
$d$	$4.8 \times 10^{-3}$	$-1/3$
$c$	1.28	$2/3$
$s$	$9.5 \times 10^{-2}$	$-1/3$
$t$	173.5	$2/3$
$b$	4.18	$-1/3$

The hallmark phenomenon associated with all quarks is that we cannot detect an isolated quark, the quark which would be far away from all other

quarks. The reason is that the strength of the strong interactions between two quarks grows with their distance. It is similar as if the quarks were connected by a spring governed by the Hook law. On the other hand, the closer quarks are the weaker the strong force is. Asymptotically, they start to behave like free particles when they approach each other. This counter-intuitive behavior of the strong force is responsible for the fact that quarks can only be found in the bound states with each other. Physicists say that the quarks are subdued to the *confinement*.

The strong interaction vertex is shown in Fig. 2.5, where  $g$  denotes gluon.

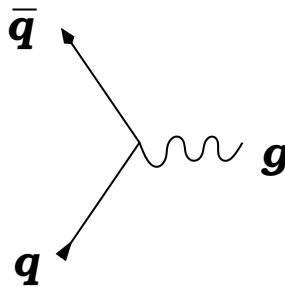


Figure 2.5: The strong vertex of quarks.

The bound states of quarks are known as *hadrons*. Experimentalists have observed two types of hadrons: *mesons* and *baryons*. The mesons are the bound states of a quark and an anti-quark. For example, the  $\pi^+$  meson is a bound state of the up quark and the anti-down quark. The baryons are the bound states of three quarks. The proton's contents is  $uud$ , the neutron consists of  $udd$ . Anti-mesons and anti-baryons are obtained by replacing all quarks with their anti-particles.

Another interesting feature of quarks is their fractional electric charges. Physicists were surprised when they discovered this fact since the general belief had been that the charge of the electron is the smallest quantum of the electric charge. As a matter of fact, only quarks break this rule. The electromagnetic vertex for quarks looks as in the case of leptons. It is shown in Fig. 2.6.

The weak interactions of quarks include the neutral-current interactions as well as the charged-current interactions. The corresponding vertices are shown in Fig. 2.7. In the case of the neutral-current vertex,  $q$  represents any quark flavor. In the case of the charged-current vertex,  $q = d, s, b$  and  $q' = u, c, t$ . The depicted charged-current vertices have their charge conjugated

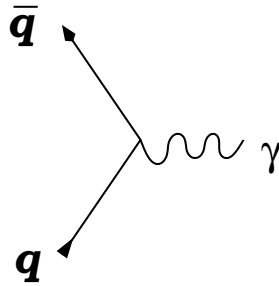


Figure 2.6: The electromagnetic vertex of quarks.

partners which are not shown in Fig. 2.7.

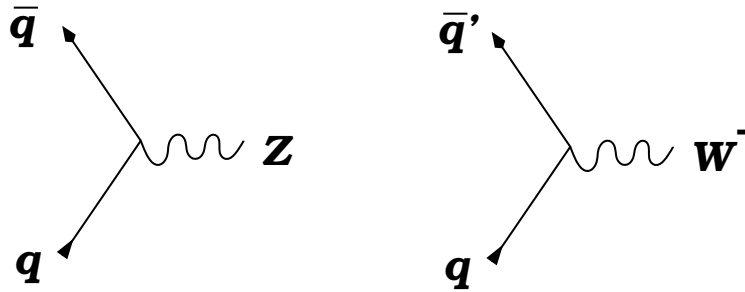


Figure 2.7: The neutral-current and charged-current weak vertices of quarks.

## 2.6 Families

In the previous sections, we have talked about all known elementary particles. We have also mentioned that their interactions — except the gravity — are described by the quantum field theory called the Standard Model. This theory interlocks the electromagnetic and weak interactions. It shows how the electroweak and strong interactions are related to various symmetries of our world.

The SM reveals that all known elementary fermions and bosons are organized to structures related to the symmetries. For example, from the symmetry point of view, there is a close relation among the three weak gauge bosons; we say they form triplet. Consequently, they share certain properties.

In the same sense, there is a connection between the electron neutrino and the electron; they form doublet. Another doublet is formed by the up

and down quarks. We are not surprised that fermions form two separate doublets — the lepton doublet and the quark doublet. After all, leptons and quarks are quite different, as we saw in the previous sections.

It is very satisfactory to see these structures and to understand the relationships among elementary particles. However, there are still facts about these structures we do not understand.

There are more lepton and quark doublets than those mentioned above. Namely, the known lepton doublets are

$$\begin{pmatrix} \nu_e \\ e^- \end{pmatrix}, \quad \begin{pmatrix} \nu_\mu \\ \mu^- \end{pmatrix}, \quad \begin{pmatrix} \nu_\tau \\ \tau^- \end{pmatrix}, \quad (2.2)$$

and the quark doublets are

$$\begin{pmatrix} u \\ d \end{pmatrix}, \quad \begin{pmatrix} c \\ s \end{pmatrix}, \quad \begin{pmatrix} t \\ b \end{pmatrix}. \quad (2.3)$$

From the point of view of their interactions the particles of the second and third lepton/quark doublets do not differ from the corresponding particles of the first lepton/quark doublet. If not for their masses, the particles of the second and third doublets would be unrecognizable from the corresponding particles of the first doublets. In this sense, the second and third doublets look like copies of the first doublets. We say there are three *families* (or *generations*) of fermions. Why there is more than one fermion family? Are there only three? If yes, why only three? The SM does not provide answers to these questions.

Our observations say that a particle from a higher family is always heavier than the corresponding particle from the lower family. We do not know why. This is just an empirical rule. Nevertheless, due to this fact all objects around us consist of the fermions of the first family. The fermions of higher families are heavier and thus unstable. They decay to the fermions of the first family which are stable because there is nothing lighter to decay to.

## 2.7 Higgs boson

The same symmetry arguments which guide the structure of the interactions of the SM and organize the elementary bosons and fermion into multiplets

imply that all the particles should be massless. This is, of course, in the direct contradiction with reality. Except for the photon and gluons, and perhaps some of the neutrinos, none of the elementary particles are massless.

Fortunately, physicists like P. Higgs, F. Englert, R. Brout, G.S. Guralnik, C.R. Hagen, T.W.B. Kibble found in 1964 a way how to reconcile the symmetry requirements of the SM with the non-zero masses. The trick is called *spontaneous symmetry breaking* (SSB). It is beyond the scope of this text to explain how it works. The only thing we would like to say is that there are many different ways how nature might have realized the trick in the case of the SM. Theorists have studied many of possible physical mechanisms behind SSB. However, only experiment can decide which one has been chosen by nature.

The simplest SSB mechanism which has been designed suggests the existence of an elementary boson of spin 0. The name of this hypothetical particle is the *SM Higgs boson*. If it were true the Higgs boson would be the first elementary particle with spin different from either 1/2 or 1.

The SM predicts that the Higgs boson should directly interact with all particles of non-zero mass. The strength of the interaction should be proportional to the mass of the particle the Higgs boson couples to. However, the SM does not predict the Higgs boson mass which is a big disadvantage when we are trying to discover it.

There are also more involved hypotheses of physics behind SSB that do not predict the existence of the Higgs boson and/or predict the existence of other particles, either elementary or composite. There are also hypotheses with more than one Higgs boson in their particle spectra.

It is quite natural that the discovery of the Higgs boson has become a goal of major experiments. Particularly, the search for the Higgs boson of the simplest SSB scenario is attracting major attention.

Of course, if the Higgs boson exists it should be produced in collisions of proper particles. Since the Higgs boson itself is not a stable particle it would exist as a short-lived virtual particle decaying through various channels. It would decay to other particles long before reaching any detectors. Thus, the existence of the Higgs boson must be inferred from the detection of its daughter particles and their behavior.

The sign of the Higgs boson existence would be the increase of the cross section when the square of the four-momentum carried by the virtual Higgs field disturbance would approach the square of its mass. (See Section 1.8) But we do not know its mass! Well, that is why the discovery of the Higgs

boson is a very difficult task.

Nevertheless, on July 4, 2012, the representatives of two major LHC experiments searching for the Higgs boson, Fabiola Gianotti of the ATLAS collaboration and Joseph Incandela of the CMS, presented at the CERN's Main Auditorium discovery of a new particle. Within the experimental accuracy of the observations the particle has properties consistent with the SM Higgs boson expectations.

Unfortunately, the accuracy achieved with the current data does not exclude interpretations of the discovery which are alternative to the SM Higgs boson. Certainly, the data does not prove that the new particle really is the SM Higgs.

Let us summarize what we know about the new particle at the moment we are writing this text:

- The mass of the new particle is about 125 GeV.
- It is not clear whether it is elementary or composite.
- The particle is electrically neutral.
- The spin of the particle is the natural number except 1. Thus, it is a boson.
- The new particle is color-neutral, i.e. it does not “feel” the strong interactions.

To answer the question about true nature of the newly discovered particle, more LHC data is required. Or even building a new  $e^+e^-$  collider parameters of which would be optimized for the production and investigation of the new particle.

For illustration, we will show one of the graphs in which the CMS collaboration demonstrates their discovery [9]. In Fig. 2.8, we can see the number of events detected by the CMS detector of the LHC collider. The detected events include the pairs of photons. The data are represented by the black dots with the error bars indicating the accuracy of the measurements. The graph depicts the observed dependence of the number of the events on the invariant mass<sup>6</sup> of the photon pair. The solid and dotted lines represent statistically optimized fits to the observed data. The red solid line is a fit to all

---

<sup>6</sup>The invariant mass  $m_{12}$  of a pair of particles with the four-momenta  $p_1$  and  $p_2$  is

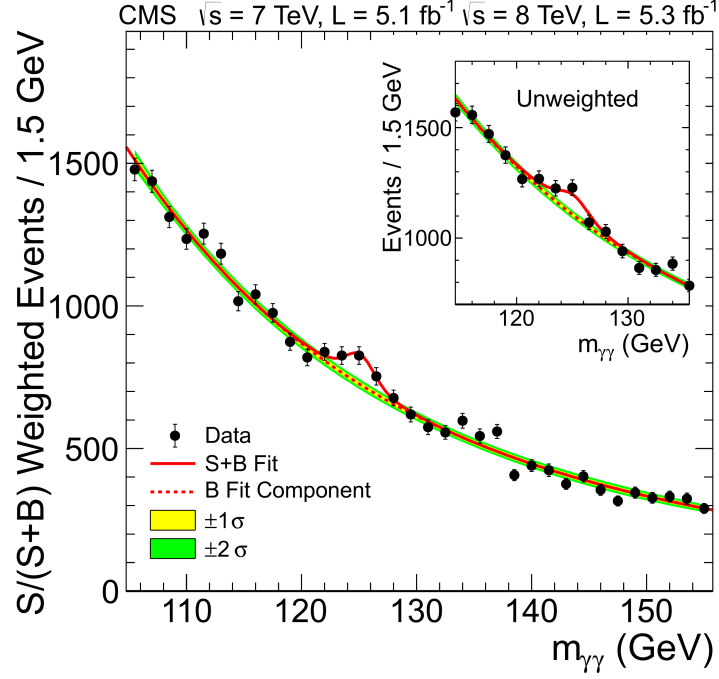


Figure 2.8: The CMS collaboration graph showing the signal of the new 125-GeV boson discovery in the  $\gamma\gamma$  channel [9].

data points, the yellow-green dotted line is a fit which does not include the points of the bump.

The bump represents the increase of the cross section which is related to the existence of a particle decaying to two photons. The mass of the particle should be equal to the value of the photon pair invariant mass at which the bump is observed.

To understand this let us imagine the process of the Higgs boson production with the subsequent decay to two photons. For example, at the LHC, it might occur in the way shown in Fig. 2.9. There, the Higgs boson could be produced in the annihilation of a quark and its anti-quark, each originating

---

defined as

$$m_{12}^2 = (p_1 + p_2)^2.$$

in one of the colliding protons.

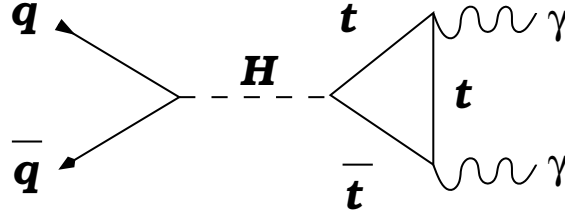


Figure 2.9: One of the Feynman diagrams of the process  $q\bar{q} \rightarrow H \rightarrow \gamma\gamma$ .

The Higgs boson cannot decay to photons directly. Recall, the Higgs boson couplings to other particles are proportional to their masses. Thus, it does not couple to the photon field. However, its coupling to the top quark field is the strongest of all. And the top quark interacts electromagnetically. Thus, it can produce photons. The Feynman diagrams that contain closed loops like in the case shown in Fig. 2.9 are called the *loop* diagrams.

The Higgs boson in the Feynman diagram of Fig. 2.9 is in the position of a virtual particle. As we discussed in Section 1.8, the virtual particle's four momentum is not bound by the condition  $E^2 - \vec{p}^2 = m^2$ . However, the cross section of the process peaks whenever the four-momentum of the virtual particle fulfills this relation.

Thanks to the conservations of energy and momentum the four-momentum  $q_H$  carried by the virtual Higgs boson in Fig. 2.9 is equal to the sum of the four-momenta  $p_1, p_2$ , of the final state photons

$$q_H = p_1 + p_2. \quad (2.4)$$

By squaring the equation we obtain

$$q_H^2 = (p_1 + p_2)^2 = m_{\gamma\gamma}^2, \quad (2.5)$$

where  $m_{\gamma\gamma}$  is the invariant mass of the photon pair. As we can see,  $m_{\gamma\gamma}^2$  is equal to the square of the four-momentum of the Higgs boson. Therefore, if we observe a peak in the  $m_{\gamma\gamma}$  distribution of the two photon production we know that the value of  $q_H^2$  approached the squared mass of the Higgs boson,  $m_{\text{Higgs}}^2$ .

Let us note that the two-photon production is only one of the channels in which the new 125-GeV particle has been observed.



## Chapter 3

# CompHEP

CompHEP is a software tool for automatic calculations of processes in particle physics [10], freely available for Linux. It is designed to calculate widths and cross sections (in the lowest order of the perturbation theory) in the Standard Model and a few other models with up to 7 particles in the final state. Events corresponding to the process can also be generated.

There are several other tools in the market which can do more or less the same thing but the advantage of CompHEP is its simplicity. The students can use it with little effort for example in their study of the Standard Model and the researchers (with a bit more effort) can add their own model to CompHEP, using LanHEP tool [11]. In fact, CompHEP has been cited by many theoretical papers on supersymmetry, extra dimensions, quantum gravity, dark matter and others. It was also used by experimentalists from LEP, Tevatron, HERA and LHC experiments.

In this chapter we describe CompHEP, its useful features and limitations, give instructions for download and installation and perform a detailed step-by-step CompHEP study of a Compton scattering, a textbook QED process. We go into details with the intention to equip the reader with skills he/she can use in his/her own studies of other processes, in particular those with  $W$  and  $Z$  bosons in the following chapters. But before we start with CompHEP, we will briefly discuss the calculation of the cross sections and the simulation chain.

### 3.1 Total and differential cross sections

We introduced the total and differential cross sections in chapter 1. Here we give you a brief idea how we calculate them.

Let us assume that particles 1 and 2 collide and produce particles 3, 4, ...,  $n$  in the final state. The total cross section is essentially given by two key ingredients, the amplitude  $M$  for the process and the Lorentz invariant phase space (LIPS), in particular [4]

$$\begin{aligned}\sigma &= \frac{1}{4\sqrt{(p_1 \cdot p_2)^2 - (m_1 m_2)^2}} \int \int \dots \int |M|^2 \text{LIPS} \\ &= \frac{S}{4\sqrt{(p_1 \cdot p_2)^2 - (m_1 m_2)^2}} \int \int \dots \int |M|^2 \left[ \left( \frac{d^3 \vec{p}_3}{(2\pi)^3 2E_3} \right) \right. \\ &\quad \left. \times \left( \frac{d^3 \vec{p}_4}{(2\pi)^3 2E_4} \right) \dots \left( \frac{d^3 \vec{p}_n}{(2\pi)^3 2E_n} \right) \right] (2\pi)^4 \delta^4(p_1 + p_2 - p_3 - p_4 \dots - p_n)\end{aligned}\quad (3.1)$$

where  $p_i = (E_i, \vec{p}_i)$  is the 4-momentum of particle  $i$  with mass  $m_i$ ,  $E_i = \sqrt{m_i^2 + \vec{p}_i^2}$  and  $S$  is a statistical factor ( $1/j!$  for each group of  $j$  identical particles in the final state).

The amplitude  $M$  contains all the dynamical information about the process (the quantum field theory behind it). We find the amplitude by calculating the Feynman diagrams for the process using *Feynman rules* derived from the *Lagrangian*. Lagrangian is the basic form in which particle physics theories are formulated. The calculation of  $M$  is usually done perturbatively, expanding the amplitude in terms of some small parameter, such as the fine structure constant  $\alpha = 1/137$  in QED. As an introduction to theoretical calculations in particle physics which includes Lagrangians, Feynman rules and amplitudes  $M$ , we highly recommend a book by David Griffiths, *Introduction to Elementary Particles* [4].

The LIPS is proportional to the number of states which the final state particles can in principle occupy if their total energy and momentum is fixed (the total energy and momentum conservation is guaranteed by the delta function). Of course, there can be many states: particle 3 can have a small or a large energy and can move in many different directions and so can particles 4 to  $n$ . If the total energy is increasing, the total number of final states is rapidly growing. If the amplitude  $M$  was a constant, the cross section would be directly proportional to the number of final states (integrals over LIPS in Eq. 3.1 count the states). However, the dynamics hidden in  $|M|^2$  usually

prefers some final states to others, acting effectively as a weight - certain states with large  $|M|^2$  will be more probable.

If we do not perform all integrals over LIPS in Eq. 3.1, we get a differential cross section. Most often you will encounter "single" differential cross sections when the integration over just a single variable is left out. The cross sections are then the functions of this single variable. We can have, e.g., the differential cross sections  $\frac{d\sigma}{dE_3}$ ,  $\frac{d\sigma}{d\cos\theta_{13}}$ , ... which show the dependence on the energy of particle 3 and the angle  $\theta$  between particles 1 and 3, respectively. We have seen in chapter 1 that the total and differential cross sections are proportional to the number of events registered by the detector. In particular, the differential cross section  $\frac{d\sigma}{dE_3}$  is proportional to the number of events  $dN$  with particle 3 having the energy  $E_3$  from the interval  $(E_3, E_3 + dE_3)$ ,

$$\frac{d\sigma}{dE_3} = \frac{1}{L} \frac{dN}{dE_3} \quad (3.2)$$

where  $L$  is the integrated luminosity and  $dN/dE_3$  is the distribution of events in variable  $E_3$ . We will see an example for the Compton scattering in Fig. 3.9b below.

## 3.2 Simulation chain

Let us now describe the great simulation chain - the chain of practical simulation steps that must be performed by particle physicists to get from the theory to the predictions of signals at the detector which can be confronted with the experimental measurement, Fig.3.1. Then we will see where the CompHEP fits. The chain has a red part, usually handled by theorists, and a green part, usually handled by experimental physicists. The theory/model is defined by its Lagrangian, from which Feynman rules are derived and Feynman diagrams drawn. Each diagram corresponds to an amplitude for the process studied within the model. The amplitudes have to be written down, squared and integrated over the phase space to yield the differential and/or total cross sections for the process.

The cross sections can be measured and compared with the calculated ones. This process is, however, not straightforward and the simulation chain continues with five more green steps. We do not deal with cross sections directly but through the number of *events* or event distributions. An event is a single collision defined by the final state particles and their 4-momenta.

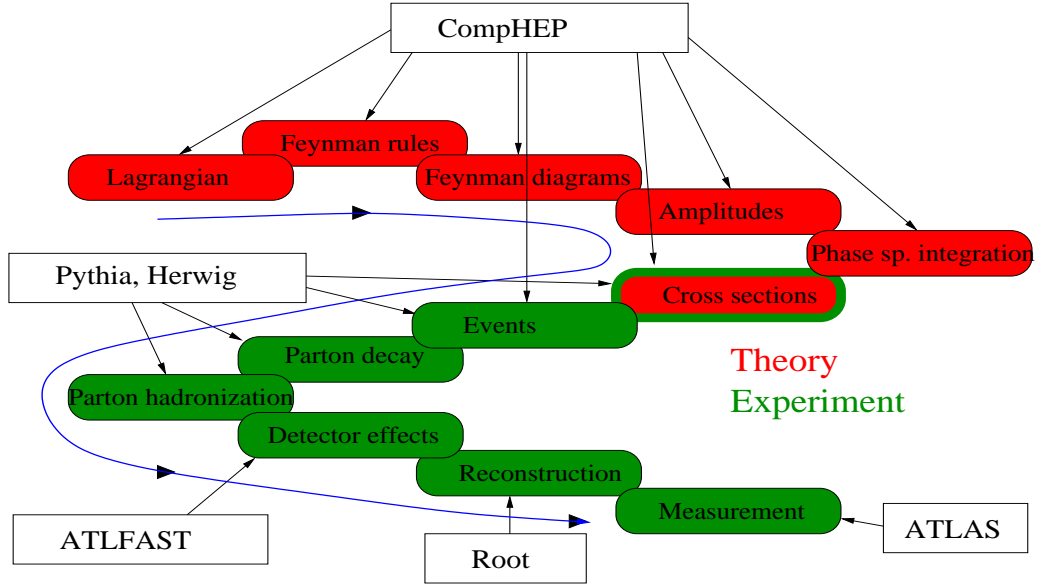


Figure 3.1: Simulation chain: steps from theory to predictions which can be tested by the measurement. CompHEP can cover the first six steps.

The number of events is given by the product of the cross section and the integrated luminosity and likewise the distribution of events is proportional to the differential cross section. Simulated events are generated from the differential cross sections in the first fully green step.

Since the theoretical calculation often includes unstable particles in the final state (such as  $W$  and  $Z$  bosons, top quarks, Higgs,  $\tau$ ,...) and involves (if present) quarks and gluons (i.e. partons) rather than hadrons seen by the detector, we must let the unstable particles decay and partons hadronize<sup>1</sup> in the next two steps of the simulation. Further, the detector is not perfect and measures particles' 4-momenta with limited precision. These effects are called the detector effects. They are simulated either quickly (e.g. with ATLFAST for the ATLAS detector) or fully and much more slowly with GEANT. The output of ATLFAST includes events with final state particles in the form of leptons, jets and missing energy, from which the originally produced particles (such as the Higgs boson) are reconstructed, using e.g. Root software.

Now, finally, the results of the simulation can be compared with the real events from the measurement. Note that the measurement itself yields events

<sup>1</sup>As a result of hadronization, quarks and gluons find themselves bound inside hadrons.

with final state particles in the form of leptons, jets and missing energy which have to be reconstructed just like the simulated events before we can compare them.

The simulation chain can be extremely demanding on computing capacities (more demanding than the analysis of real data). In fact, some of the steps are so complicated, that often a specific software tool deals with just a single step in the chain.

### 3.3 CompHEP and the simulation chain

CompHEP is not only simple to use, it is also a comprehensive tool that can cover all the red steps in the simulation chain plus the green 'events' step. Events from CompHEP can be fed into Pythia [12] or Herwig [13] to continue with decays and hadronization. The built in models/theories include QED (quantum electrodynamics), SM (Standard Model), MSSM (Minimal Supersymmetry Model) and few others. As noted above, new models can be added via LanHEP.

CompHEP is limited to the so-called *tree level* calculations of the amplitude  $M$  - the lowest order of the perturbation theory. This is normally the largest contribution. Higher order contributions include quantum corrections, so-called *loops*, which, although smaller than the tree level, can be very important for some processes. Feynman diagrams in these lecture notes are almost all tree level ones, however, we have seen examples of loop diagrams in Fig. 1.10 (one loop is represented by the  $A\bar{A}$  circle, the other loop is formed by the  $A\bar{A}B$  at the right-hand side) and in Fig. 2.9 (where the loop is the triangle formed by the top quarks). Another example is the Higgs production via gluon fusion, Fig. 6.13a. The calculation of loops can be automated to a degree and handled numerically but one has to get specific tools for that. There are plans to implement loops into CompHEP in the long run.

CompHEP can handle up to 7 particles in the final state. More particles lead to too many Feynman diagrams and too complicated phase space integrals. Even 5-7 particles (sometimes even 4 particles) require specific skills and tricks to achieve realistic computing times and converging results. For 2 or 3 particles the reader should be safe without these skills, of course, he/she is invited to try more than 3 particles. Long computing times are partly due to the method (the squaring of amplitudes) that CompHEP uses, which is very inefficient for the large number of Feynman diagrams. There are other

methods (such as helicity amplitudes) which can be more efficient.

### 3.4 CompHEP download and installation instructions

CompHEP is a Linux application, the latest stable version is Comphep-4.5.1. It can be downloaded from the CompHEP web page [10] where one has to register first, then log in. Download the file comphep-4.5.1.tgz (from the Downloads section) to your computer, e.g. to the directory called /home/COMPHEP4.5.1 (where instead of /home/COMPHEP4.5.1 any directory or name which the reader likes can be used). Now follow commands from the installation guide (this should work with most Linux distributions):

1. Untar gzip-tar distributive archive:  
`cd /home/COMPHEP4.5.1`  
`tar xzvf comphep-4.5.1.tgz`
2. Go to the comphep-4.5.1 directory:  
`cd /home/COMPHEP4.5.1/comphep-4.5.1`
3. Launch configure script:  
`./configure`
4. Compile CompHEP:  
`make`
5. In order to create a user working directory execute:  
`make setup WDIR=/home/COMPHEP4.5.1/TEST`
6. Go to your working directory and start CompHEP:  
`cd /home/COMPHEP4.5.1/TEST`  
`./comphep`

### 3.5 Compton scattering - CompHEP calculation

Compton scattering is the scattering of a photon off an electron,  $\gamma + e^- \rightarrow \gamma + e^-$ . This is the classic process which demonstrates that light can behave as a stream of particles (photons), i.e., it is not a pure wave phenomenon. It was observed early in the 20th century that when X-rays (photons) scattered off

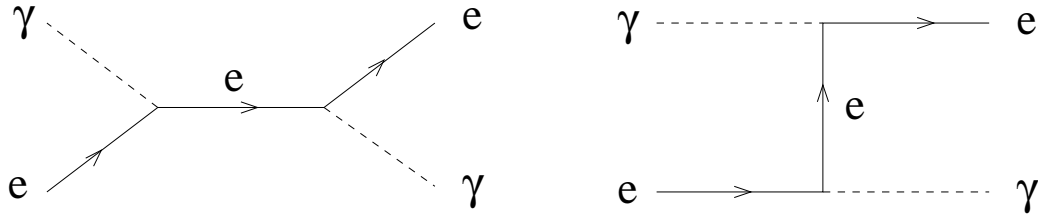


Figure 3.2: Compton scattering: two contributing Feynman diagrams.

atomic electrons by angle  $\theta$ , the scattered X-rays appeared with a wavelength  $\lambda'$  which was greater than the initial wavelength  $\lambda$ . The classical explanation, Thomson scattering, predicted wrongly that  $\lambda' = \lambda$ .

In 1923 Compton published a paper in which he treated the scattering of X-rays as the scattering of photons off electrons and derived the shift in the wavelength, which agreed with observations<sup>2</sup>:

$$\lambda' - \lambda = \frac{h}{m_e c} (1 - \cos \theta) \quad (3.3)$$

Here  $h$  is the Planck constant,  $m_e$  the electron mass and  $c$  the speed of light in the vacuum. The energy of the photon  $E_\gamma = \frac{hc}{\lambda}$ . You will derive Eq. 3.3 in *Exercise 1* at the end of the chapter.

The Compton scattering is now fully described by QED. At the lowest order of the perturbation theory two Feynman diagrams contribute, Fig. 3.2. To compute Compton cross section in CompHEP, start CompHEP and select QED model in the start-up window, Fig. 3.3. Then click Enter Scattering Process and when the list of beams appears press F3 to see the list of particles, Fig. 3.4. Enter  $A, e$  (photon and electron) for the 1st and 2nd beam (do not forget to press F3 just before you do that in both cases) and their energies.

Enter final state particles which will be again  $A, e$ , Fig. 3.5. Ignore Exclude diagrams and Keep diagrams options. Now you can view diagrams of Fig. 3.2. Click Square diagrams and Symbolic calculations in the next two steps. When all Feynman algebra is evaluated, write results in C code and run C-compiler.

A new CompHEP window for numerical calculations opens, Fig. 3.6. We can choose either a Monte Carlo integration over the phase space (a must for more than two particles) available through Numerical session or, easier in this

<sup>2</sup>Here we make an exception and do not apply  $\hbar = c = 1$

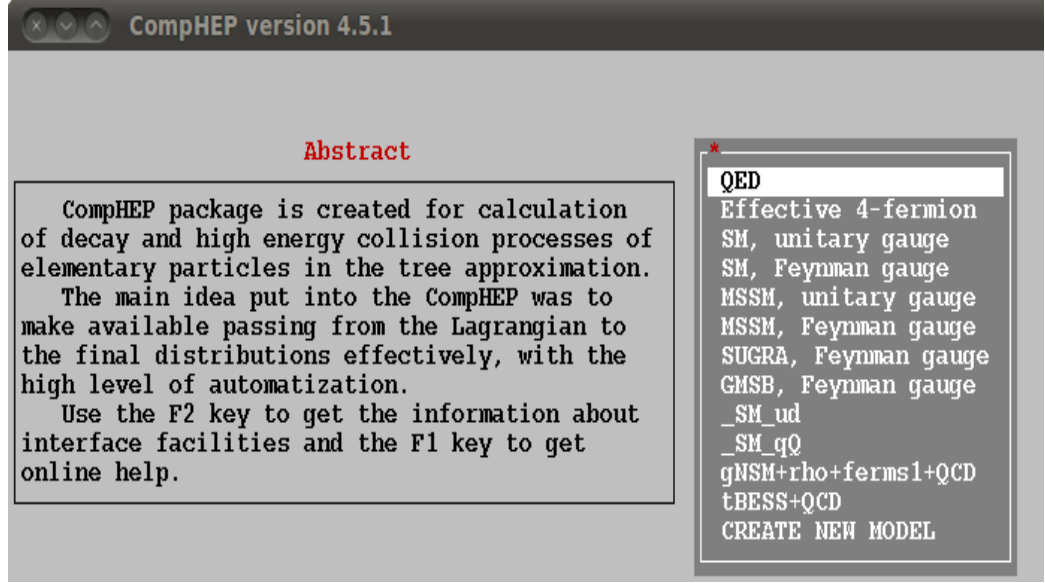


Figure 3.3: Compton scattering calculated with CompHEP. Choose QED in the list of models.

case, Simpson integration. In the next step the total cross section appears for the chosen  $\sqrt{s}$  (CM energy). Since we are interested in the behaviour of the cross section with the CM energy, click Parameter dependence, the Total Cross Section and choose parameter Sqrt(S). Finally, choose the minimum and maximum CM energy and the number of points to be plotted. The lowest possible CM energy in the case of the Compton scattering is  $\sqrt{s} = m_e + \epsilon$  where  $\epsilon \rightarrow 0$ . This corresponds to the case when the photon's energy  $\rightarrow 0$  and the electron is at rest in the CM frame. We can set the minimum at 0.00051101 GeV and maximum at 0.005 GeV. After we set the number of points a graph of the total cross section as a function of the CM energy appears, Fig. 3.7. Press an arbitrary button and a menu appears where you can change from logarithmic Y-scale to the linear. Do not forget to click the Redraw plot option.

Let us discuss the results now. The full analytical calculation (it can be done for two particles in the final state) yields for the total cross section of the Compton scattering

$$\sigma = 2\pi \frac{\alpha^2}{m_e^2} \frac{1}{x} \left\{ \left(1 - \frac{4}{x} - \frac{8}{x^2}\right) \ln(1+x) + \frac{1}{2} + \frac{8}{x} - \frac{1}{2(1+x)^2} \right\} \quad (3.4)$$

where

$$x = \frac{s - m_e^2}{m_e^2} \quad (3.5)$$

and  $\alpha = \frac{1}{137}$  is the electromagnetic fine structure constant. In the nonrelativistic limit ( $x \ll 1$  or  $s \rightarrow m_e^2$ ) we obtain the classical Thomson scattering:

$$\sigma = 8\pi \frac{\alpha^2}{3m_e^2} = 0.67 \times 10^{-24} \text{ cm}^2 = 0.67 \text{ barn} \quad (3.6)$$

This value can be found on the plot of Fig. 3.7b at the minimum CM energy  $\sqrt{s} = 0.00051101 \text{ GeV}$  where the curve touches the y-axis. In the ultrarelativistic limit  $x \gg 1$  one obtains

$$\sigma = 2\pi \frac{\alpha}{m_e^2} \frac{1}{x} \left( \ln x + \frac{1}{2} \right) \quad (3.7)$$

This limit corresponds to the curve in the right part of the plot (Fig. 3.7).

Differential cross sections can be obtained through the Numerical session button, see Fig. 3.6a. But first we redefine the problem slightly via the Initial state button in the same window. We set the 1st particle (photon) momentum at 0.01 GeV (this corresponds to the energy of  $\gamma$  ray bursts) and the 2nd particle (electron) momentum at 0 GeV (electron is at rest), Fig. 3.8a. Press Escape key. Now click the Numerical session button. A menu appears with the Set Distributions function, Fig. 3.8b. Follow the link and set distributions C13 (cosine of the angle between particle 1/incoming photon and particle 3/outgoing photon), C14 (cosine of the angle between incoming photon and outgoing electron), E3 (the energy of outgoing photon) and E4 (the energy of outgoing electron). The minimum and maximum values can be chosen as -1, 1 for C13 (C14) and 0, 0.011 GeV for E3 (E4), Fig. 3.8c. Press Escape key.

Click Clear statistics, click Clear grid. Click Start (Monte Carlo) integration. A series of five cross sections is evaluated, followed by a weighted mean. If the convergence of the five cross sections is good, the calculations are finished, if not, clear statistics (but DO NOT clear grid) and start integration again, possibly with higher statistics defined by nCall variable until you are satisfied with the convergence (equivalently, errors must be small, ideally less than 1 % for each of the five cross sections), Fig. 3.8d.

The differential cross sections can be viewed via Display Distributions function in the Numerical session window, Fig. 3.8b. We show C13 and E3

distributions in Fig. 3.9. We can see a peak at  $C13 \rightarrow 1$  ( $\theta \rightarrow 0$ ) which means that  $\gamma$ -ray photons are so energetic that they mostly continue in the forward direction after the scattering. Nevertheless, there are some which backscatter, even at  $\theta = 180$  degrees. An inspection of E3 distribution tells us, somewhat surprisingly, that there is a peak at very small energies of the scattered photons.

A further study (applying cuts via corresponding Cuts function, see Fig. 3.6a) reveals that the peak is due to backscattered photons ( $-1 < C13 < 0$ ). Forward scattered photons form the plateau which runs through most of the plot. Thus, if the photon backscatters, it loses most of its high energy as one would expect and its wavelength is shifted from small  $\lambda$  to much higher  $\lambda'$ , see Eq. 3.3.

#### *Exercise 1*

Compton scattering. Consider the scattering of photon on electron at rest. Calculate by hand the shift of the photon wavelength as the function of the scattering angle, Eq. 3.3, using the conservation of 4-momentum.

#### *Exercise 2*

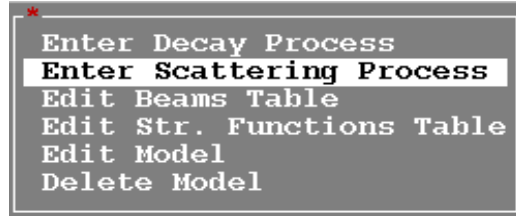
Redo in CompHEP the differential cross section calculation of the Compton scattering for visible light ( $E_\gamma = 2.75$  eV) and show that the visible light scatters in all directions more or less equally. This explains the light from the solar corona during a total eclipse.

#### *Exercise 3*

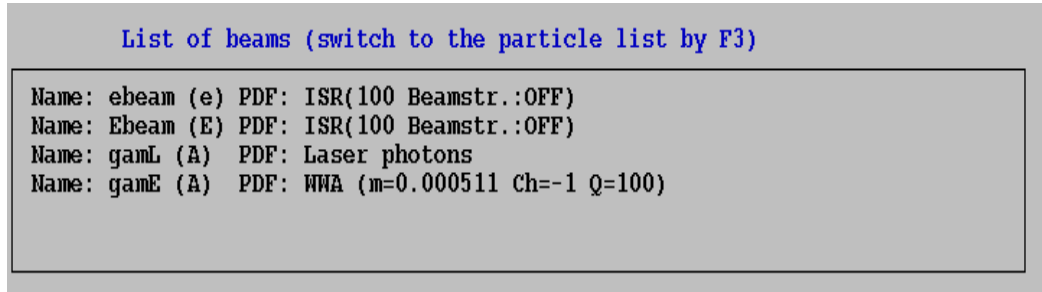
Calculate the total decay width of the Standard Model Higgs boson in CompHEP. Find all of its 2-body decay modes and find their branching fractions. Start CompHEP, choose the Standard Model (either SM, unitary gauge or SM, Feynman gauge). Rather than Enter Scattering Process, click Enter Decay Process and enter H for the Higgs boson. For the final state enter 2\*x (this trick will include all 2-body decays), Fig. 3.10. View the diagrams to see all decay modes. Square diagrams, click Symbolic calculations, write results in C code and click C-compiler. A numerical window opens up with the total decay width and all branching fractions. Click model parameters to change the Higgs mass to 125 GeV to match it with the newly discovered boson at LHC.

More CompHEP exercises will follow in chapters on  $W$  and  $Z$  bosons at

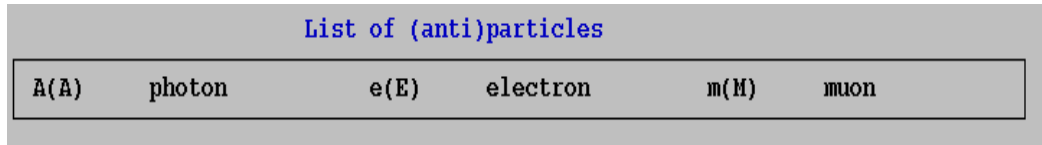
LHC.



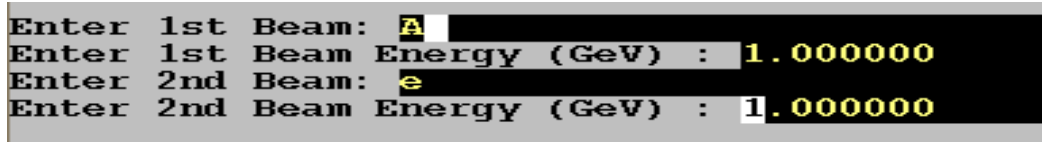
(a) Click Enter Scattering Process



(b) List of beams appears. Press F3 to switch to particle list

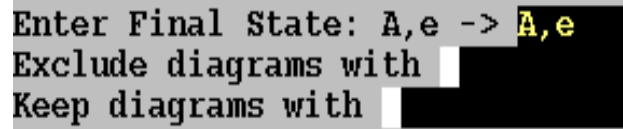


(c) List of particles appears. Enter A (photon) at the Enter 1st beam prompt



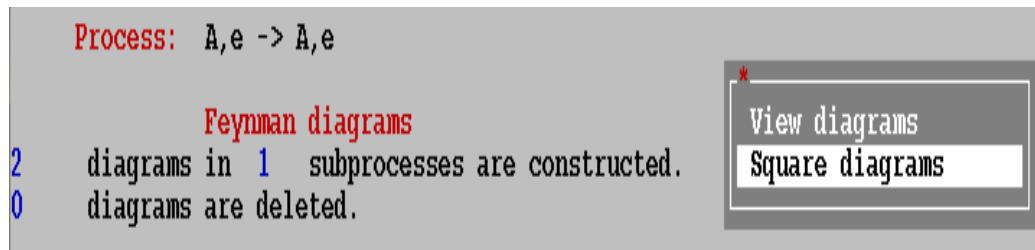
(d) Enter A, e (1st and 2nd beam) and their energies, e.g. 1 GeV

Figure 3.4: Compton scattering calculated with CompHEP continued.



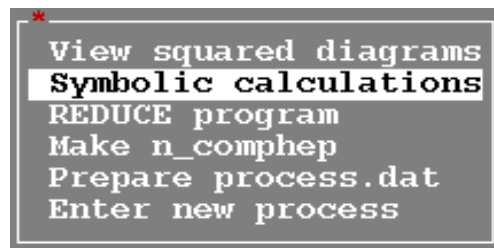
Enter Final State: A,e -> A,e  
 Exclude diagrams with  
 Keep diagrams with

(a) Enter final state A,e



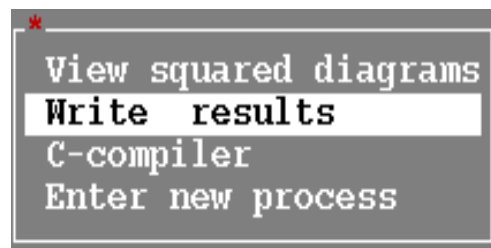
Process: A,e -> A,e  
 Feynman diagrams  
 2 diagrams in 1 subprocesses are constructed.  
 0 diagrams are deleted.  
 View diagrams  
 Square diagrams

(b) After viewing diagrams click Square diagrams



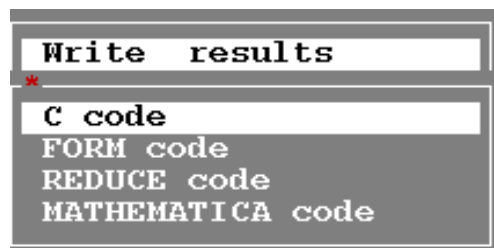
View squared diagrams  
 Symbolic calculations  
 REDUCE program  
 Make n\_comphep  
 Prepare process.dat  
 Enter new process

(c) Click Symbolic calculations



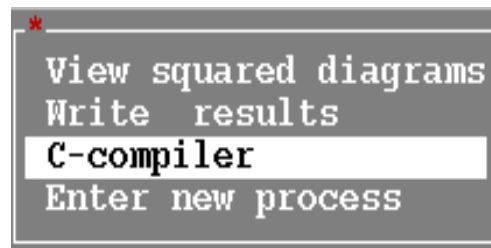
View squared diagrams  
 Write results  
 C-compiler  
 Enter new process

(d) Click Write results



Write results  
 C code  
 FORM code  
 REDUCE code  
 MATHEMATICA code

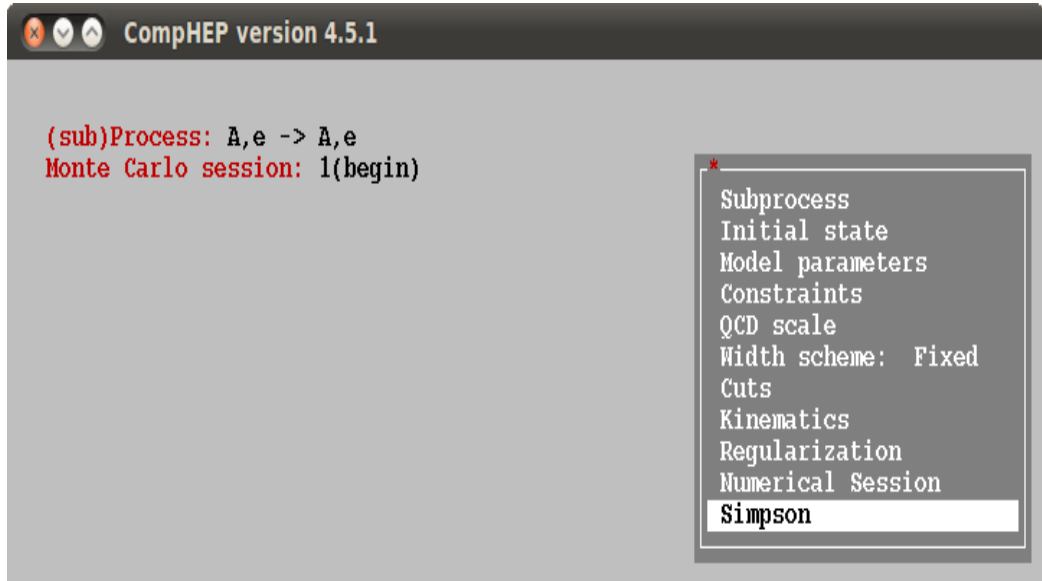
(e) Write results in C code



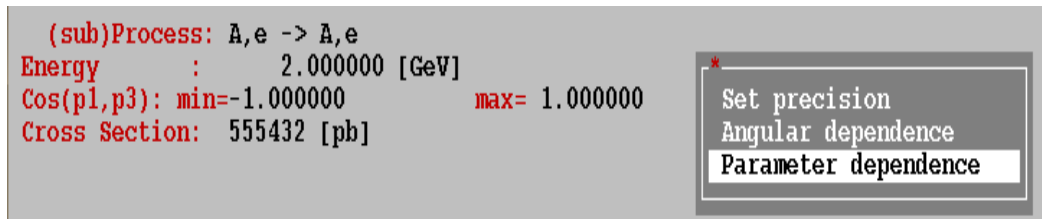
View squared diagrams  
 Write results  
 C-compiler  
 Enter new process

(f) Click C-compiler

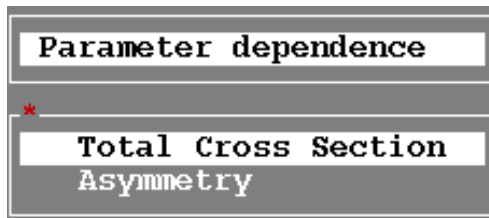
Figure 3.5: Compton scattering calculated with CompHEP continued.



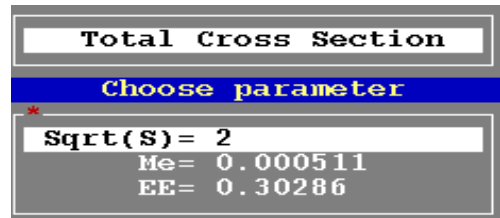
(a) A second CompHEP window for numerical calculations appears. Click Simpson integration.



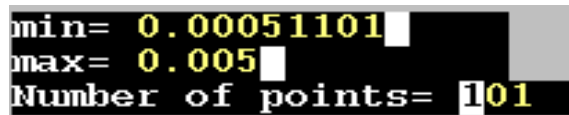
(b) Results of Simpson integration appear (cross section). Choose Parameter dependence.



(c) Click Total cross section



(d) Click Sqrt(S)



(e) Choose minimum and maximum CM energy in GeV and No. of points plotted.

Figure 3.6: Compton scattering calculated with CompHEP continued.

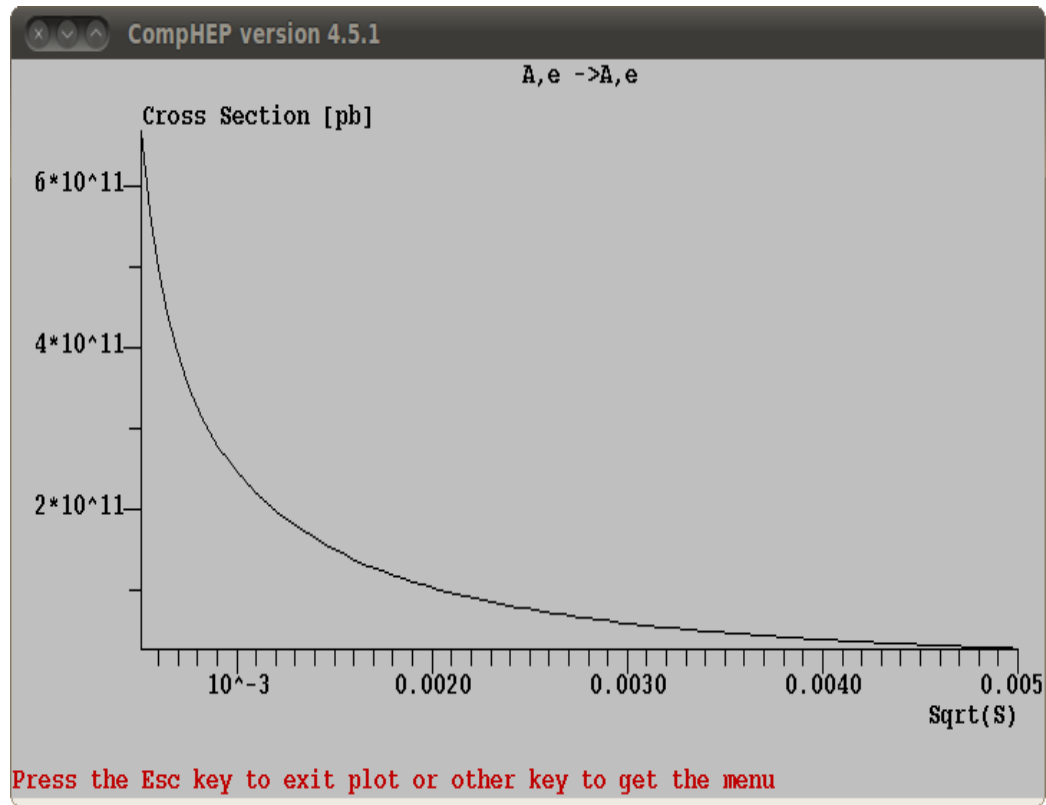


Figure 3.7: A total cross section in pb for Compton scattering as a function of  $\sqrt{s}$  (CM energy) in GeV.

```

*
Beam particle 1: parton
Beam particle 2: parton
Str.Fun.1: OFF
Str.Fun.2: OFF
1 particle momentum[GeV] = 0.01
2 particle momentum[GeV] = 0

```

(a) Initial state settings

```

Numerical Session
*
Itmx = 5
nCall = 10000
Set Distributions
Start integration
Display Distributions
Combine ROOT-hist
Clear statistic
Clear grid
Generate events

```

(b) Numerical session window with many useful functions

(sub)Process: A,e -> A,e

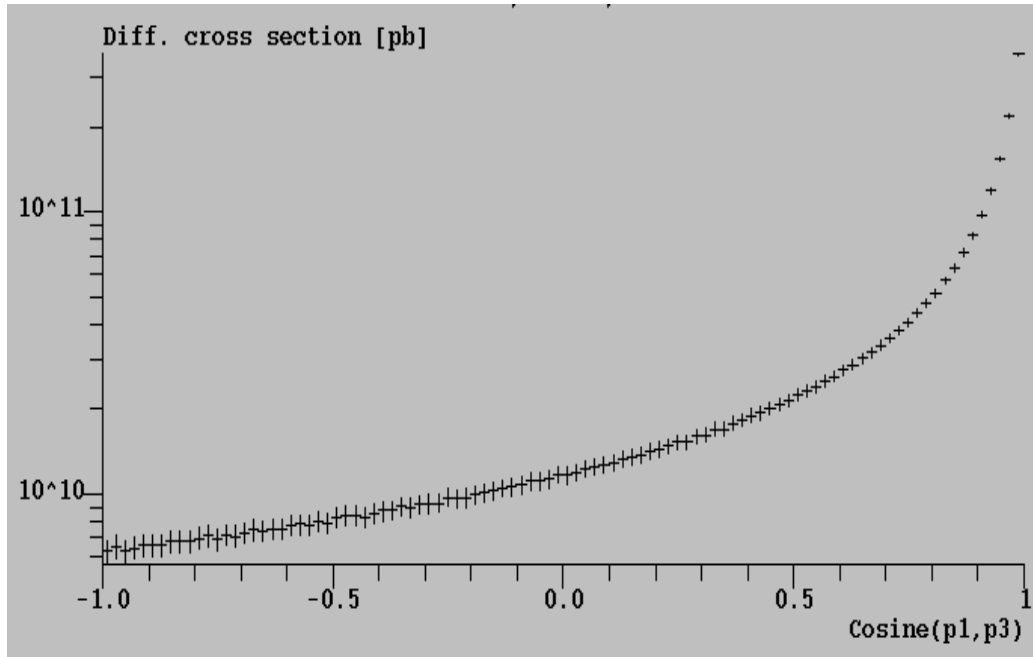
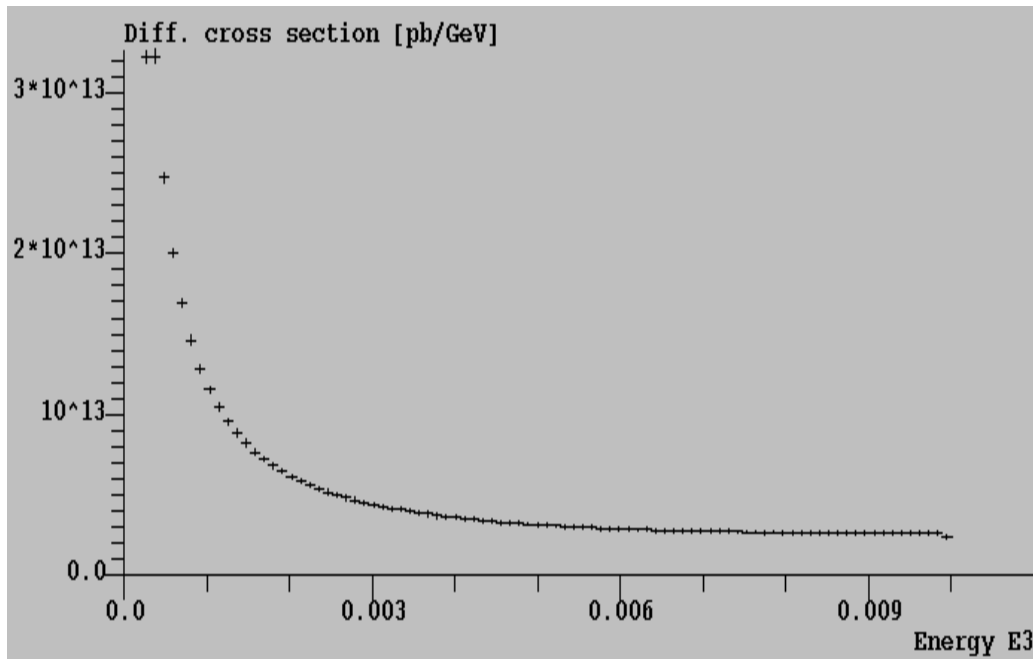
Distributions				
Clr	Rest	Del	Size	
Parameter	>	Min bound	< >	Max bound < > Rest Frame <
C13		-1		1
C14		-1		1
E3		0		0.011
E4		0		0.011

(c) Definition of distributions

#IT	Cross section [pb]	Error %	nCall	chi**2
11	5.1014E+10	1.98E-04	10000	
12	5.1014E+10	1.92E-04	10000	
13	5.1014E+10	1.94E-04	10000	
14	5.1014E+10	1.98E-04	10000	
15	5.1014E+10	1.93E-04	10000	
< >	5.6411E+10	5.21E-05	150000	1E+10

(d) Total cross sections. Monte Carlo integration results

Figure 3.8: Compton scattering calculated with CompHEP continued.

(a) C13 ( $\cos \theta$ ) distribution

(b) E3 (energy of the scattered photon in GeV) distribution

Figure 3.9: Differential cross sections in pb/GeV for Compton scattering.

```
Enter decayed particle: H
Enter Final State: H -> 2*x
Exclude diagrams with 
Keep diagrams with
```

Figure 3.10: Enter final state as 2\*x to include all 2-body decay modes.

# Chapter 4

## ATLAS detector and particle ID

### 4.1 ATLAS detector at LHC

CERN, the European Organization for Nuclear Research, is located in Geneva, Switzerland. It is the largest particle physics center in the world, established in 1954. W and Z bosons were discovered at CERN SPS collider in 1983-84. The aerial view of the Geneva region with CERN, LHC and ATLAS detector is shown in Fig. 4.1.

Large Hadron Collider (LHC) is a proton-proton collider which is in operation since 2009 at CERN. It is the world's largest accelerator. Its purpose is to look for the mechanism of electroweak symmetry breaking (the way by which W and Z bosons and possibly all elementary particles get their masses), to look for candidates for the dark matter of the Universe, to search for the solution of the baryon asymmetry in the Universe (why there seems to be more matter than antimatter), to study properties of the quark-gluon plasma (the form of matter with free quarks and gluons which existed  $1\mu\text{s}$  after the Big Bang) and, finally, to search for possible extra dimensions.

The most important goal is the mechanism of electroweak symmetry breaking. The Standard Model offers a simple solution - the Higgs mechanism which leads to the prediction of the Standard Model Higgs boson. Another solution (the most popular one among physicists) is offered by the Supersymmetric theories (SUSY). SUSY predicts at least 5 Higgs bosons and a supersymmetric partner for each elementary particle. Many of the SUSY

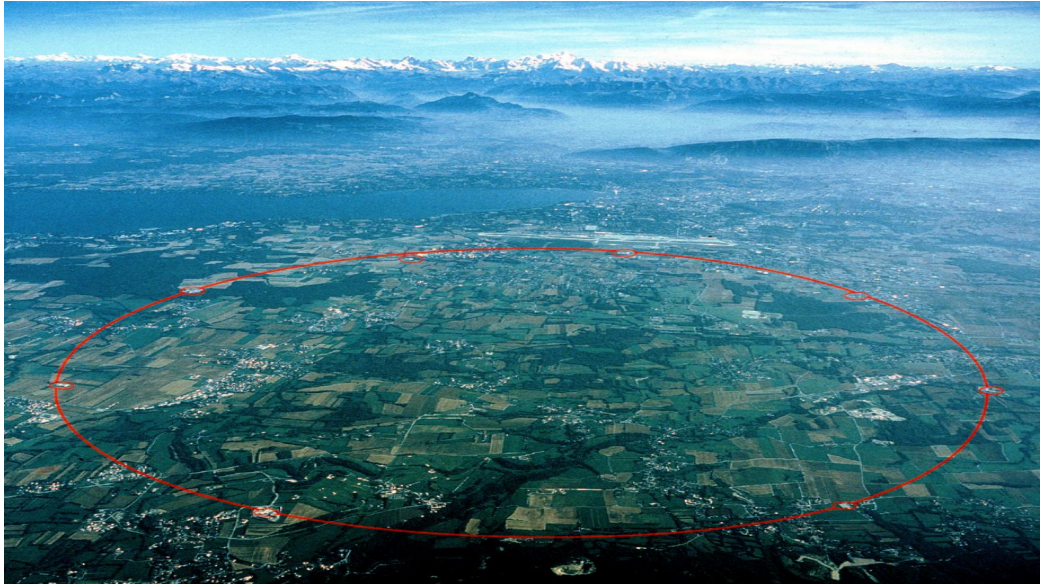


Figure 4.1: The aerial view of Geneva and CERN. The red circle indicates the position of the LHC tunnel. The ATLAS site is at the 2 o'clock position, near the main CERN site. The French Alps with Mont Blanc can be seen in the background. ATLAS Experiment ©2012 CERN

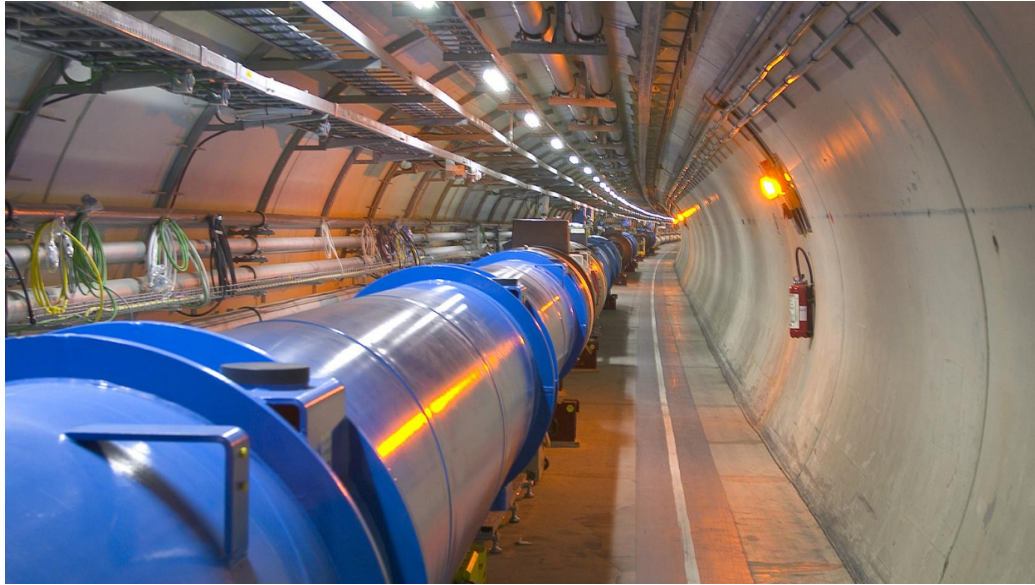


Figure 4.2: LHC tunnel with dipole magnets. ATLAS Experiment ©2012 CERN

partners are expected to be within the reach of LHC. We note that there are also solutions of the electroweak symmetry breaking problem without Higgs bosons, e.g. theories of dynamical symmetry breaking.

LHC is housed in the 27 km long circular tunnel approximately 100m under the surface. The protons move in two vacuum beam pipes, one for protons moving clockwise, the other for those moving counterclockwise (LHC is actually two accelerators in one). They move in groups called bunches. There are  $10^{11}$  protons in a single bunch and there will be 2835 bunches around the ring in each direction in full operation. The protons are kept on circular orbits by the magnetic force due to magnetic dipoles which make up most of the LHC's length (Fig. 4.2). They are accelerated by strong electric fields in RF (Radiofrequency) cavities which comprise only a short section of the LHC, about 3m long. The bunches are squeezed by the magnetic quadrupoles to as small size as possible in order to increase the chance of collisions among protons as the two counter-rotating beams of protons cross their paths in the interaction regions.

The maximum design energy of LHC, 7 TeV per proton, is limited by the maximum size of the magnetic field which can be achieved by the supercon-

ducting magnetic dipoles, 8.3 Tesla. A higher energy would require a higher field or a larger radius of the accelerator ring. High energies are required in order to produce new massive particles, heavier than anything we know so far. The second most important parameter of the LHC is its luminosity, the number of protons per  $\text{cm}^2$  per second. The number of collisions and hence the number of new particles produced is directly proportional to the luminosity. One can see that the luminosity goes up with the number of protons in the bunch, with the number of bunches and with the decreasing size of the bunches. The maximum design luminosity is  $10^{34} \text{ cm}^{-2} \text{ s}^{-1}$ .

There are 4 interaction regions, each housing a large detector: ATLAS, CMS, LHCb and ALICE. ATLAS and CMS are the two main detectors designed to search for new physics directly, detecting the signatures of the new particles produced in the collisions, LHCb is searching for the new physics indirectly, in the quantum corrections to the processes (decays and mixing) with B mesons (contain one b quark), and ALICE is a detector specialized to study the quark-gluon plasma created in the lead-lead collisions (for one month in a year LHC will collide lead ions instead of protons).

ATLAS (A Toroidal LHC Apparatus) detector is 44 metres long and 25 metres in diameter, the largest of the four main detectors (Fig. 4.3). Geometrically speaking, it consists of the central barrel and the two end caps, from the operational point of view it consists of four main subdetectors and two magnet systems. The subdetectors include the Tracker (SCT Tracker, Pixel detector, TRT Tracker), the Electromagnetic calorimeter (Liquid argon), the Hadronic calorimeter (Tile) and the Muon detectors. The two magnets are the solenoid and the toroid magnets (Fig. 4.4).

The Tracker (Inner detector) is the subdetector which is the closest to the interaction point (Fig. 4.5). Its purpose is to detect the tracks of the charged particles. The Tracker is in the magnetic field of the solenoid magnet which bends the tracks of the charged particles and from the resulting curvatures their momenta and electric charges can be found. In the Tracker particles lose little energy.

The next subdetector after the Tracker is the Electromagnetic calorimeter. Its task is to measure energies of electrons, positrons and photons and also their positions. It is designed in such a way so as to completely absorb these electromagnetically interacting particles. It consists of lead plates and sensing parts with liquid argon. The energy of electrons (positrons or photons) is absorbed in the lead plates where the electron creates a shower of many  $e^-$ ,  $e^+$ ,  $\gamma$  particles. The number of these shower particles, which is

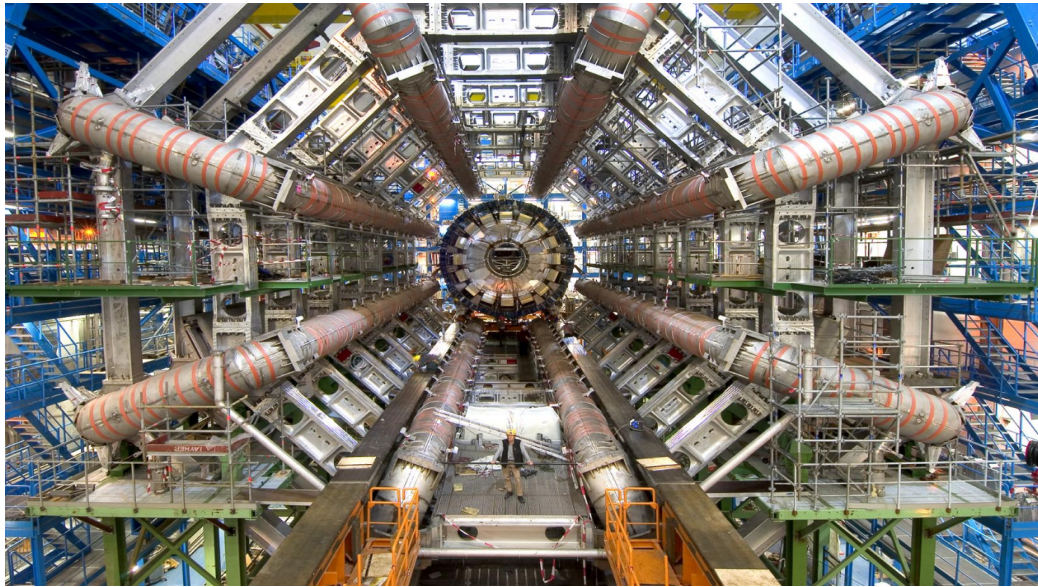


Figure 4.3: ATLAS detector. The eight toroid magnets can be seen surrounding the calorimeter that is later moved into the middle of the detector. ATLAS Experiment ©2012 CERN

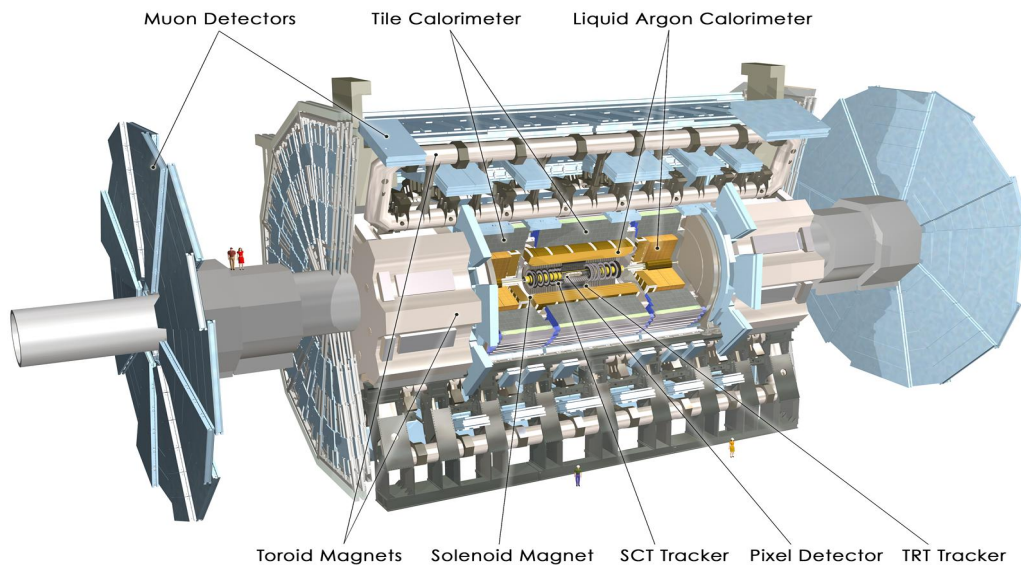


Figure 4.4: A detailed computer-generated image of the ATLAS detector and its systems. ATLAS Experiment ©2012 CERN

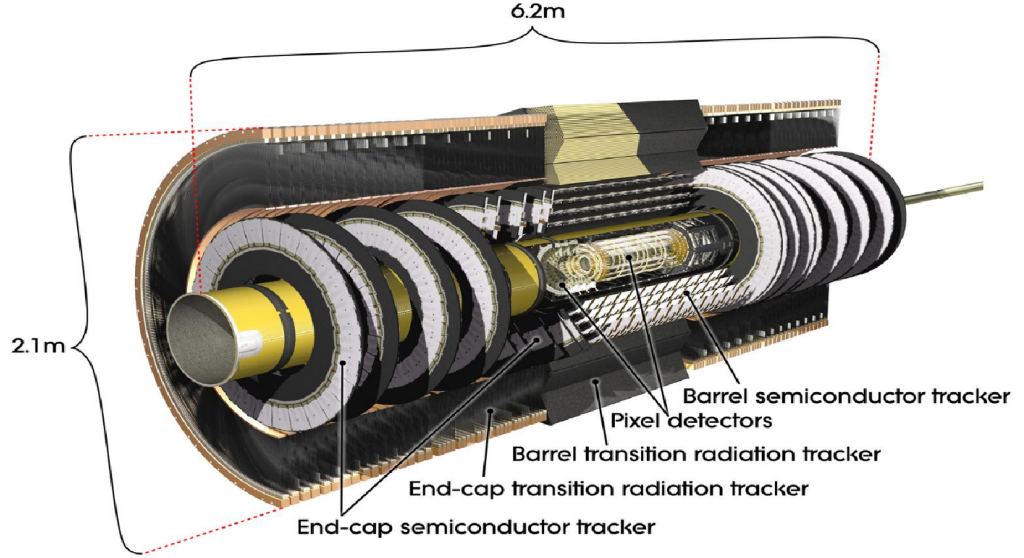


Figure 4.5: Enlarged view of the Tracker with its components: Pixel detector, SCT Tracker and TRT Tracker. ATLAS Experiment ©2012 CERN

proportional to the energy of the original electron, is then transformed into an electronic signal in the liquid argon elements.

The Hadronic calorimeter, likewise, measures energies and positions of hadrons, particles which interact mainly via the strong force. It consists of steel plates where hadrons generate showers of particles and sensing elements (scintillating tiles) where an electronic signal proportional to the energy of the original hadron is generated.

Finally, the muon detectors form the outermost layer of the ATLAS detector system. Their task is to identify muons and measure their momenta and charges from the curvature of their tracks. The curvature of the tracks is the result of the second large magnet system, the toroid magnets, in the field of which the muon detectors are placed. The toroid magnets give ATLAS its "T".

## 4.2 Particle identification

Particle identification is based on the information recorded by the four main subdetector systems. Electrons and positrons leave a track in the Tracker and

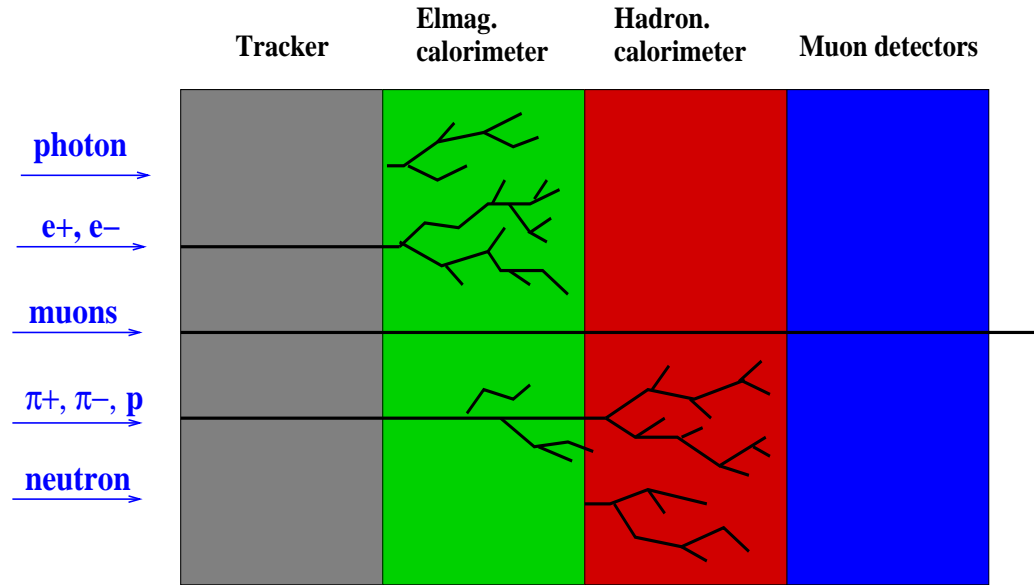


Figure 4.6: Particle identification. Particles are recognized according to the characteristic signals left in the tracker, electromagnetic and hadronic calorimeters and muon detectors

lose all of its energy in the Electromagnetic calorimeter, at the place to which the track in the Tracker points. There is no signal in the Hadronic calorimeter and the muon detectors (in the direction of the electron/positron track), see Fig. 4.6. Electron (or positron) as detected by ATLAS is shown in Fig. 4.7 in both end view (the beam pipe with protons is perpendicular to the page) and side view (beam pipe runs in the left-right direction). The innermost subdetector (black & grey) is the Tracker, followed by the Electromagnetic calorimeter (green), Hadronic calorimeter (red) and Muon detectors (blue). The electron/positron is shown by the red solid line at 10 o'clock in the end view with the corresponding energy deposition in the Electromagnetic calorimeter (yellow spots).

Muons and antimuons leave a track in the Tracker, lose little energy in the Electromagnetic and Hadronic calorimeters, leave a track in the muon detectors and leave ATLAS. Muons are the only particles along with neutrinos which fly through the whole ATLAS and normally the only particles which originate in the collision and leave a signature in the muon detectors. It may seem strange that muons, which have very similar properties as elec-

trons, their lighter brothers, behave so differently in the detector. The reason is that muons,  $200\times$  more massive than electrons, mainly lose their energy through ionisation rather than pair creation. High energy electrons, on the other hand, mainly lose their energy through pair creation, which is a very effective energy loss. The result is that electrons/positrons should not get beyond the Electromagnetic calorimeter while muons/antimuons may continue hundreds of meters beyond ATLAS in the ground. Fig. 4.8 shows muon (or antimuon) as seen by ATLAS. It is the solid orange line at 11 o'clock in the Tracker in the end view with the corresponding small energy depositions (yellow) in the calorimeters and three muon chambers reporting hits (orange) in the direction of the original track. We should caution here that not every signal from the muon detectors can be attributed to the muons produced in the collision of the two protons in the beam pipe. Many muons originate in the collisions of the cosmic ray particles in the atmosphere, in particular in the pion decays and easily make it through to the ATLAS cavern 100 m underground and to the muon detectors. This unwanted background can be usually easily removed if we see no corresponding track in the Tracker pointing to the so-called vertex (the point of the collision of two LHC protons).

Charged hadrons (pions, protons, kaons, ...) leave tracks in the Tracker, lose some energy in the Electromagnetic calorimeter and if they make it to the Hadronic calorimeter, they lose all of the remaining energy there.

Photons as neutral particles do not leave tracks in the Tracker and lose all energy in the Electromagnetic calorimeter. Neutrons as neutral particles do not leave tracks in the Tracker, do not lose energy in the Electromagnetic calorimeter and lose all their energy in the Hadronic calorimeter.

The particles discussed so far are detected directly. The remaining ones are for various reasons detected indirectly. Neutrinos interact only via weak force and do not leave any direct signature in the ATLAS detector. Nevertheless, they can be measured indirectly, using momentum conservation (see below).

The top quark, W and Z bosons are unstable particles and decay immediately at the primary vertex (where the two protons collided) and hence can only be detected indirectly via their decay products (W and Z decays are discussed in chapters 6 and 7). Tau/antitau particles and B mesons are also unstable particles: they live long enough to move away from the primary vertex but not enough to get too far. Typically it can be a fraction of a mm or a few mm before they decay. Identification of taus and B's is quite challenging. In the case of B's it is based on the reconstruction of the *secondary*

*vertex*, the point where B decayed and from which the tracks of the decay products originate.

Quarks and gluons are not seen directly due to the confinement: if produced in the collision, they immediately generate a shower of hadrons (jet) during the process called hadronization. Hadrons in the jet travel approximately in the direction of the original quark/gluon, making a cone of tracks in the Tracker. The number of hadrons in the jet can vary from a few (minijets) to tens of particles (rich jets). The jet cone is more focused for quarks/gluons with a higher energy. It is very difficult to tell the gluon jet from the quark jet. We can see at least three jets in the ATLAS event shown in Fig. 4.9. Note the many tracks in the Tracker and the energy depositions in the calorimeters (yellow spots). It is not unusual to find leptons inside jets. They are most likely decay products of jet hadrons and have to be distinguished from the leptons emerging directly from the hard collision at the primary vertex. The latter ones are typically isolated (not part of a jet) and isolated leptons with high energies are often the most important clue in the search for new physics.

## 4.3 Important kinematic variables

ATLAS detector measures and records information on particles' energies, momenta and charges. Out of these many kinematic variables can be constructed, several of particular importance: *rapidity*, *transverse momentum*, *missing transverse energy* and *invariant masses of systems of particles*. We will discuss them one by one.

### 4.3.1 Rapidity and pseudorapidity

Rapidity *relative to the beam axis of a single particle* is defined as

$$y = \frac{1}{2} \ln \frac{E + p_z}{E - p_z} = \frac{1}{2} \ln \frac{1 + v_z}{1 - v_z} \quad (4.1)$$

where  $E = \sqrt{p^2 + m^2}$  is the total energy of the particle,  $p_z$  the  $z$  component (along the proton beam axis) of its momentum  $p$  and  $v_z$  the  $z$  component of its velocity<sup>1</sup>. Rapidity is thus seen as a measure of the along-the-beam

---

<sup>1</sup>Since we work in units in which the speed of light  $c = 1$ ,  $v_z$  can take on any (dimensionless) value between 0 and 1.

component of the particle's velocity. It is used due to its properties under Lorentz transformations: it is additive under the boost along the beam axis.

If we deal with highly relativistic particles, it is useful to define pseudo-rapidity  $\eta$  as

$$\eta = -\ln \left[ \tan \frac{\theta}{2} \right] = \frac{1}{2} \ln \frac{p + p_z}{p - p_z} \quad (4.2)$$

where  $\theta$  is the angle between the particle momentum and the beam axis,  $p$  is the size of the particle momentum.

The usefulness of the pseudorapidity is that for highly relativistic particles rapidity and pseudorapidity become equal and we can relate the rapidity with the scattering angle  $\theta$  which is easy to measure. A very small rapidity then means that the particle is moving almost perpendicular to the  $z$ -axis and a large rapidity  $y$  means that the particle is moving close to the beam, left or right, according to the sign of  $y$ .

#### *Exercise*

Show that if a particle of mass  $m$  is highly relativistic ( $v \rightarrow c$ ,  $m \ll E$ ), pseudorapidity becomes equal to rapidity.

### 4.3.2 Transverse momentum

Transverse momentum is the component of the particle momentum perpendicular to the collision axis. It is used because it is invariant with respect to the Lorentz boost along the beam axis. There are additional reasons for using transverse momentum.

During the high energy proton-proton collisions at LHC energies the two protons do not collide as a whole. We will see in chapter 5 (Sec. 5.1) that the proton is a complex object consisting of many partons (parton = quark, antiquark or gluon). The high energy proton-proton collision is rather a parton-parton collision with a parton from one proton colliding with another parton from the other proton (Fig. 4.10). The remaining partons ignore the collision and escape down the beam pipe undetected. We know the momenta of the colliding protons but we do not know the momenta  $\vec{p}_1, \vec{p}_2$  of the two colliding partons. A parton's momentum is a fraction of the proton momentum which fluctuates all the time due to the interactions of partons within the proton. The fraction can be anything from 0 to 1 and we can only assign a probability for a parton to have a certain value of the fraction. More

precisely, we do not know the longitudinal (along the beam pipe) components of  $\vec{p}_1, \vec{p}_2$  since, to a good precision, the transverse (perpendicular to the beam pipe) components are negligibly small (partons are boosted with the proton along the beam pipe).

To sum it up, the total initial momentum  $\vec{p}_1 + \vec{p}_2$  has only longitudinal component which fluctuates collision by collision and, for a given collision, we do not know its value. This has two consequences. First, the distribution of momenta  $\vec{p}_3$  and  $\vec{p}_4$  of the particles 3 and 4 emerging from the hard collision (Fig. 4.10) depends besides the fundamental physics also on the along-the-beam boost of the CM system of the colliding partons 1 and 2 (the boost fluctuates with the fluctuating longitudinal component of  $\vec{p}_1 + \vec{p}_2$ ). The boost dependence thus gets in the way of the physics we would like to study. On the other hand the distributions of the transverse momenta  $\vec{p}_{T3}, \vec{p}_{T4}$  depend only on this physics, not on the boost fluctuations. The second consequence is discussed below.

### 4.3.3 Missing transverse momentum and missing transverse energy

Since we do not know the total initial momentum  $\vec{p}_1 + \vec{p}_2$ , we cannot take advantage of a very important tool in the physics analysis - the total momentum conservation for a given parton collision<sup>2</sup>. However, since the total initial transverse momentum of partons 1 and 2 is zero, we can use momentum conservation for the transverse components,  $\vec{p}_{T3} + \vec{p}_{T4} = 0$ . Generally, for  $n$  particles in the final state

$$\sum_i^n \vec{p}_{T_i} = 0. \quad (4.3)$$

This allows us to define another extremely useful quantity, missing transverse momentum,  $\vec{p}_T^{miss}$ ,

$$\vec{p}_T^{miss} = - \sum_i \vec{p}_{T_i}. \quad (4.4)$$

---

<sup>2</sup>For protons we do know initial momentum, however we cannot measure total final longitudinal momentum because we cannot build totally hermetic detector, especially along the pipe.

The missing transverse momentum allows us to detect neutrinos (or some new particles which interact extremely weakly) indirectly. The neutrinos escape ATLAS undetected, however, they carry transverse momentum with them. This neutrino  $p_T$  will appear as  $\vec{p}_T^{miss}$  assuming that the  $p_T$  momenta of all other particles were precisely measured. Since ATLAS is not perfect, one can expect that  $p_T^{miss}$  up to 20 GeV may arise naturally as a result of some particles hitting the dead parts of the detector. If  $p_T^{miss} > 20$  GeV, it is very likely that a neutrino or more neutrinos were produced in the hard collision.

Often a related quantity is used, missing transverse energy,  $E_T^{miss}$ . This has to do with the fact that ATLAS calorimeters measure energy, not momentum. For LHC energies the energy of a particle is to a very good approximation equal to its momentum and hence we can put

$$E_T^{miss} \doteq |\vec{p}_T^{miss}| = p_T^{miss} \quad (4.5)$$

and use them as synonyms.

#### 4.3.4 Invariant mass

Finally, we discuss invariant mass of a system of  $n$  particles with 4-momenta  $p_1, p_2, \dots, p_n$  where  $p_i = (E_i, \vec{p}_i)$  and  $E_i, \vec{p}_i$  are the energy and momentum of particle  $i$ , respectively. It is defined as

$$\begin{aligned} M &= (p_1 + p_2 + \dots + p_n)^2 \\ &= (E_1 + E_2 + \dots + E_n)^2 - (\vec{p}_1 + \vec{p}_2 + \dots + \vec{p}_n)^2 \end{aligned} \quad (4.6)$$

For a system of two particles we also get

$$\begin{aligned} M &= (p_1 + p_2)^2 = p_1^2 + 2p_1 \cdot p_2 + p_2^2 \\ &= m_1^2 + 2E_1E_2 - 2\vec{p}_1 \cdot \vec{p}_2 + m_2^2 \end{aligned} \quad (4.7)$$

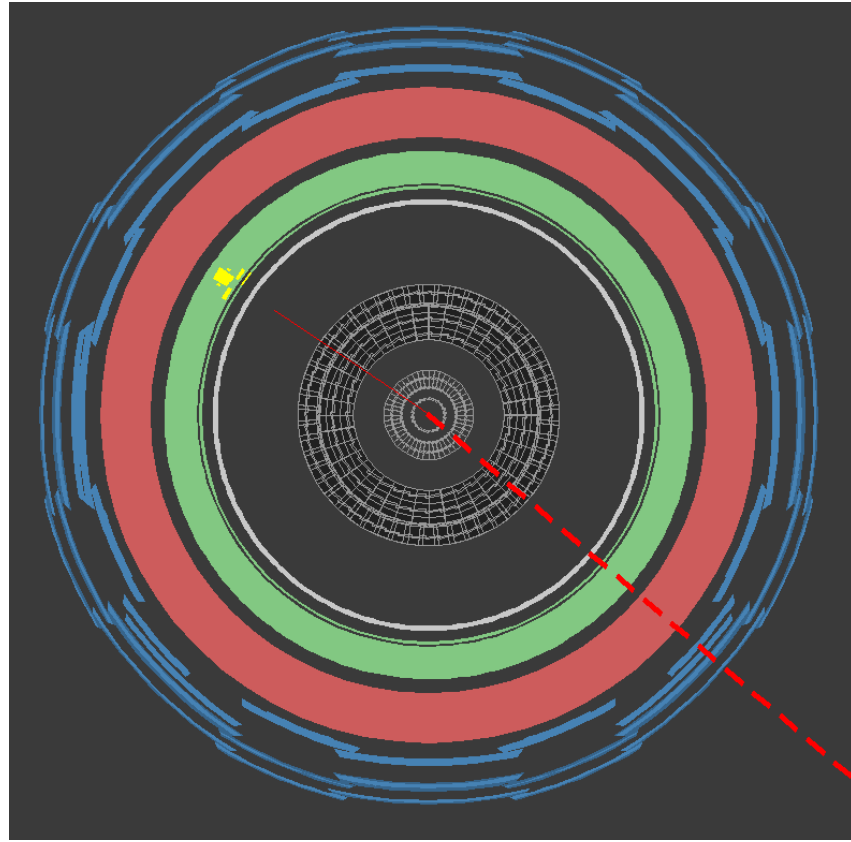
Invariant mass is an extremely useful concept for the search of new particles which can be seen as peaks above the background in the invariant mass distribution. We have seen this in Sec. 2.7 where we discussed the possible Higgs boson discovery in its decay to two photons. A peak, or bump, appeared in the invariant mass of the photon pair distribution at  $M = 125$  GeV (Fig. 2.8), interpreted as due to a new particle consistent with the SM

Higgs of mass  $M_H = M$ . The background is represented by the continuous distribution at the sides of the peak and below it.

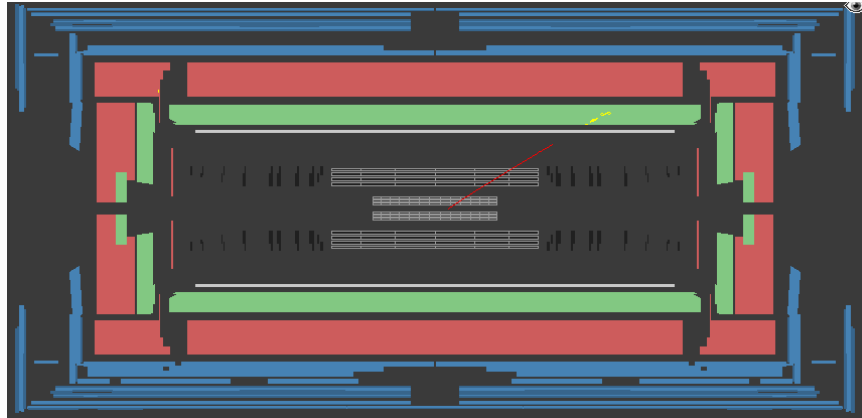
We give another example in chapter 6, Fig. 6.15b, where we show the ATLAS results of the Standard Model Higgs searches in the channel  $H \rightarrow ZZ \rightarrow llll$ . The Higgs signal appears as a peak in the distribution of the invariant mass of the system of the four leptons  $m_{4l}$ , at 125 GeV.

*Exercise*

Show from Eq. 4.6 that if  $X$  decayed to  $n$  particles then the invariant mass  $M$  of these  $n$  particles is equal to  $M_X$ . Hint: use energy and momentum conservation for the decay.

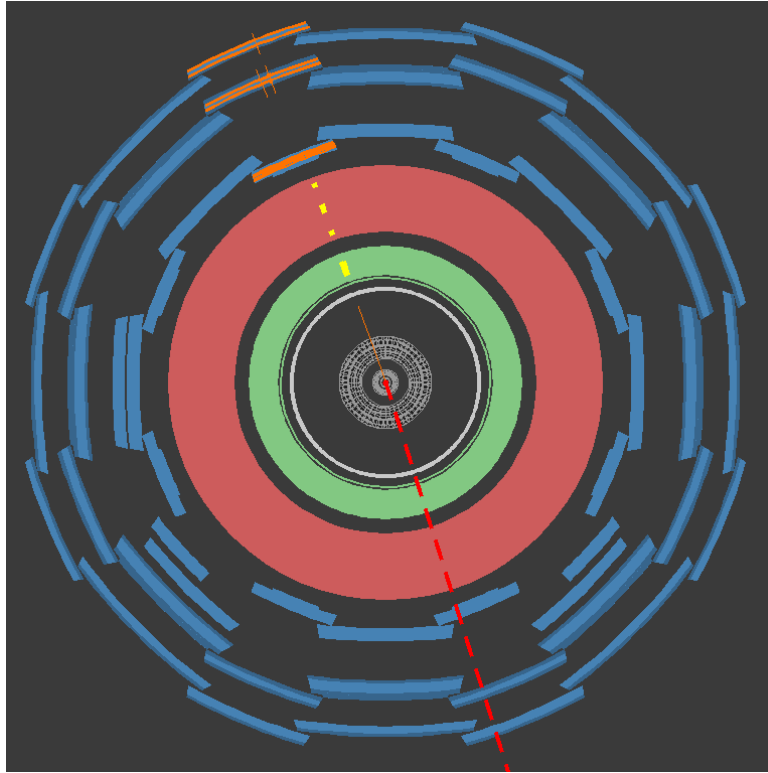


(a) End view

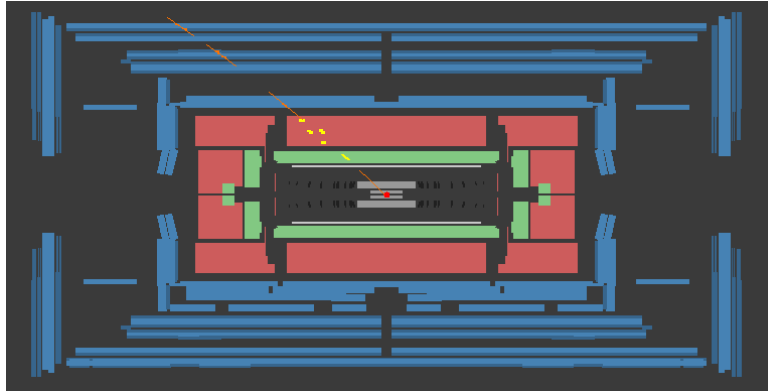


(b) Side view

Figure 4.7: Electron/positron signature in ATLAS detector. The electron/positron is shown by the red solid line at 10 o'clock in the end view with the corresponding energy deposition in the Electromagnetic calorimeter (yellow spots). The red dashed line indicates the missing momentum  $\vec{p}_T^{miss}$  in the event, in this case most likely due to a neutrino.

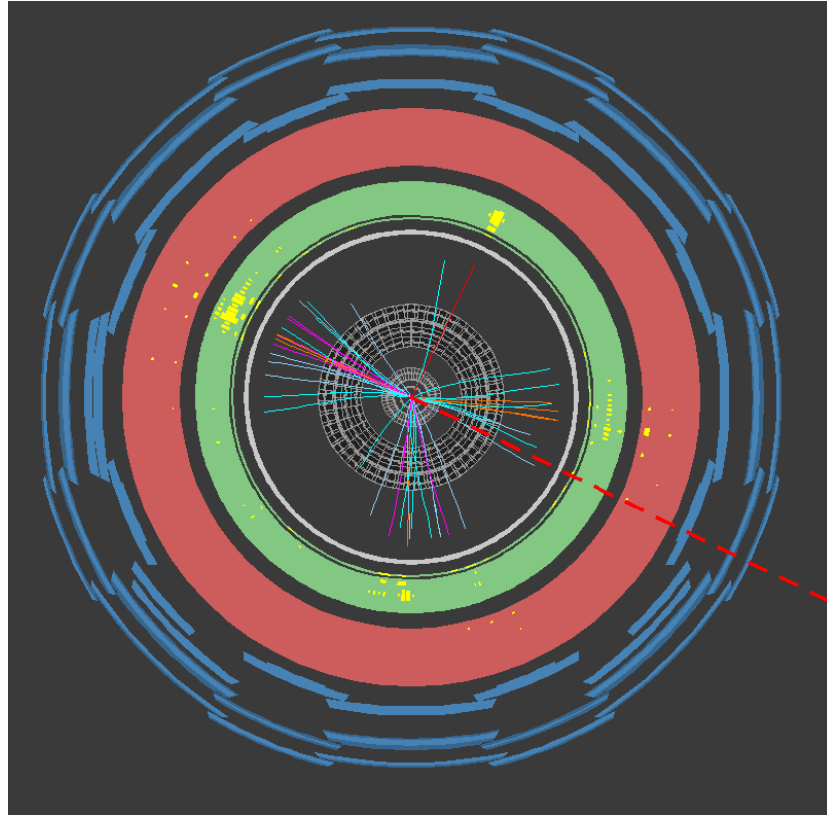


(a) End view

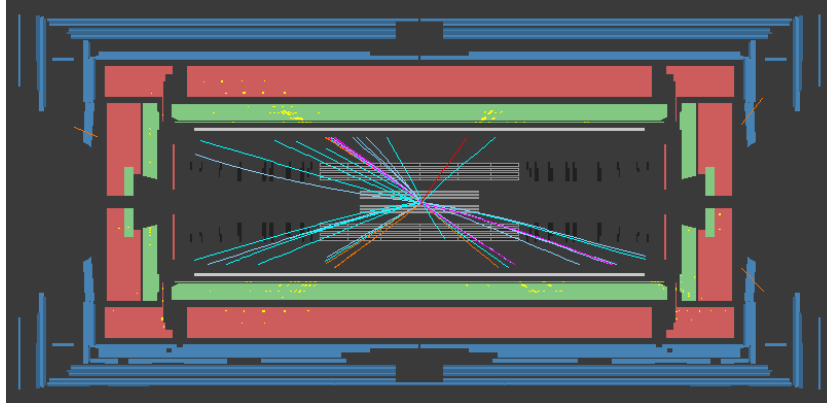


(b) Side view

Figure 4.8: Muon/antimuon signature in ATLAS detector. The muon/antimuon is the solid orange line at 11 o'clock in the Tracker in the end view with the corresponding small energy depositions (yellow) in the calorimeters and three muon chambers reporting hits (orange) in the direction of the original track. The red dashed line indicates the missing momentum  $\vec{p}_T^{miss}$  in the event, in this case most likely due to a neutrino.



(a) End view



(b) Side view

Figure 4.9: Jet signature in ATLAS detector

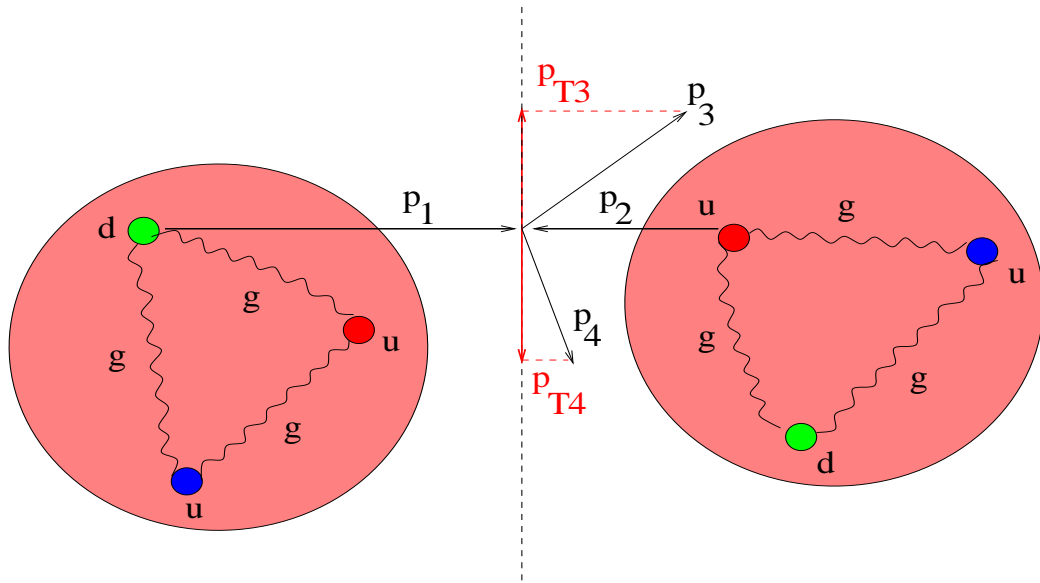


Figure 4.10: Proton-proton collision at high energies: just two partons inside protons ( $u$  and  $d$  quark in this case) collide while the remaining partons ignore the collision and escape down the beam pipe. The two interacting partons with momenta  $p_1, p_2$  create in the collision particles with momenta  $p_3$  and  $p_4$ . The transverse components of  $p_3, p_4$  are  $p_{T3}, p_{T4}$ .



# Chapter 5

## Proton structure

Proton is not an elementary particle, it has its own complex structure which goes well beyond the familiar two  $u$  quarks and one  $d$  quark. The proton structure complicates somewhat studies of the proton-proton collisions at LHC - the cross sections depend not only on the processes we would like to analyze (such as new physics) but also on this structure. We need to understand it very well. And in the region where it has not been explored yet, we can use some Standard Model processes at LHC (the physics we know) to extract the relevant information and learn more about the proton.

### 5.1 Scattering of electrons off protons

Much of what we know about the proton structure comes from the scattering of electrons off the proton. At the lowest energies the electron "perceives" the proton as a simple point charge (Mott scattering), as verified by the Rutherford type experiment with the scattering of electrons off the hydrogen atom, Fig. 5.1a. If the positive charge was distributed in the whole volume of the atom we would expect that the number of electrons scattered at large angles is small. The observed numbers at these angles are actually large and consistent with the scattering off a point charge, the proton.

At higher energies, Fig. 5.1b, electron starts to "see" proton not as a point but as a spherical charge distribution over a volume with the effective size of 1 fm ( $10^{-15}$  m, the size of the proton). This is evidenced as the drop of electrons scattered at large angles with respect to the now expected pointlike behavior of the proton. The electron energy chosen,  $E = 188$  MeV, is the

one used by R. Hofstadter in 1954 in the classic study of the proton size for which he received the Nobel prize.

So far we are talking about elastic scattering of electrons during which the proton simply recoils. At yet higher energies the proton breaks up and all sorts of hadrons like pions, kaons, delta baryons, ... fly out. This we call *inelastic scattering*.

If we keep increasing the energy of electrons, we discover that the numbers scattered at large angles are again large and consistent with the scattering off the free, pointlike spin 1/2 constituents inside the proton - the quarks, Fig. 5.1c. This regime is called the *deep inelastic scattering* (DIS). Here the structure of the proton is revealed.

The series of many DIS experiments (not only electron proton scattering) at different energies confirmed the prediction of the quark model that the proton is composed of two  $u$  quarks and one  $d$  quark. This, however, is not the whole story. According to QCD, the theory of strong interactions, the three quarks interact with each other emitting gluons and a gluon can, for a moment, change into a quark-antiquark pair. In fact, DIS confirmed the presence of all these constituents (partons) in the proton. The three original quarks ( $u, u, d$ ) are called *valence* quarks, the gluons and the quark-antiquark pairs represent the *sea*, see Fig.5.2. Sea quarks/antiquarks may include all flavors:  $u, \bar{u}, d, \bar{d}, c, \bar{c}, s, \bar{s}, t, \bar{t}, b, \bar{b}$ .

Let us look at the deep inelastic scattering of the electron off the proton more closely. The kinematics of DIS is shown in Fig.5.3. Two variables are useful for DIS description,

$$Q^2 = -q^2 = -(k - k')^2 \quad (5.1)$$

where  $k, k'$  are the 4-momenta of the incoming and outgoing electron, respectively, and

$$x = \frac{Q^2}{2p \cdot q}, \quad 0 < x < 1 \quad (5.2)$$

where  $p$  is the 4-momentum of the proton.  $Q^2$  defines the energy scale of the process, or the resolution power of the photon: the higher  $Q^2$ , the smaller structure is seen by the photon inside proton and  $x$  is a measure of inelasticity of the process. For  $x = 1$  the electron scattering is elastic (the proton is not broken apart). For  $x < 1$  the process is inelastic and if also  $Q^2 > 1$  GeV and  $x$  is less than about 0.25, the regime of DIS sets in. In this regime  $x$  gives

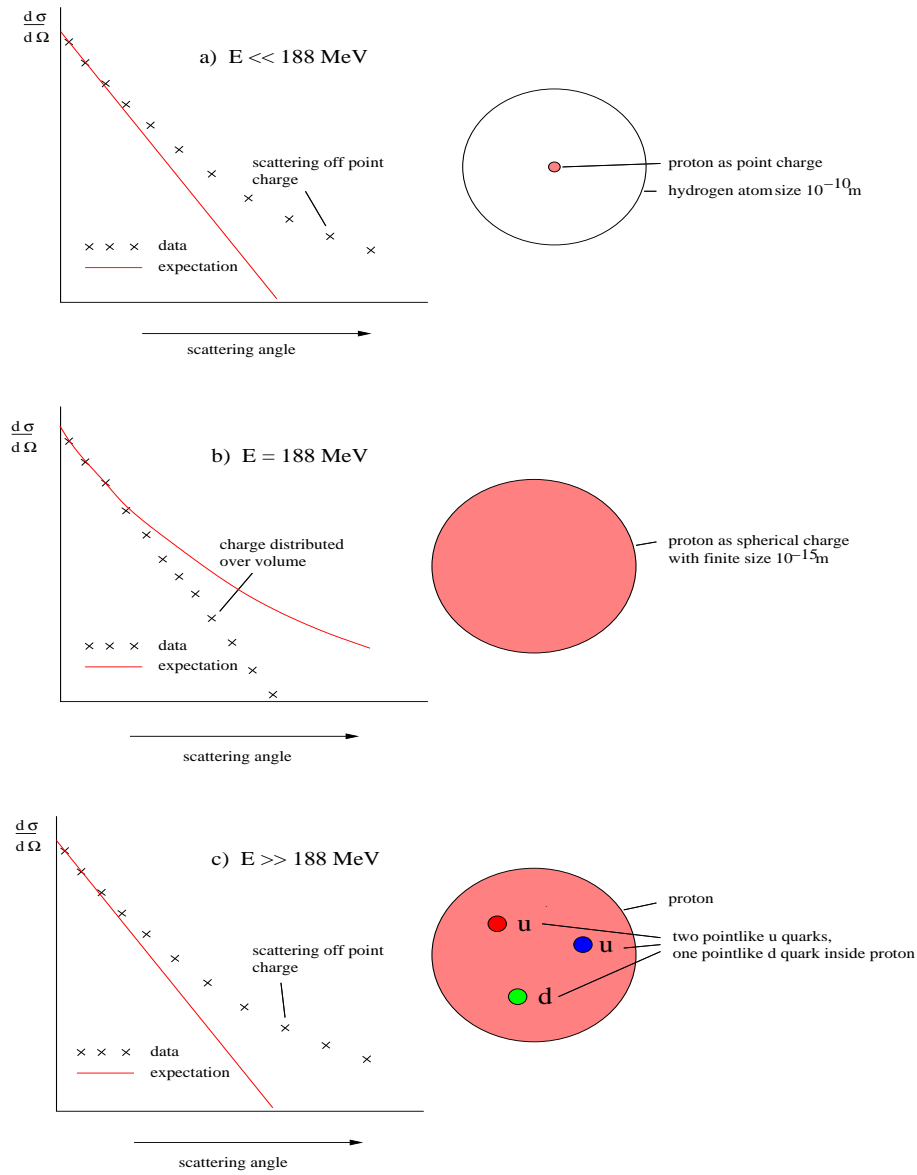


Figure 5.1: Scattering of electron off the hydrogen atom. Differential cross section as a function of the scattering angle is shown. a) At very low energies, in an analogue of the Rutherford scattering the data shows that the positive charge in the atom is not distributed over the volume of the atom but at a point. b) At the energy of electron  $E = 188 \text{ MeV}$ , the cross section drops below the value for the scattering off the pointlike proton - indication that the proton has the finite size. c) At high energies, when deep inelastic scattering sets in, the cross section goes back to the values corresponding to the scattering off the pointlike particles - the quarks.

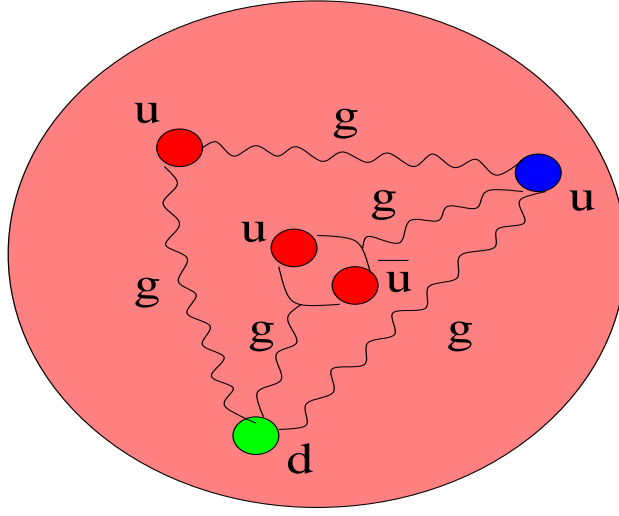


Figure 5.2: Constituents of the proton: valence quarks  $u, u, d$  with red, blue and green colors, gluons (wavy objects) and quark-antiquark pairs (also red color) from the sea.

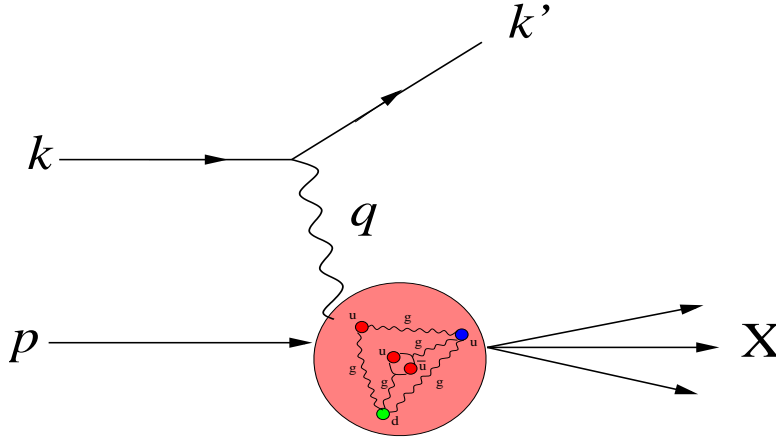


Figure 5.3: Kinematic quantities for the description of DIS.  $k$  and  $k'$  are the 4-momenta of the incoming and outgoing electron,  $p$  is the 4-momentum of the proton with mass  $m_p$ ,  $X$  is the collection of hadrons with invariant mass  $M_X$  which emerges as a result of breaking the proton apart,  $q = k - k'$  is the 4-momentum of the photon, it is the momentum transferred to the proton by the photon.

the fraction of the proton momentum carried by the quark or gluon struck by the photon.

## 5.2 Parton Distribution Functions

Our knowledge of the proton structure at energies where DIS applies is embodied by the knowledge of the so-called *Parton Distribution Functions* (PDF's). PDF's describe the probability to find a given parton (quark, anti-quark or gluon) carrying a given fraction  $x$  of the proton momentum inside the proton. More precisely, PDF's are number densities which depend on  $x$  and  $Q^2$ . In particular, if we denote the  $d$  quark PDF as  $d(x, Q^2)$ , the number of  $d$  quarks,  $N_d(Q^2)$ , with  $x$  between  $x_1$  and  $x_2$  is given by

$$N_d(Q^2) = \int_{x_1}^{x_2} d(x, Q^2) dx. \quad (5.3)$$

The number of  $d$  quarks,  $N_d(Q^2)$ , is given by the sum of valence  $d$  quarks and sea  $d$  quarks. Further, the number of sea  $d$  quarks is equal to the number of anti- $d$  quarks. Likewise  $d(x, Q^2)$  is the sum of the valence  $d$  quark PDF,  $d_V(x, Q^2)$ , and the sea  $d$  quark PDF,  $d_s(x, Q^2)$ , the latter being the same as anti- $d$  sea contribution,  $d_s(x, Q^2) \equiv \bar{d}(x, Q^2)$ :

$$d(x, Q^2) = d_V(x, Q^2) + d_s(x, Q^2). \quad (5.4)$$

The same also applies to the  $u$  quark and the  $u$  quark PDF,  $u(x, Q^2)$ .

If we subtract the sea contributions, we obtain the valence quarks numbers (the so-called Valence sum rules),

$$\begin{aligned} \int_0^1 [d(x, Q^2) - d_s(x, Q^2)] dx &= \int_0^1 d_V(x, Q^2) dx = 1 \\ \int_0^1 [u(x, Q^2) - u_s(x, Q^2)] dx &= \int_0^1 u_V(x, Q^2) dx = 2 \end{aligned} \quad (5.5)$$

The mean value of  $x$  for  $d$  quark is given by  $\bar{x}_d = \int_0^1 x d(x, Q^2) dx$ . The sum of mean values of  $x$  of all partons should equal to 1 (fractions of proton momentum should add to 1), yielding the Momentum sum rule

$$\int_0^1 x [u(x, Q^2) + d(x, Q^2) + \bar{u}(x, Q^2) + \bar{d}(x, Q^2) + \dots] dx = 1 \quad (5.6)$$

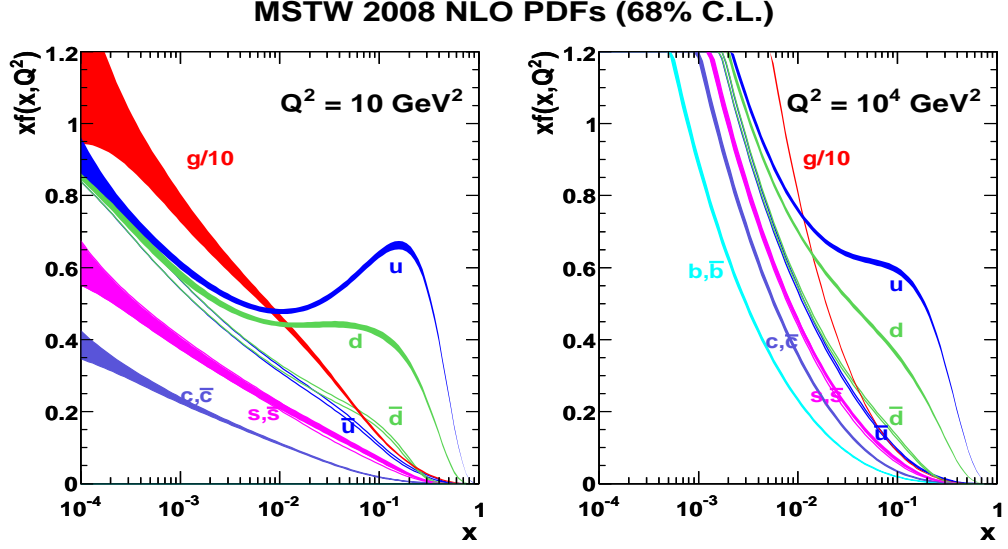


Figure 5.4: Distributions of  $x$  times PDFs of the proton at scales  $Q^2 = 10 \text{ GeV}^2$  (left) and  $Q^2 = 10^4 \text{ GeV}^2$  (right). Reprinted with permission from MSTW collaboration, <http://mstwpdf.hepforge.org/>

where ellipses indicate contributions of PDF's of all other quarks, antiquarks and gluons:  $c, \bar{c}, s, \bar{s}, t, \bar{t}, b, \bar{b}, g$ .

Physicists have not been able to calculate PDF's from QCD, they are found experimentally at some  $Q^2$  (once we have them at some  $Q^2$ , QCD is used to evolve them to higher values of  $Q^2$ ). Our knowledge of the proton PDF's is summarized in Fig. 5.4 for two different energy scales  $Q^2 = 10 \text{ GeV}^2$  and  $Q^2 = 10^4 \text{ GeV}^2$ . This is the summary of results of many experiments with fixed targets, electron-proton collider HERA experiments<sup>1</sup> and proton-antiproton experiments at the Tevatron collider<sup>2</sup>. The width of the bands indicates the uncertainty of a particular PDF. Using these PDF's we can calculate mean values of  $x$  for  $u$  and  $d$  quarks (mean values are basically given by the area under the curves in Fig. 5.4, do not forget though that the

<sup>1</sup>The Hadron Electron Ring Accelerator, HERA, at DESY, Hamburg, is the first electron-proton collider in the world. It was closed in 2007.

<sup>2</sup>Tevatron was the proton-antiproton collider at the Fermi National Accelerator Laboratory (Fermilab), near Chicago. Here the top quark was discovered. Tevatron closed in 2011.

$x$ -axis is logarithmic),

$$\begin{aligned}\bar{x}_u &= \int_0^1 x u(x, Q^2) dx \sim 0.36 \\ \bar{x}_d &= \int_0^1 x d(x, Q^2) dx \sim 0.18.\end{aligned}\tag{5.7}$$

This means that  $u$  and  $d$  quarks carry on average approximately  $36\% + 18\% = 54\%$  of the proton momentum (exact numbers depend on the scale  $Q^2$ ). The remaining momentum is carried mostly by gluons and a tiny fraction by the remaining quarks.

### 5.3 Proton-proton collisions

Precise knowledge of PDF's is much needed in the whole  $x$  range in order to better understand signal and backgrounds in searches for new physics in high-energy colliders. The cross sections for both new physics and the backgrounds depend on PDF's and the uncertainty of the prediction of the cross sections due to the PDFs' uncertainties is often larger than the experimental error. For this purpose, Standard Model  $W$  and  $Z$  production processes,  $pp \rightarrow W^\pm X$ ,  $pp \rightarrow ZX$ , will be used to tightly constrain some of the PDF's at LHC. The improved PDF's can be subsequently used to predict signal and backgrounds for new physics. Here we will show how the processes at LHC depend on PDF's in general, later in chapter 6 we will be more specific and concentrate on a single  $W$  boson production.

First we have to discuss kinematics of the proton-proton collision. At the LHC the proton structure is probed not by the electron but by one of the partons of one proton scattering off one of partons of the other proton, see Fig.5.5. The DIS collision is divided into two parts, the PDF part (proton structure) and the *hard-scattering process* (blue). PDF's describe which partons and with what probabilities take part in the hard-scattering. In the hard-scattering part two or more particles with invariant mass  $M$  are produced from the two initial partons. The adjective 'hard-scattering' indicates that a lot of energy is involved ( $M$  is typically few tens of GeV) and perturbative calculations can be applied. On the other hand the PDF part is *soft*, meaning that PDF's cannot be calculated perturbatively from QCD.

The collision energy is  $\sqrt{s}$  and if we neglect the proton mass which is

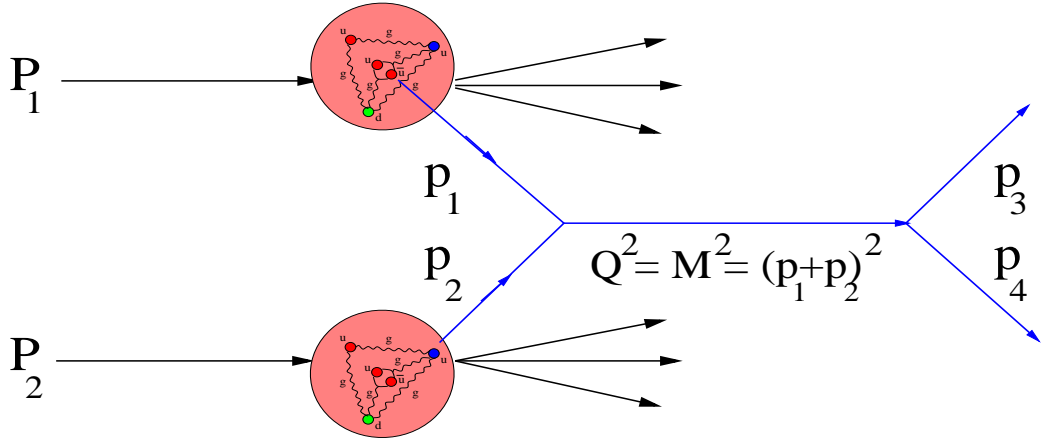


Figure 5.5: Scheme of the proton-proton collision at LHC. Two protons with 4-momenta  $P_1, P_2$  collide head-on. Among many partons inside the protons only two take part in the hard-scattering process (blue), one with 4-momentum  $p_1 = x_1 P_1$ , the other with  $p_2 = x_2 P_2$ . The invariant mass of the system of the two partons is  $M$ . As a result of the hard-scattering, two (or more) particles with 4-momenta  $p_3, p_4$  and invariant mass  $M$  leave the interaction point.

much smaller than  $\sqrt{s}$ , the two protons have 4-momenta

$$\begin{aligned} P_1^\mu &= \frac{\sqrt{s}}{2}(1, 0, 0, 1) \\ P_2^\mu &= \frac{\sqrt{s}}{2}(1, 0, 0, -1), \end{aligned} \quad (5.8)$$

the two partons have 4-momenta

$$\begin{aligned} p_1^\mu &= x_1 P_1^\mu \\ p_2^\mu &= x_2 P_2^\mu, \end{aligned} \quad (5.9)$$

and the invariant mass squared of the two partons is

$$M^2 = (p_1 + p_2)^2 = x_1 x_2 s. \quad (5.10)$$

Before we continue we define the rapidity of the system of two partons. Recall first the definition of rapidity relative to a beam axis, Eq. 4.1. The rapidity of the system of two partons can be defined as ( $E$  is now the sum of total energies  $E_1 + E_2$  of the two partons and likewise the  $p_z$ )

$$y = \frac{1}{2} \ln \frac{E + p_z}{E - p_z} = \frac{1}{2} \ln \frac{x_1}{x_2}. \quad (5.11)$$

For the fractions of the proton momenta carried by the partons we get

$$\begin{aligned} x_1 &= \frac{M}{\sqrt{s}} e^y \\ x_2 &= \frac{M}{\sqrt{s}} e^{-y} \end{aligned} \quad (5.12)$$

It is time to show the crucial dependence of the cross sections of LHC processes on the proton structure. In the regime of DIS the cross section for some process  $pp \rightarrow X$  (where  $X$  can be a single particle or a collection of particles with invariant mass  $M$ ) can be written as

$$\sigma_X = \sum_{a,b} \int_0^1 dx_1 \int_0^1 dx_2 f_a(x_1, Q^2) f_b(x_2, Q^2) \hat{\sigma}_{ab \rightarrow X} \quad (5.13)$$

where  $a, b$  identify parton flavors: for a given  $a$  PDF  $f_a(x_1, Q^2)$  represents one PDF from the set of all PDF's,  $\{u(x_1, Q^2), \bar{u}, d, \bar{d}, c, \bar{c}, \dots, g(x_1, Q^2)\}$ , and

the sum over  $a, b$  indicates that many different partons can take part in the production of  $X$  in the hard process  $ab \rightarrow X$ .  $\hat{\sigma}_{ab \rightarrow X} \equiv \hat{\sigma}_{ab \rightarrow X}(x_1, x_2)$  is a function of  $x_1, x_2$  and  $Q^2$  is identified as  $Q^2 \equiv M^2$ .

Perhaps an example will help to clarify things a bit: a single Higgs boson  $H$  is produced in the gluon-gluon fusion (other partons contribution is negligible hence we have only one term in the sum):

$$\sigma_H = \int_0^1 dx_1 \int_0^1 dx_2 g(x_1, Q^2) g(x_2, Q^2) \hat{\sigma}_{gg \rightarrow H}(x_1, x_2) \quad (5.14)$$

The hard-scattering process is illustrated by a Feynman diagram in Fig.6.13a. This is where the most interesting physics is hidden (the Higgs) and the calculation of  $\hat{\sigma}_{gg \rightarrow H}(x_1, x_2)$  is usually the most difficult part. If we could collide two gluons instead of two protons,  $\sigma_H$  would be equal to  $\hat{\sigma}_{gg \rightarrow H}$  ( $x_1 = x_2 = 1$ ). But since we collide protons, we have to take into account that gluons inside protons can have different momenta ( $0 < x_1, x_2 < 1$ ) with different probabilities and this is taken care of by weighting the  $\hat{\sigma}_{gg \rightarrow H}$  with gluon PDF's and integrating over  $x_1, x_2$ . In chapter 6 we will show more examples with more parton species contributing to the sum over  $a, b$ .

Generally, the LHC is sensitive to PDF's in a region in the  $x$ - $Q^2$  plane which is to a large degree different from the regions probed by Tevatron, HERA and fixed target experiments, see Fig. 5.6. The ATLAS sensitivity to  $u(x, Q^2)$  and  $d(x, Q^2)$  through the  $W$  boson production, studied in chapter 6, is defined by  $Q^2 = M_W^2$  and the  $W$  boson rapidity interval measured by ATLAS,  $-3 < y < 3$ .

### *Exercise*

Verify Eqs. 5.10 - 5.12

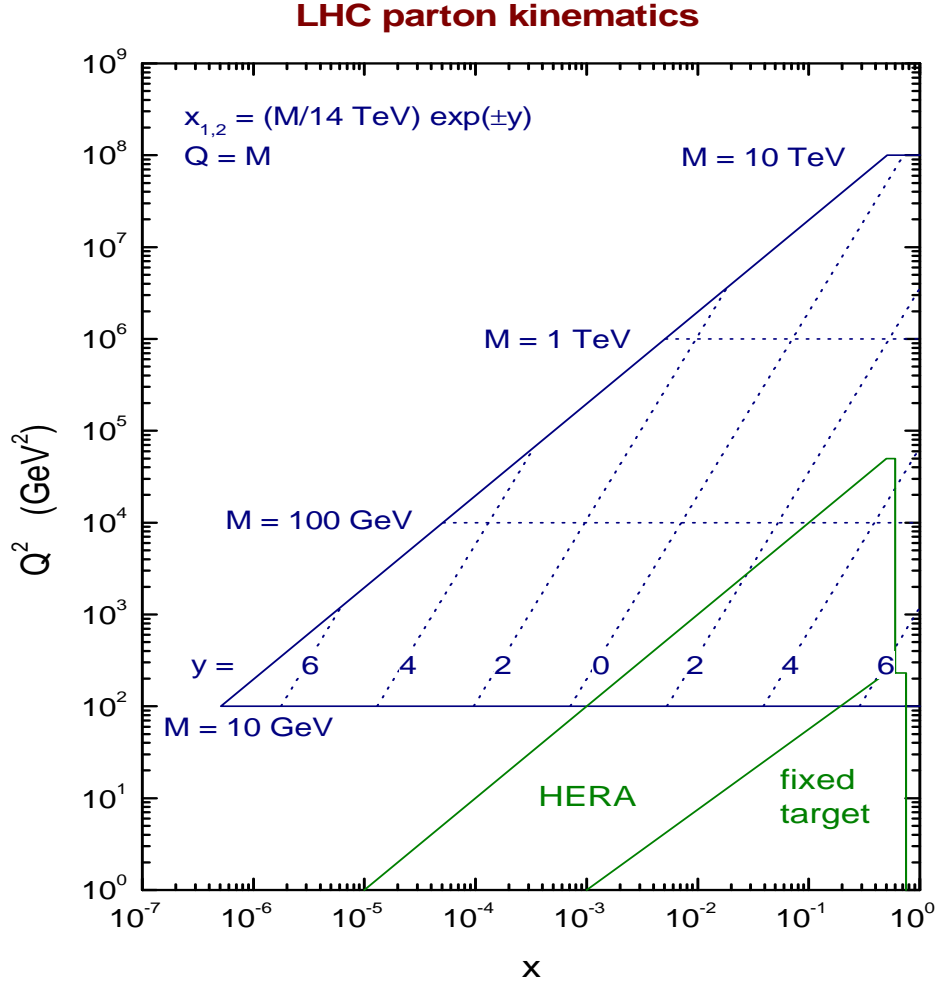


Figure 5.6: Regions of sensitivity to PDFs in the  $x$ - $Q^2$  plane for fixed target experiments (green), HERA (green) and LHC (blue). ATLAS sensitivity through  $W$  boson production is at  $M = M_W = 80.398 \text{ GeV}$  ( $Q^2 = M_W^2$ ). Reprinted with permission from MSTW collaboration, <http://mstwpdf.hepforge.org/>



# Chapter 6

## $W$ bosons at LHC

Study of  $W$  bosons is important for at least two reasons. First,  $W$  boson production probes the proton structure and can be used to improve proton structure functions needed in the predictions of new physics signals and corresponding backgrounds at LHC. Second,  $W$  boson searches represent an important step in the search for new particles, such as Higgs boson.

### 6.1 $W$ boson production cross sections

$W^+$  bosons are produced at LHC mainly by one of these 4 mechanisms

$$pp \rightarrow ug X \rightarrow W^+ d X \quad (6.1)$$

$$pp \rightarrow gg X \rightarrow W^+ d\bar{u} (s\bar{c}) X \quad (6.2)$$

$$pp \rightarrow u\bar{d} X \rightarrow W^+ X \quad (6.3)$$

$$pp \rightarrow u\bar{d} X \rightarrow W^+ g X \quad (6.4)$$

Several remarks are in order. The first part of these equations (take, e.g.,  $pp \rightarrow ug X$ ) tells us that we collide protons but only two partons, one in each proton, ( $u$  and  $g$  in this case) take part in the hard process. The rest of the two protons (these remnants are called underlying event) is denoted  $X$ . The remnants typically escape down the beampipe undetected. In CompHEP calculations one ignores the remnants assuming correctly that they do not have impact on DIS processes. The second part ( $ug X \rightarrow W^+ d X$ ) describes the hard process in which two initial partons collide and create  $W^+ d$  in the final state.

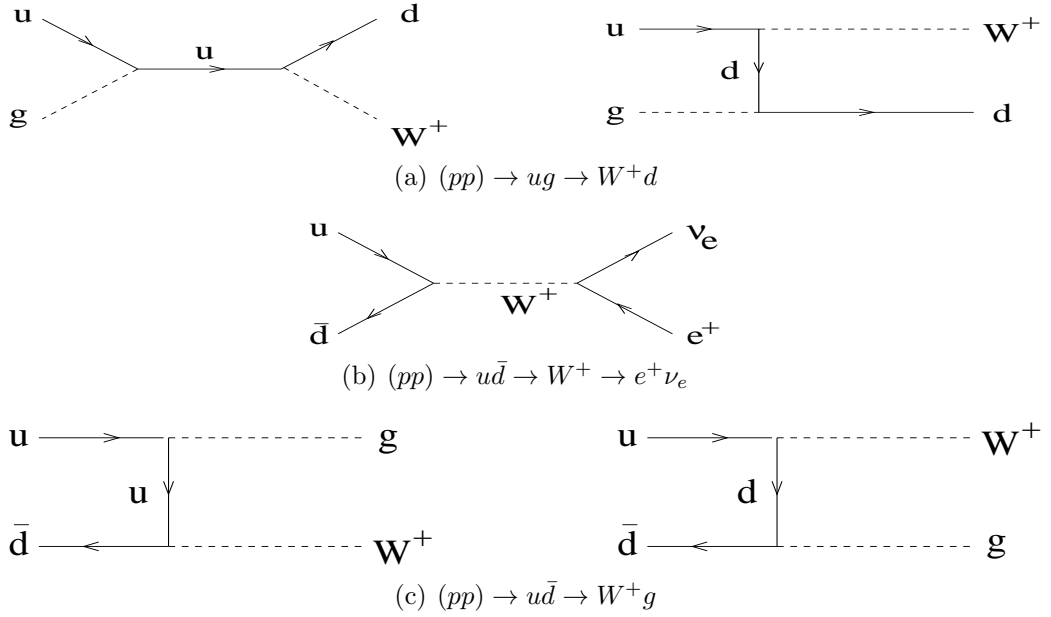


Figure 6.1: Feynman diagrams for  $W^+$  boson production mechanisms.  $W$  boson decay, to be discussed in Sec.6.3, is present in each mechanism but shown only for the case (b).

$W^+$  boson production can actually proceed through more than one pair of partons for a given mechanism. For example,  $W^+ d$  production (the first mechanism) can go not only via  $ug$  pair but also via  $cg$  pair;  $W^+ d\bar{u}$  production (the second mechanism) can go not only via  $gg$  but also via  $u\bar{u}, u\bar{c}, d\bar{d}$  and many other pairs. These different possibilities are called subprocesses. The list of available subprocesses can be easily found during the CompHEP calculation of the process. In Eqs. 6.1-6.4 we show only the dominant subprocesses - those which contribute typically around 90 % of the total cross section.

Feynman diagrams for the first, third and fourth mechanisms and the dominant subprocesses are shown in Fig. 6.1, the second (not shown) has 8 diagrams.

Similarly,  $W^-$  bosons are produced by one of these 4 mechanisms

$$pp \rightarrow dg X \rightarrow W^- u X \quad (6.5)$$

$$pp \rightarrow gg X \rightarrow W^- u \bar{d} (c \bar{s}) X \quad (6.6)$$

$$pp \rightarrow \bar{u} d X \rightarrow W^- X \quad (6.7)$$

$$pp \rightarrow \bar{u} d X \rightarrow W^- g X \quad (6.8)$$

The quark-gluon mechanism (Eqs. 6.1,6.5) and the quark-antiquark mechanism (Eqs. 6.3,6.4,6.7,6.8) produce more  $W^+$  than  $W^-$  bosons. The gluon-gluon mechanism (Eqs. 6.2,6.6) is symmetric, producing equal numbers of  $W^+$  and  $W^-$  bosons. We can see this when we specify the total production cross sections using Eq. 5.13. For  $W^+$  bosons we get for the four mechanisms, respectively,

$$\sigma_1^+ = \int_0^1 dx_1 \int_0^1 dx_2 u(x_1) g(x_2) \hat{\sigma}_{ug \rightarrow W^+ d}(x_1, x_2) + (1 \leftrightarrow 2), \quad (6.9)$$

$$\sigma_2^+ = \int_0^1 dx_1 \int_0^1 dx_2 g(x_1) g(x_2) \hat{\sigma}_{gg \rightarrow W^+ d \bar{u}}(x_1, x_2) + (1 \leftrightarrow 2), \quad (6.10)$$

$$\sigma_3^+ = \int_0^1 dx_1 \int_0^1 dx_2 u(x_1) \bar{d}(x_2) \hat{\sigma}_{u \bar{d} \rightarrow W^+}(x_1, x_2) + (1 \leftrightarrow 2), \quad (6.11)$$

$$\sigma_4^+ = \int_0^1 dx_1 \int_0^1 dx_2 u(x_1) \bar{d}(x_2) \hat{\sigma}_{u \bar{d} \rightarrow W^+ g}(x_1, x_2) + (1 \leftrightarrow 2) \quad (6.12)$$

Here  $1 \leftrightarrow 2$  denotes terms where partons, e.g.  $u$  and  $g$ , change their places:  $u(x_1) g(x_2)$  becomes  $u(x_2) g(x_1)$  ( $u$  is now from proton 2 and  $g$  is from proton 1). These terms are equal in size to the original unchanged terms and the net effect is that they double the cross section. Note that we dropped the  $Q^2$  dependence of the PDF's and the hard cross sections.

For  $W^-$  bosons we get for the four mechanisms, respectively,

$$\sigma_1^- = \int_0^1 dx_1 \int_0^1 dx_2 d(x_1) g(x_2) \hat{\sigma}_{dg \rightarrow W^- u}(x_1, x_2) + (1 \leftrightarrow 2), \quad (6.13)$$

$$\sigma_2^- = \int_0^1 dx_1 \int_0^1 dx_2 g(x_1) g(x_2) \hat{\sigma}_{gg \rightarrow W^- u \bar{d}}(x_1, x_2) + (1 \leftrightarrow 2), \quad (6.14)$$

$$\sigma_3^- = \int_0^1 dx_1 \int_0^1 dx_2 d(x_1) \bar{u}(x_2) \hat{\sigma}_{d \bar{u} \rightarrow W^-}(x_1, x_2) + (1 \leftrightarrow 2), \quad (6.15)$$

$$\sigma_4^- = \int_0^1 dx_1 \int_0^1 dx_2 d(x_1) \bar{u}(x_2) \hat{\sigma}_{d \bar{u} \rightarrow W^- g}(x_1, x_2) + (1 \leftrightarrow 2) \quad (6.16)$$

Since all hard cross sections  $\hat{\sigma}$  for  $W^+$  are equal to those for  $W^-$ , the only difference between  $\sigma_i^+$  and  $\sigma_i^-$  can come from PDF's. For  $\sigma_2^+, \sigma_2^-$  there is no difference, the same gluon PDF's appear in both cross sections with the consequence that the gluon-gluon mechanism contributes equal numbers of  $W^+$  and  $W^-$  bosons.

The situation is different for mechanisms 1 (quark-gluon) and 3,4 (quark-antiquark):  $\sigma_1^+$  depends on  $u(x_1, Q^2)g(x_2, Q^2)$ ,  $\sigma_1^-$  on  $d(x_1, Q^2)g(x_2, Q^2)$  and since  $u(x, Q^2) > d(x, Q^2)$  (there are more  $u$  quarks than  $d$  quarks in the proton), mechanism 1 produces more  $W^+$  than  $W^-$  bosons.  $\sigma_3^+$  and  $\sigma_4^+$  both depend on  $u(x_1, Q^2)\bar{d}(x_2, Q^2)$  and  $\sigma_3^-$  and  $\sigma_4^-$  both on  $d(x_1, Q^2)\bar{u}(x_2, Q^2)$ . Since we expect that  $\bar{u}(x, Q^2) \doteq \bar{d}(x, Q^2)$ <sup>1</sup> and this expectation is experimentally supported (Fig. 5.4), the only difference is again the difference between  $u(x, Q^2)$  and  $d(x, Q^2)$  and also mechanisms 3 and 4 produce preferentially  $W^+$  bosons.

## 6.2 Charge asymmetry

To quantify preferential production of  $W^+$  over  $W^-$  bosons we define charge asymmetry as<sup>2</sup>

$$R^\pm = \frac{N(W^+)}{N(W^-)} = \frac{L\sigma(W^+)}{L\sigma(W^-)} = \frac{\sigma(W^+)}{\sigma(W^-)} > 1 \quad (6.17)$$

where  $N(W^+), N(W^-)$  are the total numbers of  $W^+, W^-$  produced, respectively,  $L$  is the integrated luminosity and  $\sigma(W^\pm)$  are the total cross-sections for the production of  $W^\pm$  bosons given as

$$\sigma(W^\pm) = \sigma_1^\pm + \sigma_2^\pm + \sigma_3^\pm + \sigma_4^\pm \quad (6.18)$$

Since the charge asymmetry  $R^\pm$  is the consequence of the difference between  $u(x, Q^2)$  and  $d(x, Q^2)$ , these two PDF's can be studied through the measured charge asymmetry  $R^\pm$ .

We will now try to make an intelligent guess of the numerical value of  $R^\pm$ . First we will neglect the gluon-gluon contribution in Eq.6.18 which is

<sup>1</sup>Production mechanism is the same for the sea  $\bar{u}$  and  $\bar{d}$  quarks and both are almost massless.

<sup>2</sup>Another option would be  $R^\pm = \frac{N(W^+) - N(W^-)}{N(W^+) + N(W^-)}$  but we stick with the simpler definition in order to compare with the ATLAS result in Fig. 6.16.

the smallest one as we will see below (it contributes about 2-3% to  $\sigma(W^\pm)$ ). If we then substitute Eq. 6.18 and individual  $\sigma_i^\pm$  into Eq. 6.17 we get

$$R^\pm = \frac{\int_0^1 dx_1 \int_0^1 dx_2 [u g \hat{\sigma}(W^+d) + u \bar{d} \hat{\sigma}(W^+) + u \bar{d} \hat{\sigma}(W^+g)]}{\int_0^1 dx_1 \int_0^1 dx_2 [d g \hat{\sigma}(W^-u) + d \bar{u} \hat{\sigma}(W^-) + d \bar{u} \hat{\sigma}(W^-g)]} \quad (6.19)$$

where we dropped  $x_1, x_2, Q^2$  dependence in PDF's and introduced obvious short notation  $\hat{\sigma}_{ug \rightarrow W^+d}(x_1, x_2, Q^2) \equiv \hat{\sigma}(W^+d)$ , etc.

Hard process cross sections for  $W^+$  are equal to those for  $W^-$ :  $\hat{\sigma}(W^+d) = \hat{\sigma}(W^-u)$ ,  $\hat{\sigma}(W^+g) = \hat{\sigma}(W^-g)$  and  $\hat{\sigma}(W^+) = \hat{\sigma}(W^-)$ . Using this plus  $\bar{u}(x, Q^2) \doteq \bar{d}(x, Q^2)$  gives

$$R^\pm = \frac{\int_0^1 dx_1 \int_0^1 dx_2 u [g \hat{\sigma}(W^+d) + \bar{d} \hat{\sigma}(W^+) + \bar{d} \hat{\sigma}(W^+g)]}{\int_0^1 dx_1 \int_0^1 dx_2 d [g \hat{\sigma}(W^+d) + \bar{d} \hat{\sigma}(W^+) + \bar{d} \hat{\sigma}(W^+g)]} \quad (6.20)$$

This looks simple, the only difference between the numerator and the denominator is the difference between the  $u(x, Q^2)$  and  $d(x, Q^2)$ . One might assume that  $u(x, Q^2) = 2 d(x, Q^2)$  (after all, there are two  $u$  quarks and one  $d$  quark in the proton) which would immediately yield  $R^\pm = 2$ . However, things are not that simple. Our assumption is not experimentally supported. From Fig. 5.4 we can see that at low  $x$

$$u(x, Q^2) \doteq d(x, Q^2) \quad (6.21)$$

and at  $x \rightarrow 1$

$$u(x, Q^2) \doteq 4 d(x, Q^2) \quad (6.22)$$

It turns out that in order to predict  $R^\pm$ , we need to calculate hard cross sections and perform integration over  $x_1, x_2$ . We will do it below with Com-  
pHEP.

From the experimental point of view the procedure seems simple: it suffices to recognize events where  $W$  bosons were produced, count  $W^+, W^-$  separately and find the asymmetry as  $R^\pm = \frac{N(W^+)}{N(W^-)}$ . There is, however, one complication:  $W$  bosons decay and this decay changes the prediction of  $R^\pm$ .

## 6.3 W boson decay

$W$  bosons have a very short lifetime ( $\sim 10^{-25}$ s) which prevents them from being detected directly. Instead we detect their decay products. About 70%

of the time they decay hadronically ( $W \rightarrow q\bar{q}$ ) and about 30% of the time leptonically ( $W \rightarrow l\nu_l$ ) where the lepton can be  $e, \mu$  or  $\tau$ . We will consider only leptonic decays with  $e$  or  $\mu$  as signals because of their clean experimental signatures.  $\tau$  decays and hadronic decays will be treated as backgrounds.

The four  $W^+$  boson production mechanisms (Eqs. 6.1 - 6.4) with the  $W$  boson decay included look like

$$pp \rightarrow ug X \rightarrow W^+ d X \rightarrow l^+ \nu_l d X \quad (6.23)$$

$$pp \rightarrow gg X \rightarrow W^+ d\bar{u} X \rightarrow l^+ \nu_l d \bar{u} X \quad (6.24)$$

$$pp \rightarrow u\bar{d} X \rightarrow W^+ X \rightarrow l^+ \nu_l X \quad (6.25)$$

$$pp \rightarrow u\bar{d} X \rightarrow W^+ g X \rightarrow l^+ \nu_l g X \quad (6.26)$$

and the four  $W^-$  boson production mechanisms (Eqs. 6.1 - 6.4) are now

$$pp \rightarrow dg X \rightarrow W^- u X \rightarrow l^- \bar{\nu}_l u X \quad (6.27)$$

$$pp \rightarrow gg X \rightarrow W^- u\bar{d} X \rightarrow l^- \bar{\nu}_l u \bar{d} X \quad (6.28)$$

$$pp \rightarrow \bar{u}d X \rightarrow W^- X \rightarrow l^- \bar{\nu}_l X \quad (6.29)$$

$$pp \rightarrow \bar{u}d X \rightarrow W^- g X \rightarrow l^- \bar{\nu}_l g X \quad (6.30)$$

Inclusion of  $W$  decays means that we will have to modify the hard cross sections in our estimate of  $R^\pm$  in Eq. 6.20:

$$R^\pm = \frac{\int_0^1 dx_1 \int_0^1 dx_2 u [g \hat{\sigma}(l^+ \nu_l d) + \bar{d} \hat{\sigma}(l^+ \nu_l) + \bar{d} \hat{\sigma}(l^+ \nu_l g)]}{\int_0^1 dx_1 \int_0^1 dx_2 d [g \hat{\sigma}(l^+ \nu_l d) + \bar{d} \hat{\sigma}(l^+ \nu_l) + \bar{d} \hat{\sigma}(l^+ \nu_l g)]} \quad (6.31)$$

which include the decay of  $W$  bosons into either an  $e$  or  $\mu$  channel.  $\hat{\sigma}(l^+ \nu_l d)$  is a short for  $\hat{\sigma}_{ug \rightarrow l^+ \nu_l d}(x_1, x_2, Q^2)$  etc.

We are ready to calculate in CompHEP the total cross sections for the four  $W^\pm$  production mechanisms including the decays via electron and muon channels. In order to mimic the ATLAS acceptance we introduce the cut on the lepton rapidity:

$$-2.47 < y_l < 2.47 \quad (6.32)$$

Further, to suppress the backgrounds we impose the cuts on the lepton  $p_T(l)$  and the missing  $E_T^{miss}$

$$\begin{aligned} p_T(l) &> 25 \text{ GeV} \\ E_T^{miss} &> 25 \text{ GeV} \end{aligned} \quad (6.33)$$

and, if jets are present, it is also required that at least one has  $p_T(j)$  from the interval

$$15 \text{ GeV} < p_T(j) < 75 \text{ GeV} \quad (6.34)$$

Using these cuts and the *cteq6l1* structure functions<sup>3</sup> we get at  $\sqrt{s} = 7 \text{ TeV}$  following cross sections

$$\sigma_{W^+d} = 108.8 \text{ pb} \quad \sigma_{W^-u} = 59.0 \text{ pb} \quad (6.35)$$

$$\sigma_{W^+d\bar{u}} = 23.7 \text{ pb} \quad \sigma_{W^-u\bar{d}} = 23.7 \text{ pb} \quad (6.36)$$

$$\sigma_{W^+} = 1073.6 \text{ pb} \quad \sigma_{W^-} = 615.4 \text{ pb} \quad (6.37)$$

$$\sigma_{W^+g} = 91.2 \text{ pb} \quad \sigma_{W^-g} = 50.7 \text{ pb} \quad (6.38)$$

This shows that the gluon-gluon contribution (Eq.6.36) is indeed the smallest one. For the charge asymmetry we get

$$R^\pm = 1.76 \text{ (1.73)} \quad (6.39)$$

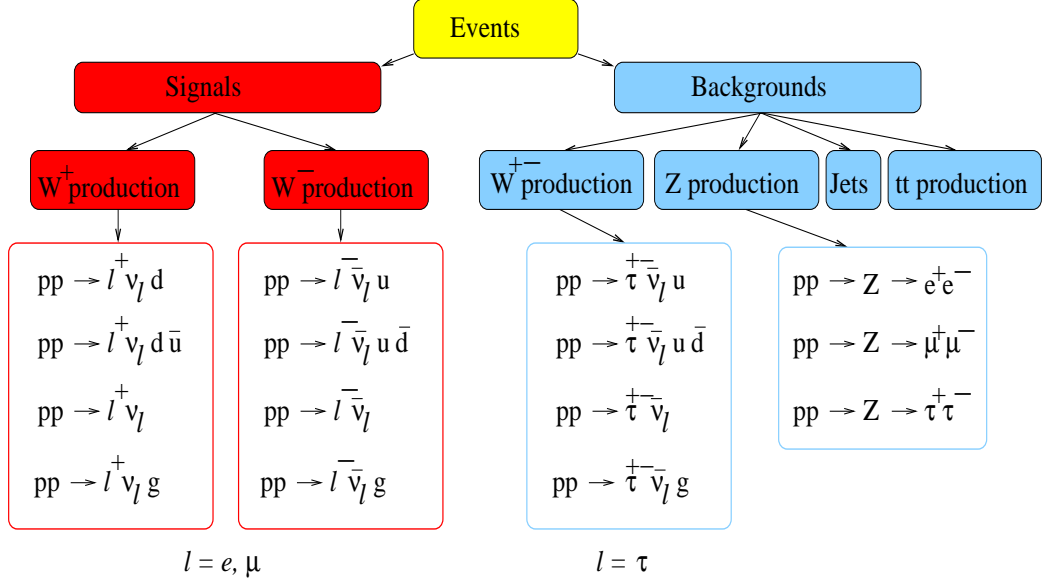
for the gluon-gluon contribution neglected (included), respectively.

This asymmetry is essentially generated by the difference between the PDF's  $u(x, Q^2)$  and  $d(x, Q^2)$  but this is not the only source. We can see that it depends also on the hard process cross sections (Eq. 6.31) and, as more subtle effect, it depends also on the applied cuts, in particular on the lepton rapidity cut. The reason for the latter is that  $W$  boson decays make the lepton rapidity distribution for  $l^+$  different from  $l^-$  and the same rapidity cut (Eq. 6.32) generates charge asymmetry of about 14% (if subtracted from Eq. 6.39, the result would change from 1.76 to  $R^\pm \sim 1.62$ ). Finally, as we will show in Exercise in Sec.6.7.1, the charge asymmetry also depends on the collision energy  $\sqrt{s}$ . The higher the energy, the smaller the asymmetry.

All this points to the many difficulties that experimental physicists face when they try to interpret their results. The cuts are needed in order to suppress the backgrounds but the cuts introduce unwanted asymmetry which has to be accounted for if we want to interpret the charge asymmetry as due to the difference between  $u(x, Q^2)$  and  $d(x, Q^2)$ .

---

<sup>3</sup>CompHEP offers a set of different structure functions which mildly differ from each other. They are available through Initial state option in the CompHEP window for numerical calculations, see Fig. 3.6a.

Figure 6.2:  $W$  boson signal and main background processes.

## 6.4 Signals vs Backgrounds

Signals are the processes we look for in the data, in our case  $W^\pm$  boson production followed by its leptonic decay either to electron or muon, represented by the four production mechanisms, Eqs. 6.23-6.30. The challenge of experimental particle physics is to find  $W^\pm$  bosons due to these mechanisms among the many background processes. The background processes can appear like events with  $W$  bosons but in fact they are really something else. Fig. 6.2 shows the list of signals along with the most "dangerous" backgrounds.

The typical single  $W$  boson signal event contains an isolated electron or muon which has a large  $p_T$ , Figs. 6.3-6.4, a large missing transverse energy  $E_T^{miss}$ , Fig. 6.5, and either no jets or one, two or more jets. The isolated lepton means that it is not close in space to any of the jets which can be present in the event. A lepton close to a jet is most likely a decay product of one of the hadrons inside the jet, i.e., it is not a direct decay product of the  $W$  boson. Large  $p_T$  (typically more than 20 GeV) is due to the large mass of the  $W$  boson,  $M_W = 80$  GeV. The large missing transverse energy,  $E_T^{miss} > 25$  GeV is typically required since the neutrino, the second decay product of the  $W$  leptonic decay, escapes the detector undetected, taking

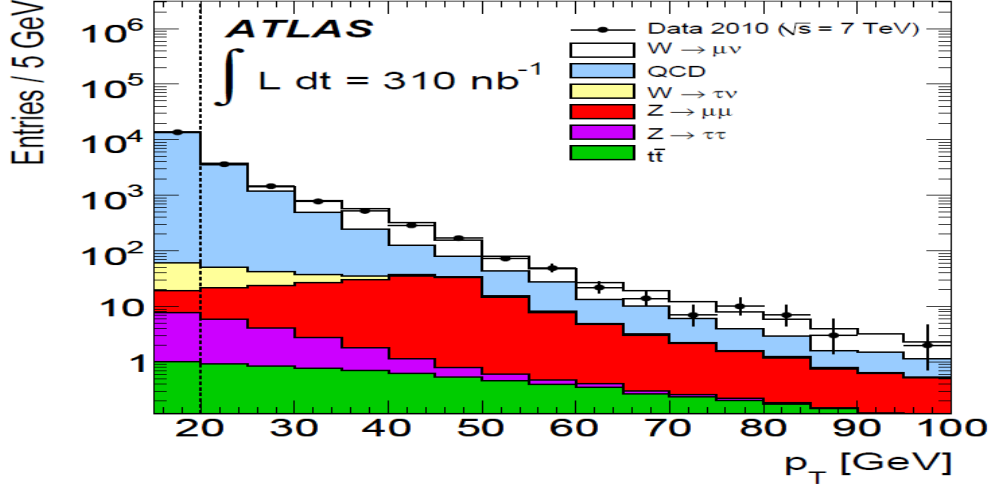


Figure 6.3: Distribution of the transverse momentum of muon. Signal is shown in white, background processes in colors. Both signal and background are Monte Carlo simulations. Also shown are experimental data (dots). Reprinted from the "Measurement of the  $W \rightarrow l\nu_l$  and  $Z/\gamma^* \rightarrow ll$  production cross sections in proton-proton collisions at  $\sqrt{s} = 7$  TeV with the ATLAS detector" [14].

a large amount of  $E_T$  with itself. Let us see now why the background events can, under certain conditions, look like the typical signal event. The  $Z$  boson production processes of Fig. 6.2 can be falsely interpreted as single  $W$  signal processes if  $Z$  decays leptonically and one of the two leptons escapes undetected or is misidentified as jet or part of the jet.

The top quark pair production,  $pp \rightarrow t\bar{t}X$ , can also mimic single  $W$  boson signal if, e.g., the top quarks decay in the following chain ( $W^-$  boson decays hadronically to two jets,  $jj$  and  $W^+$  leptonically):

$$t\bar{t} \rightarrow W^+ b W^- \bar{b} \rightarrow l^+ \nu_l b jj \bar{b} \quad (6.40)$$

This looks like a single  $W$  boson production with two light jets  $jj$ , and two  $b$  jets (signal events tend to have smaller number of jets but through the so-called parton showers even a single original jet can turn into four or more jets).

The "jets" background is the QCD background which is generally huge. On many occasions a lepton can appear inside a jet as a result of the lep-

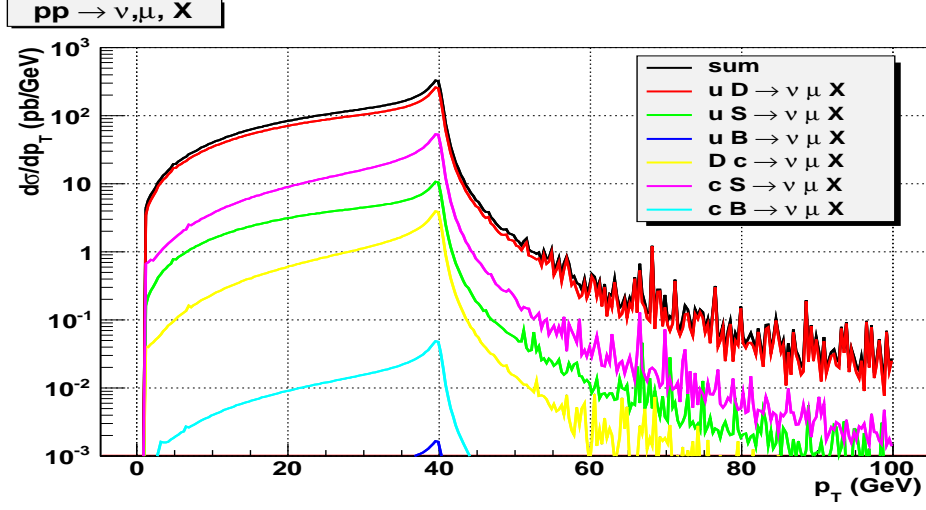


Figure 6.4: Distribution of the transverse momentum of muon for  $pp \rightarrow W^+ \rightarrow \mu^+ \nu_\mu$ , simulated with CompHEP. Besides the dominant parton contribution,  $u\bar{d}$  (red) all other parton contributions are shown.

tonic decay of one of the hadrons and rarely this lepton can be emitted at a relatively large angle with respect to the jet axis and thus appear as isolated. An isolated lepton with high  $p_T$  is exactly a typical feature of the  $W$  boson signal events.

Finally,  $W$  production tau channel is the genuine single  $W$  production where  $W$  decays into tau lepton,  $W \rightarrow \tau \nu_\tau$ . We consider it as background since the tau can further decay either to an electron or a muon inside the detector and pretend it comes from a direct decay  $W \rightarrow e, \nu_e$  or  $W \rightarrow \mu, \nu_\mu$ .

Typically only a small fraction of the background events look like the typical signal events. If, however, the background is much larger than the signal, even the small fraction can make a lot of problems. It is very important to get the backgrounds under control suggesting appropriate cuts. The cuts are applied to various kinematical variables of the event with the goal to remove as much background events from the data as possible and to keep as much signal events as possible.

To see which cuts are appropriate, we have to compare differential cross sections for the signal and the background. Let us start with the muon  $p_T$  distribution (for electron we get almost the same thing) see Fig. 6.3.

Backgrounds with one exception all peak in the region of small  $p_T$  below

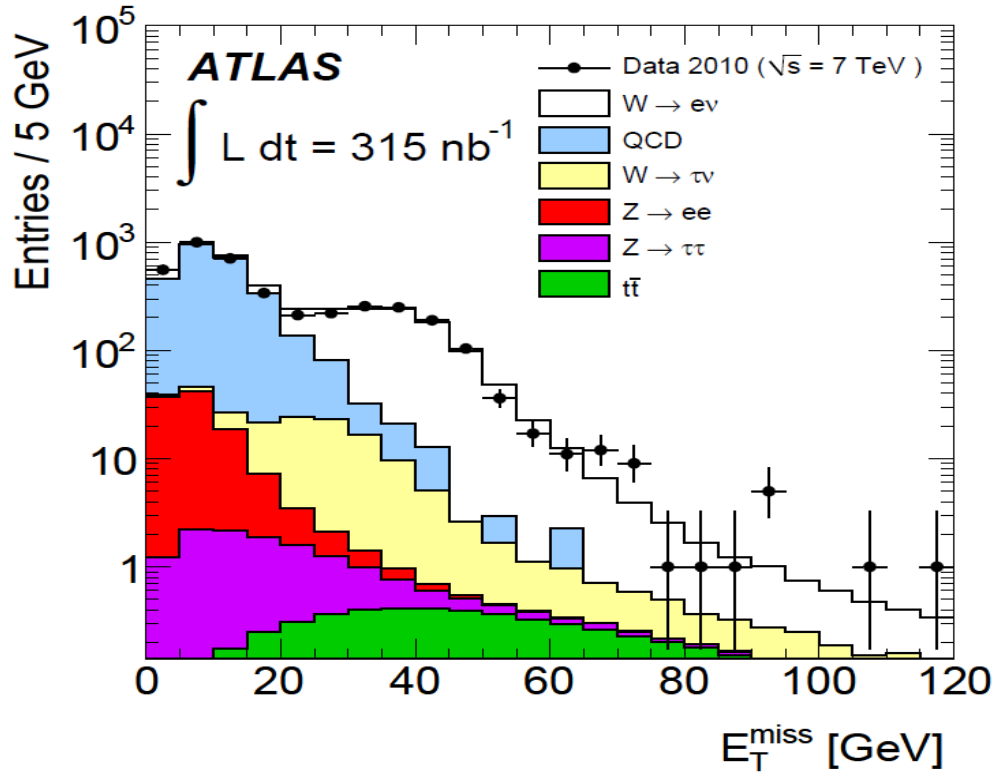


Figure 6.5: Distribution of the missing transverse energy,  $E_T^{\text{miss}}$ , for events with  $W \rightarrow e\nu_e$  candidate. The cut  $p_T(e) > 20 \text{ GeV}$  was already applied. Signal is shown in white, background processes in colors. Also shown are experimental data (dots). Reprinted from the "Measurement of the  $W \rightarrow l\nu_l$  and  $Z/\gamma^* \rightarrow ll$  production cross sections in proton-proton collisions at  $\sqrt{s} = 7 \text{ TeV}$  with the ATLAS detector" [14].

20 GeV. The signal shown in white is hidden behind the backgrounds in this region. In order to see it we simulate the signal muon  $p_T$  distribution with CompHEP for the dominant production mechanism,  $pp \rightarrow W^+ \rightarrow \mu^+ \nu_\mu$ . With the minimum cut  $-2.47 < y_\mu < 2.47$  and  $p_T(\mu) > 1$  GeV we get for  $\sqrt{s} = 7$  TeV and cteq6l1 PDF's Fig. 6.4.

The signal peaks in the region 25–40 GeV and hence we propose  $p_T(\mu) > 25$  GeV cut for the experimental analysis.

Fig. 6.4 shows another important thing - individual parton contributions to the total process. So far we have considered only the contribution from  $u\bar{d}$  (red). We can see that this is indeed the dominant contribution, however,  $c\bar{s}$  (magenta) is not completely negligible and has to be included in the serious studies.

The distribution of the missing transverse energy is shown in Fig. 6.5. The cut on the electron transverse momentum,  $p_T(e) > 20$  GeV, was already applied. It is evident that most backgrounds peak below  $E_T^{miss} = 25$  GeV while the signal has significant amount of events above this value. We propose  $E_T^{miss} > 25$  GeV cut.

## 6.5 *W* boson events in Minerva

MINERVA is a software tool developed for students so they could learn more about the ATLAS experiment and particle physics at CERN. It is a simplified version of Atlantis, the event display used by ATLAS physicists to visualise what happens in the detector. It can be downloaded from its home page [15] or from the International Masterclasses ATLAS exercise page (follow the *W* path-Measurement link) [16]. ATLAS data can be downloaded from the Slovak Masterclasses page (follow link *Fyzika*) [17]. Events are packed in the zipped files, 50 events each, labeled by letters A-Z.

Start Minerva and two windows will open up: Atlantis Canvas and Atlantis GUI. Load your 50 events through File-Read Event Locally functions in the Atlantis GUI Window. You can browse events by clicking the Next and Previous functions (or equivalently the back and forth arrows). The Atlantis Canvas window has three subwindows which offer an end view (Fig. 6.6(a)) and a side view (Fig. 6.6(b)) of the collision event in the detector, and the spatial distribution of energy absorbed by the calorimeters (Fig. 6.7). The Atlantis GUI window has control functions at the top (Fig. 6.8) and a window at the bottom (Fig. 6.9) where further numerical information about

the event is displayed.

In the end and side views of the event (Fig. 6.6) we can see the tracker (black & grey), the electromagnetic calorimeter (green), the hadronic calorimeter (red) and muon detectors (blue). The tracks of charged particles are drawn in cyan, purple, orange and red colours in the order of increasing momentum. Energy absorbed by the calorimeters is shown as yellow spots and the missing transverse momentum,  $\vec{p}_T^{miss}$ , as dashed red line where the thickness of the line indicates the amount missing. The muon chambers with registered hits are coloured orange. Note that most of the hits do not correspond to muons from the hard proton proton collision (there is no corresponding track in the tracker).

Fig. 6.7 shows a rolled-out calorimeter with the details of the spatial distribution of energy (yellow towers). Variables  $\Phi$  (azimuth) and  $\eta$  (rapidity) are used to describe the position where a particle lost its energy. In the upper right corner we can find a very important information about the missing transverse energy,  $E_T^{miss}$ .

Atlantis GUI window features further important functions which include event Zoom/Move/Rotate functions accessible through the magnifier icon, detailed information for a picked item, e.g. a track in the Tracker (index finger icon) and nonlinear zoom (fish-eye icon). A very useful feature in the event analysis is the 'Cuts' button through which we can set cuts on various variables, in particular the  $p_T$  cut.  $p_T > 20$  GeV means that only tracks with the transverse momentum larger than this value will be displayed.

To pick a track, we first click on the index finger icon, then click on a track in the Tracker and the information about the track displays at the bottom part of the Atlantis GUI window (Fig. 6.9). The sign of  $PT$  variable indicates the electric charge of a particle:  $PT = -26$  GeV means the negative charge with the transverse momentum of 26 GeV.

### 6.5.1 Tips for event analysis

1. Load a sample of events, start with the first one.
2. Check  $E_T^{miss}$  value in the rolled-out calorimeter window (Fig. 6.7). If larger than 25 GeV, a neutrino was likely present.
3. Study event in both end and side views, look especially for energetic ( $p_T > 25$  GeV) isolated leptons.
4. Zoom in to see the primary collision vertex in detail. Is there just one collision or perhaps two, three or more (so-called pile-up)? Note that at

large zoom even the tracks from a single vertex will appear as not to come from a single point - they will be spread along the beam axis (z coordinate). However, if the z coordinates of the tracks all fit within 1 cm interval, we will treat them as coming from a single vertex.

5. You can cut off low momentum particles with a suitable  $p_T$  cut.
6. If, after the  $p_T$  cut, you are left with a high  $p_T$  isolated lepton (or more which all originate in the same vertex), you should decide if it is a muon, antimuon, electron or positron.
7. Pick the lepton track in the 'index finger regime' and find the electric charge and check the  $p_T$  momentum value.
8. The rest depends on the task you solve - you may look for  $W$  bosons,  $Z$  bosons, Higgs bosons and other particles.

### 6.5.2 Typical $W \rightarrow e^- \bar{\nu}_e$ event

A typical  $W \rightarrow e^- \bar{\nu}_e$  event is in Figs. 6.6 -6.9. The first thing to note is  $E_T^{miss} = 49$  GeV in Fig.6.7. This is more than the required 25 GeV and we conclude that neutrino is likely present in this event.

Note now the orange track at 7 o'clock in the end view. It points to a lot of energy deposited in the electromagnetic calorimeter (yellow spot). Check the track also in the side view. The track appears isolated, the orange color indicates a high  $p_T$  particle. The isolation of the track is confirmed in the distribution of energy losses in the calorimeters - the track points to the tall yellow tower which is isolated in the  $\eta - \Phi$  plane (no other towers near by). Let's extend the orange track through the outer detectors. Since no significant signals are present on the extension's path in the hadronic calorimeter and muon detectors (well, two muon chambers in the end view shine orange but not the third one and, more importantly, there is no sign of anything in the muon chambers in the side view), this event is an electron/positron candidate.

Click on the index finger icon, then click on the orange track and a detailed information about the track is displayed in the bottom part of the GUI window, Fig. 6.9. We can see that  $p_T = -31.314$  GeV, more than the required 25 GeV for the signal. The minus sign indicates that we deal with an electron candidate.

Note also the angle between the orange track and the red dashed line (missing  $p_T$  line) in the end view. It is close to 180 degrees which is very typical for  $W$  boson events but beware that there are a few  $W$  events where

this angle can be very different from this value.

### 6.5.3 Typical $W \rightarrow \mu^+\nu_\mu$ event

A typical  $W \rightarrow \mu^+\nu_\mu$  event is in Figs. 6.10 -6.12. The first thing to note is  $E_T^{miss} = 37$  GeV in Fig.6.11. This is more than the required 25 GeV and we conclude that neutrino is likely present in this event.

Note now the orange track at 10 o'clock in the end view. First, it is isolated. Second, if we extend its path there is no energy deposited in the electromagnetic calorimeter and little in the hadron calorimeter. Third, all muon chambers on its path indicate hits (check also side view). These signatures indicate a muon/antimuon candidate and the orange color tells us this is a high  $p_T$  particle. There is no specifically tall yellow tower in the distribution of energy losses in the calorimeters which is OK for muons (unlike electrons).

Click on the index finger icon, then click on the orange track and a detailed information about the track is displayed in the bottom part of the GUI window, Fig. 6.12. We can see that  $p_T = 38.163$  GeV, more than the required 25 GeV for the signal. The plus sign indicates that we deal with an antimuon candidate.

Note again the angle between the orange track and the red dashed line (missing  $p_T$  line) in the end view. It is close to 180 degrees which is very typical for  $W$  boson events but beware that there are a few  $W$  events where this angle can be very different from this value.

## 6.6 Higgs boson in $H \rightarrow W^+W^-$ channel

### 6.6.1 Higgs production and decay

The Standard model Higgs boson is at LHC produced via gluon fusion (Fig. 6.13a), vector boson fusion (Fig. 6.13b), associated production with  $W$  or  $Z$  bosons (Fig. 6.13c) or associated production with top quark pair (Fig. 6.13d). The most important mechanism is the gluon fusion, followed by the vector boson fusion which is about 10 times weaker than the gluon fusion in the region of small Higgs masses. The Higgs boson decays quickly by many channels. The probability of Higgs to decay via a particular channel (so-called branching ratio) depends strongly on the Higgs mass  $M_H$ , Fig. 6.14.

For small Higgs masses the decay to  $b$  quark pair dominates, for large masses the decays to  $W^+W^-$  pair and  $ZZ$  pair take over. Also shown is a very important decay channel to a pair of photons.

### 6.6.2 Discovery of a new particle consistent with the Higgs

It was announced by CERN on July 4, 2012 that a new particle consistent with the Standard model Higgs at  $M_H = 125$  GeV had been found by both ATLAS and CMS. The most important information comes from the Higgs decay to photon pairs ( $H \rightarrow \gamma\gamma$ ) and  $ZZ$  pairs and the next important channel is the  $W^+W^-$  decay channel<sup>4</sup>. Note that this is not what one would guess from Fig.6.14 for  $M_H = 125$  GeV. It is important to realize that the dominant decay channel is not necessarily the most sensitive one. The  $ZZ$  and  $W^+W^-$  pairs decay further hadronically or leptonically and among many possibilities the most sensitive subchannels are  $H \rightarrow ZZ \rightarrow l^+l^-l'^+l'^-$  and  $H \rightarrow W^+W^- \rightarrow l^+\nu l'^-\nu$  where  $l, l'$  stand either for  $e$  or  $\mu$ .

In Fig. 6.15 we show invariant mass or transverse mass distributions for these channels found by the ATLAS collaboration [19]. For  $H \rightarrow \gamma\gamma$  channel one can see in Fig. 6.15a at least two data points around 126 GeV, each representing about one hundred of events above the expected background. In Fig. 6.15b there are six and seven  $H \rightarrow ZZ$  events found in two bins at about 125 GeV while about three events are expected from the background in each bin. These two figures support each other since both have excesses of events and both point to the same mass (within the experimental uncertainty) around 126 GeV.

The  $H \rightarrow W^+W^- \rightarrow l^+\nu l'^-\nu$  channel, which we will search for in the data, adds further support with an excess of some events in the broad transverse mass interval between 100 and 140 GeV. The global significance of all three channels combined is estimated to be  $5.1 \sigma$  (5.0 is required for discovery).

---

<sup>4</sup>We note that for  $M_H = 125$  GeV we have  $2M_W > M_H$  and  $2M_Z > M_H$ , hence at least one of the  $Z$  bosons in the  $H \rightarrow ZZ$  channel and one of the  $W$  bosons in the  $H \rightarrow W^+W^-$  channel has to be virtual.

## 6.7 Exercises and measurements

### 6.7.1 Charge asymmetry dependence on the collision energy

This is a CompHEP exercise. You will explore how the structure of the proton changes with the collision energy  $\sqrt{s}$ . Assume that only the quark-gluon mechanism contributes to the charge asymmetry  $R^\pm$  and ignore the  $W$  boson decay effects. This will not change the main point. To calculate quark-gluon mechanism cross sections of Eqs. 6.1, 6.5, introduce minimal cuts on the transverse momentum of the final state particles, e.g.,

$$p_T(W^+), p_T(d) > 0.1 \text{ GeV} \quad (6.41)$$

$$p_T(W^-), p_T(u) > 0.1 \text{ GeV} \quad (6.42)$$

The cuts remove the divergence in the t-channel diagram, leading to stable numerical result for the cross sections. Calculate the total cross sections and the charge asymmetry for  $\sqrt{s} = 2 \text{ TeV}$  and  $\sqrt{s} = 7 \text{ TeV}$  using cteq6l1 PDF's.

#### Answer

At  $\sqrt{s} = 2 \text{ TeV}$  you should get

$$\sigma_{pp \rightarrow W^+d} = 2.650 \times 10^3 \text{ pb} \quad (6.43)$$

$$\sigma_{pp \rightarrow W^-u} = 1.325 \times 10^3 \text{ pb} \quad (6.44)$$

$$R^\pm = 2.00 \quad (6.45)$$

At  $\sqrt{s} = 7 \text{ TeV}$  you should get

$$\sigma_{pp \rightarrow W^+d} = 1.889 \times 10^4 \text{ pb} \quad (6.46)$$

$$\sigma_{pp \rightarrow W^-u} = 1.092 \times 10^4 \text{ pb} \quad (6.47)$$

$$R^\pm = 1.73 \quad (6.48)$$

We observe that  $R^\pm$  decreases with  $\sqrt{s}$ .

#### Explanation

Why is this so? The invariant mass of the two partons has to be larger than  $M_W$  (otherwise  $W$  boson would not be produced):

$$M = \sqrt{(p_1 + p_2)^2} = \sqrt{x_1 x_2} \sqrt{s} \geq M_W \quad (6.49)$$

Further, the differential cross section in the invariant mass  $M$  peaks just above  $M_W$ , falling quickly with  $M$ . The consequence is that the total cross section and the charge asymmetry are sensitive only to invariant masses in the narrow region of  $W$  boson mass

$$M \sim M_W \quad (6.50)$$

For  $\sqrt{s} = 7$  TeV we thus have

$$\sqrt{x_1 x_2} \sim \frac{M_W}{\sqrt{s}} = 0.0114 \quad (6.51)$$

and for  $\sqrt{s} = 2$  TeV

$$\sqrt{x_1 x_2} \sim \frac{M_W}{\sqrt{s}} = 0.040. \quad (6.52)$$

We can see that lower  $\sqrt{s}$  require higher  $x$  values and vice versa. We remind (see Eq. 6.21 or Fig. 5.4) that at low  $x$  the PDF  $u(x, Q^2)$  becomes equal to  $d(x, Q^2)$ , driving  $R^\pm$  closer to 1 for very high  $\sqrt{s}$ . On the other hand at  $x \rightarrow 1$  (see Eq. 6.22 or Fig. 5.4)  $u(x, Q^2) \doteq 4 d(x, Q^2)$  which leads to  $R^\pm \rightarrow 4$  at  $\sqrt{s} \rightarrow M_W$ . The conclusion is that at high  $\sqrt{s}$  the sea quarks and antiquarks become increasingly more important constituents of the proton, changing the ratio of  $u(x, Q^2)/d(x, Q^2)$  and driving  $R^\pm$  below 2.

### 6.7.2 Search for $W$ bosons in the ATLAS data

This is the original International Masterclasses measurement described in [16]. You will search for signatures of  $W$  bosons in the ATLAS data and find the charge asymmetry  $R^\pm$ . You can download the data from the Slovak Masterclasses page (follow the 'Fyzika' link) [17]. Each package of 50 events is labeled by a letter. You should analyze at least 50 events, working either on your own or, preferably, in a pair with your fellow student.

Start Minerva and load you 50 events through File - Read Event Locally functions in the Atlantis GUI Window. The .zip file with events will be read by Minerva as is (do not try to unzip it). Browse events with the Previous and Next functions in the GUI Window.

Look for  $W^+ \rightarrow l^+ \nu_l$  and  $W^- \rightarrow l^- \bar{\nu}_l$  candidate events which should meet the following criteria:

1. A single isolated lepton, electron/positron or muon/antimuon.
2.  $p_T(l) > 25$  GeV for each lepton
3.  $E_T^{miss} > 25$  GeV

If the event meets ALL three criteria, check the charge of the lepton to distinguish  $W^+$  candidate from the  $W^-$  candidate and write down the event number so that you could return to it later. If the event does not meet the criteria (even if it is just one of the three) we conclude that it is likely a background event (see Sec. 6.4). The level of backgrounds was reduced significantly by the pre-selection cuts applied to ATLAS data.

After you have analyzed at least 50 events, count the number of  $W^+$  and  $W^-$  candidates separately and find the charge asymmetry  $R^\pm$  from Eq. 6.17. You do not have to subtract the gluon gluon production mechanism since it contributes just 2% to the total numbers of  $W^\pm$  bosons.

Compare your results with the official ATLAS results [20], Fig.6.16.

### 6.7.3 Search for the Higgs in $W^+W^-$ channel.

This is also the original International Masterclasses measurement [16]. Your task is to find simulated  $H \rightarrow W^+W^- \rightarrow l^+\nu l'^-\nu$  candidate events which were mixed in with the real data. Use the same data sample as in the search for  $W$  bosons measurement. Selection criteria will be slightly different from those for  $W$  bosons. We will discuss them now.

Depending on the decay modes of the  $W^+W^-$  pair we may end up with the following particles in the final state:

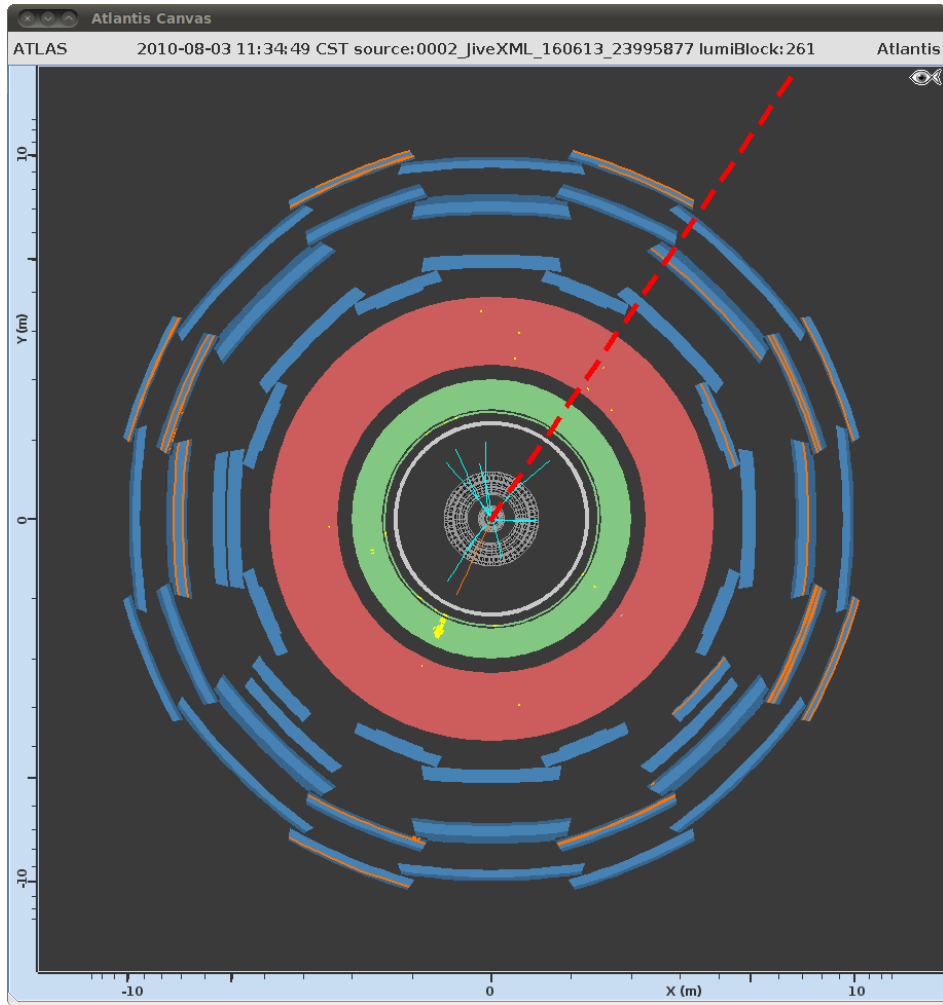
- a)  $e^+e^-\nu\nu$
  - b)  $e^+\mu^-\nu\nu$
  - c)  $\mu^+e^-\nu\nu$
  - d)  $\mu^+\mu^-\nu\nu$
- (6.53)

Based on this and on the study of the lepton  $p_T$  distributions and event  $E_T^{miss}$  distributions of signal and backgrounds we come to the following criteria which have to be passed by the  $H \rightarrow W^+W^- \rightarrow l^+\nu l'^-\nu$  candidate events [16]:

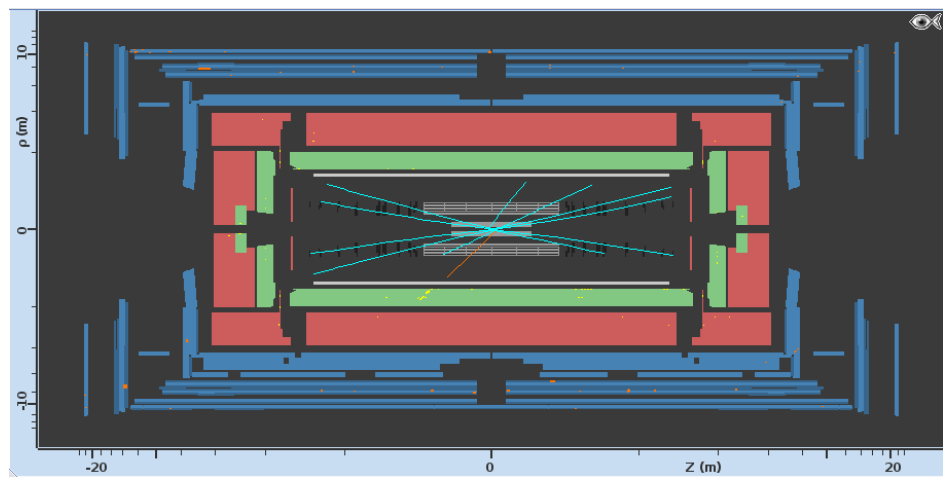
- 1) Events must contain exactly two leptons with opposite electric charge
- 2) The two leptons must be isolated (away from jets)
- 3) Watch for pile-up: the two leptons must originate from the same vertex (the same collision)
- 4) the leading lepton (the one with higher  $p_T$ ) should have  $p_T > 25$  GeV while the sub-leading lepton (the one with lower  $p_T$ ) should have  $p_T > 15$  GeV
- 5)  $E_T^{miss} > 40$  GeV if both leptons are coming from the same family (cases (a) and (d) in Eq. 6.53) and  $E_T^{miss} > 25$  GeV if not (cases (b) and (c) in Eq. 6.53).

Criterion (5) is based on the presence of two neutrinos in the event. The neutrinos, as discussed before, escape undetected, which results in typically large  $E_T^{miss}$ . Backgrounds have typically smaller  $E_T^{miss}$ . For leptons not coming from the same family the backgrounds are smaller than for the leptons from the same family, leading us to the smaller  $E_T^{miss}$  cut of 25 GeV in the former case.

Events which pass all five criteria are your  $H \rightarrow W^+W^- \rightarrow l^+\nu\ l'^-\nu$  candidates.



(a) End view



(b) Side view

Figure 6.6: View of a  $W \rightarrow e^- \bar{\nu}_e$  event in Minerva

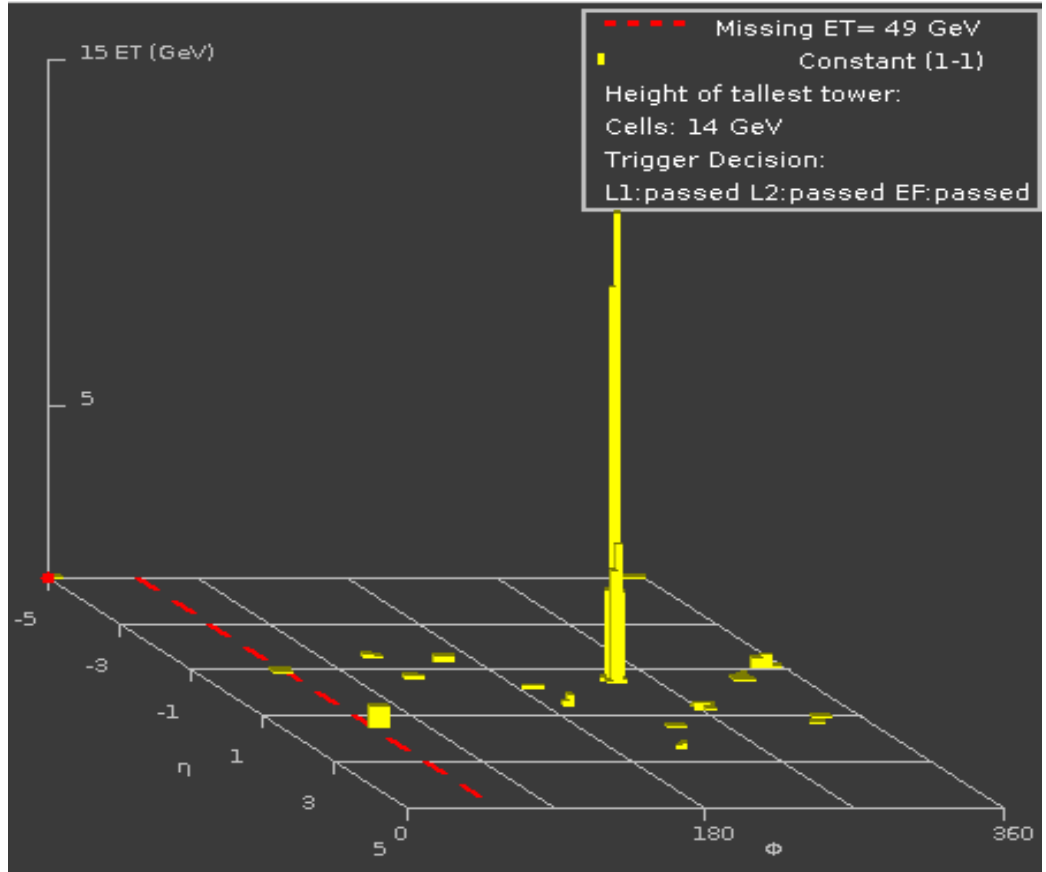


Figure 6.7: Distribution of energy losses in the calorimeters for the same  $W \rightarrow e^- \bar{\nu}_e$  event in Minerva.

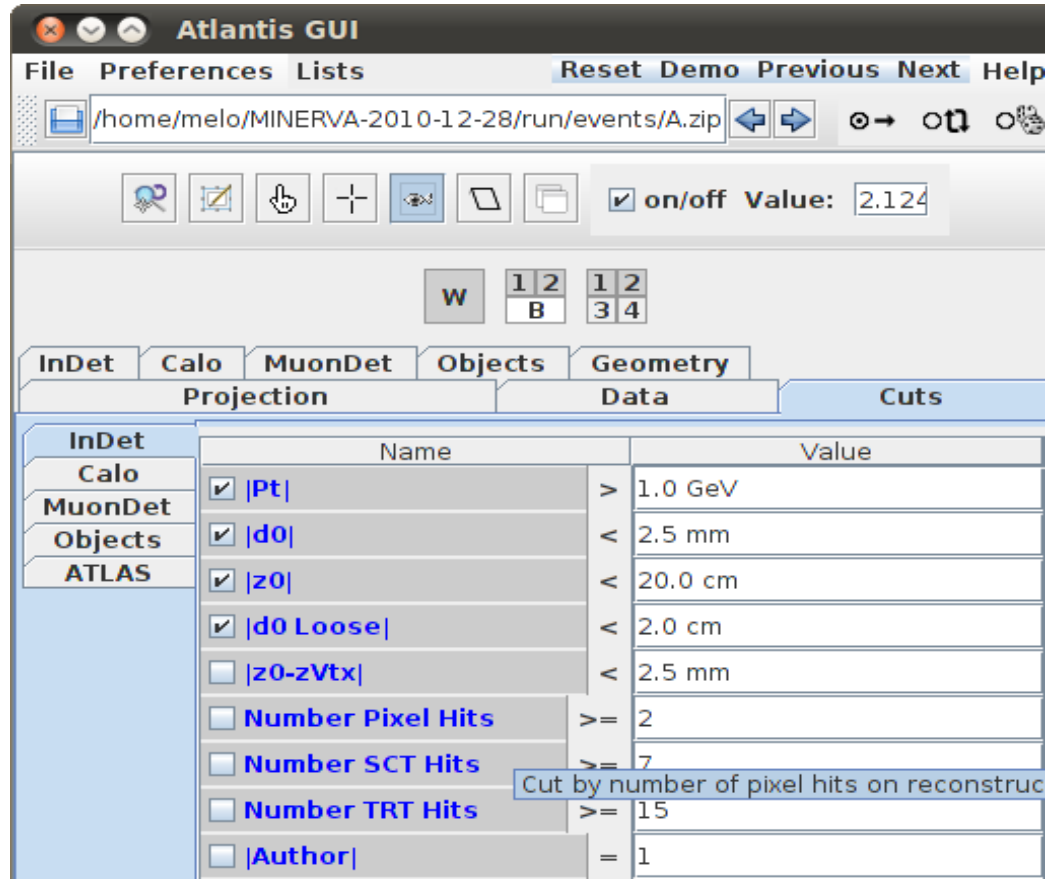


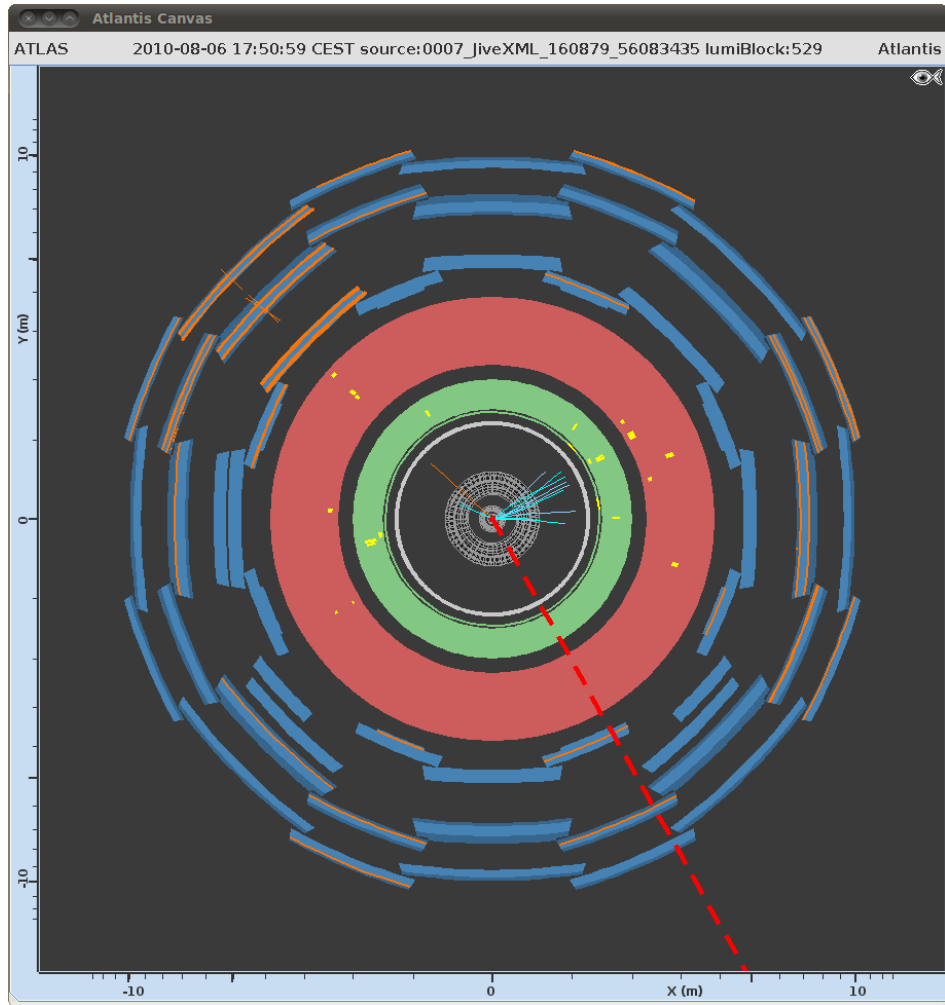
Figure 6.8: The top part of Atlantis GUI window with control functions.

```

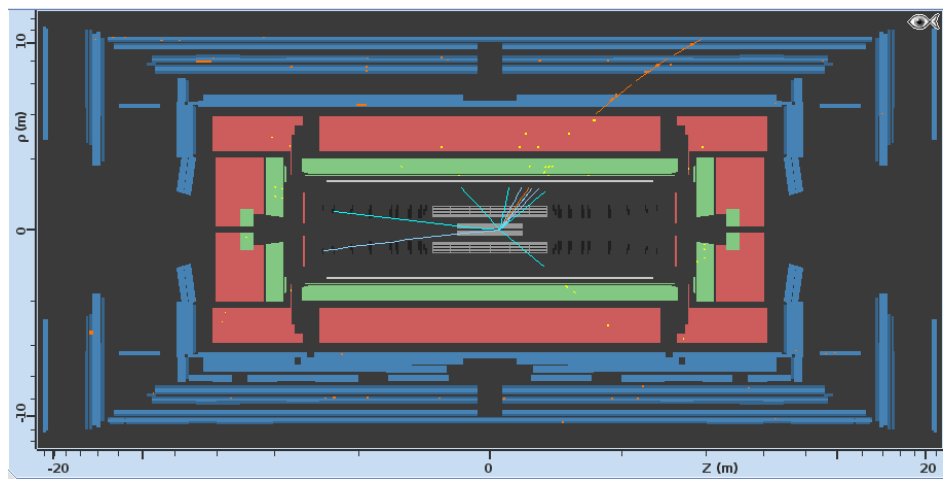
InDetTrack index: 4
PT=-31.314 GeV
η = -0.465
Φ = 244.630°
Px=-13.417 GeV
Py=-28.294 GeV
Pz=-15.097 GeV
numPixelHits = 3
numSCTHits = 8
numTRTHits = 36

```

Figure 6.9: A detailed track info from the bottom part of the GUI window for the same  $W \rightarrow e^- \bar{\nu}_e$  event in Minerva.



(a) End view



(b) Side view

Figure 6.10: View of a  $W \rightarrow \mu^+ \nu_\mu$  event in Minerva

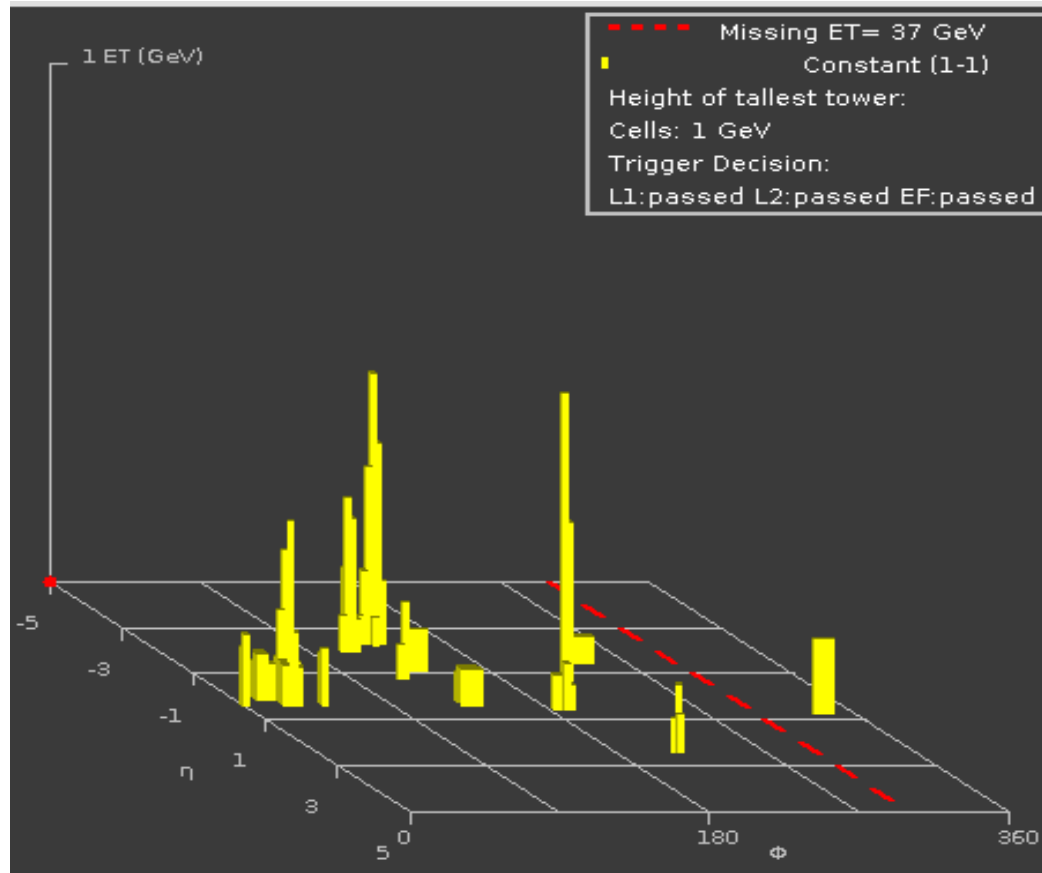


Figure 6.11: Distribution of energy losses in the calorimeters. The same  $W \rightarrow \mu^+ \nu_\mu$  event in Minerva

```

InDetTrack index: 0
PT=38.163 GeV
η = 0.341
Φ = 138.306°
Px=-28.497 GeV
Py=25.384 GeV
Pz=13.284 GeV
numPixelHits = 4
numSCTHits = 8
numTRTHits = 30

```

Figure 6.12: A detailed track info on the orange track taken from the bottom GUI window. The same  $W \rightarrow \mu^+ \nu_\mu$  event in Minerva

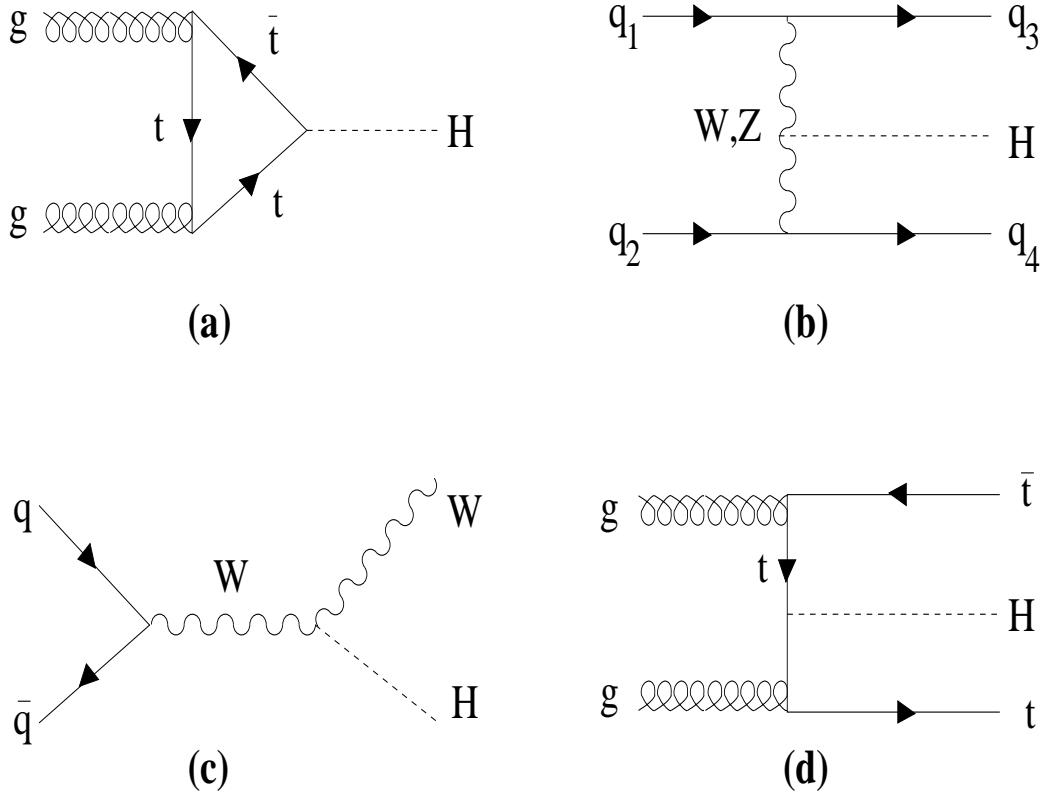


Figure 6.13: Dominant mechanisms of Higgs production at LHC: a) gluon fusion, b) vector boson fusion, c) associative production with  $W$  boson and d) associative production with top quark pair.

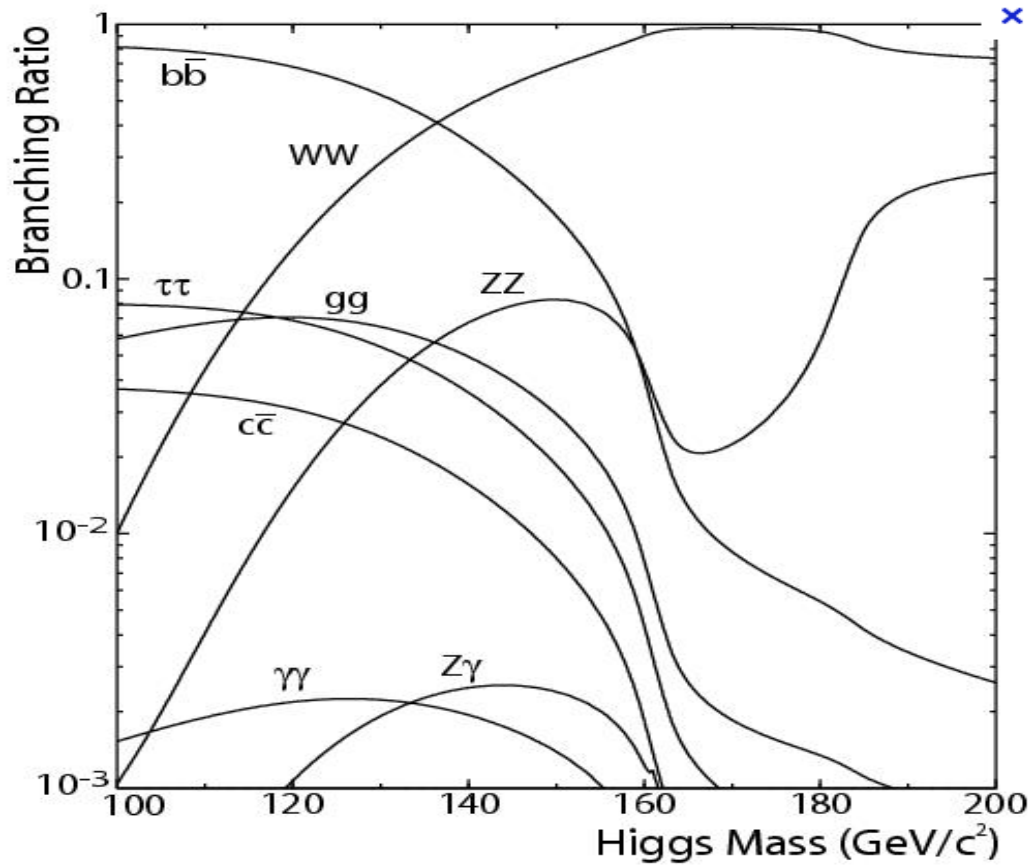


Figure 6.14: Probability that Higgs will decay through a particular channel. At small masses the decay to  $b\bar{b}$  pair dominates, at high masses decays to  $W^+W^-$  and  $ZZ$  pairs take over. The plot was originally published here [18].

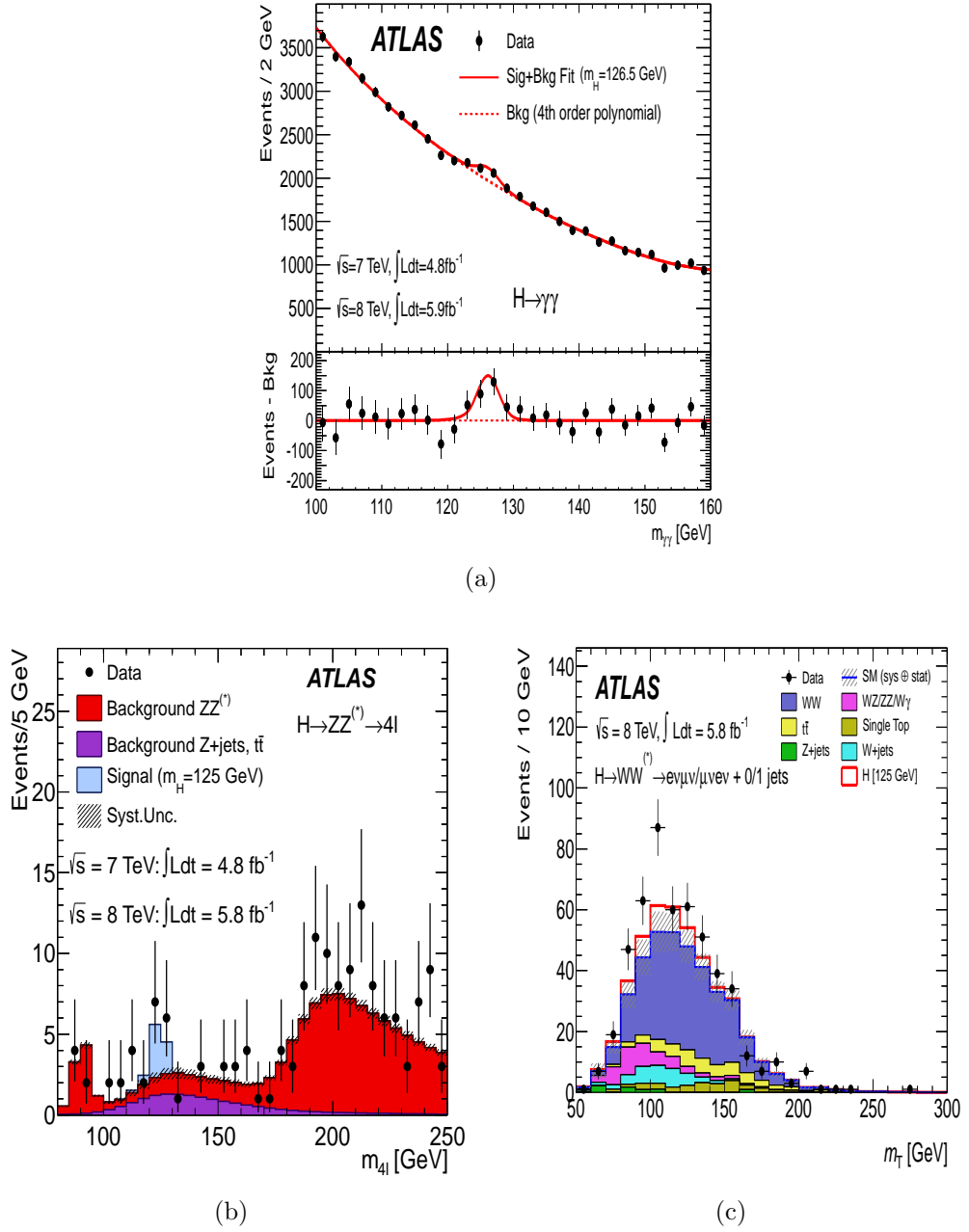


Figure 6.15: Discovery of a new particle consistent with SM Higgs boson: (a) Invariant mass distribution for  $H \rightarrow \gamma\gamma$ , (b) Invariant mass distribution for  $H \rightarrow ZZ \rightarrow l^+l^-l'^+l'^-$  and (c) Transverse mass distribution for  $H \rightarrow W^+W^- \rightarrow l^+\nu l'^-\nu$  channel. ©ATLAS collaboration 2012 [19].

Comparison with results of the ATLAS collaboration (from 2011):						
<i>Measurement of the <math>W \rightarrow l\nu</math> and <math>Z/\gamma^* \rightarrow ll</math> production cross sections in proton-proton collisions at <math>\sqrt{s} = 7 \text{ TeV}</math> with the ATLAS detector *)</i>						
<i>Search for the Standard Model Higgs boson in the <math>H \rightarrow WW(*) \rightarrow l\nu l\nu</math> decay mode using 1.7 fb<sup>-1</sup> of data collected with the ATLAS detector at <math>\sqrt{s} = 7 \text{ TeV}</math> **)</i>						
*) Authors: The ATLAS Collaboration (Submitted on 5 Dec 2011): <a href="http://arxiv.org/abs/1109.5141.pdf">http://arxiv.org/abs/1109.5141.pdf</a>						
**) Authors: The ATLAS Collaboration (24 Aug 2011): ATLAS-CONF-2011-134						
W → ... + ν					Background	WW+0J cand.
	positron	electron	antimuon	muon		
Total	77885	52856	84514	55234.0	21930.0	469
Total W+/W-	number of W+	162399	number of W-	108090		
W+ / W-	1.50		±	0.01		

Figure 6.16: Charge asymmetry  $R^\pm$ . Official ATLAS results as presented at [16].



# Chapter 7

## Z bosons at LHC

We will study Z boson production processes at LHC, find their cross sections using CompHEP and for the dominant process also differential cross sections. As a result of this study we suggest criteria which should be met by the Z boson candidate events. We will introduce Hypatia, a tool we will use to search for the Z bosons in the real LHC data from ATLAS, describe the search and finally discuss the results of the final measurement.

### 7.1 Z boson production

Z bosons are produced at LHC through these 3 main mechanisms (we show only dominant partons contribution)

$$pp \rightarrow u(d)g X \rightarrow Zu(d) X \quad (7.1)$$

$$pp \rightarrow u\bar{u}(d\bar{d}) X \rightarrow Z X \quad (7.2)$$

$$pp \rightarrow u\bar{u}(d\bar{d}) X \rightarrow Zg X \quad (7.3)$$

They (just like  $W$  bosons) have a very short lifetime ( $\sim 10^{-25}$ s) and decay before they move any measurable distance from the vertex. The dominant decay modes are

$$Z \rightarrow \nu\bar{\nu} \quad (20.0\%) \quad (7.4)$$

$$Z \rightarrow e^+e^- \quad (3.36\%) \quad (7.5)$$

$$Z \rightarrow \mu^+\mu^- \quad (3.36\%) \quad (7.6)$$

$$Z \rightarrow \tau^+\tau^- \quad (3.36\%) \quad (7.7)$$

$$Z \rightarrow q\bar{q} \quad (69.9\%) \quad (7.8)$$

The neutrino mode, summed over the three neutrino flavours ( $\nu = \nu_e, \nu_\mu, \nu_\tau$ ), is invisible at LHC detectors. The hadronic mode, summed over the five quark flavours ( $q = u, d, c, s, b$ ), is difficult to distinguish from the huge hadronic backgrounds intrinsic to pp colliders. The tau mode, although easier than the hadronic mode, is still difficult for our purposes and we will also treat it as background. We are left with the electron and the muon modes which will be used in our search for Z bosons due to clear experimental signatures.

## 7.2 Z production cross sections

We will use CompHEP to compute the total cross sections of the Z boson production processes where Z decays into  $l^+l^-$  pair ( $l = \mu, e$ ) at  $\sqrt{s} = 7$  TeV, Eqs. 7.9-7.11. For the process with the largest cross section we will also study  $p_T$  and  $m_{ll}$  distributions.

$$pp \rightarrow u(d)g X \rightarrow Zu(d) X \rightarrow l^+l^-u(d) X \quad (7.9)$$

$$pp \rightarrow u\bar{u}(d\bar{d}) X \rightarrow Z X \rightarrow l^+l^- X \quad (7.10)$$

$$pp \rightarrow u\bar{u}(d\bar{d}) X \rightarrow Zg X \rightarrow l^+l^-g X \quad (7.11)$$

Feynman diagrams for these processes are depicted in Figs. 7.1 - 7.3. Note that the same final state particles can be reached not only via the Z boson diagrams but also via the photon ( $\gamma$ ) diagrams.

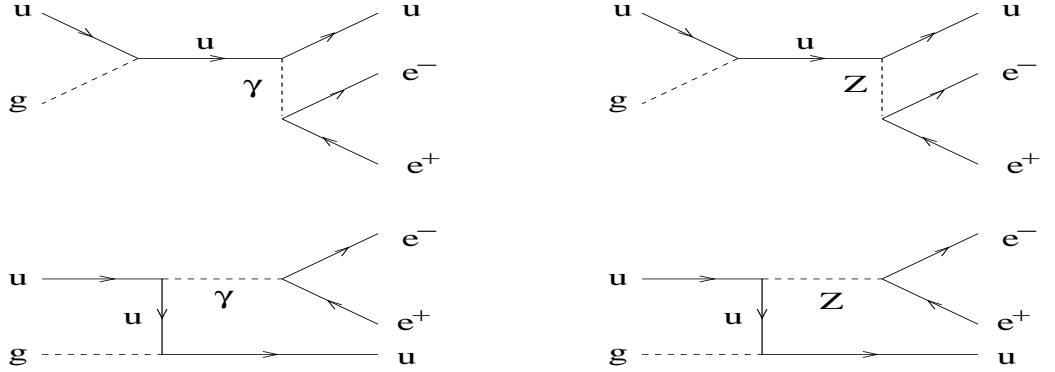


Figure 7.1: Feynman diagrams for  $pp \rightarrow ug \rightarrow Zu \rightarrow e^+e^-u$ .



Figure 7.2: Feynman diagrams for the dominant  $u\bar{u}$  subprocess of  $pp \rightarrow u\bar{u} \rightarrow Z \rightarrow e^+e^-$ . Other subprocesses include  $d\bar{d}$ ,  $c\bar{c}$ ,  $s\bar{s}$ ,  $b\bar{b}$ .

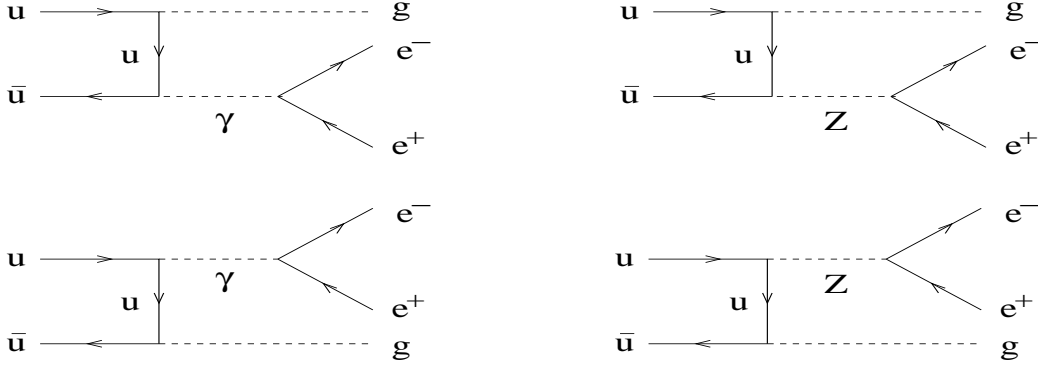


Figure 7.3: Feynman diagrams for the dominant  $u\bar{u}$  subprocess of  $pp \rightarrow u\bar{u} \rightarrow Zg \rightarrow e^+e^-g$ . Other subprocesses include  $d\bar{d}$ ,  $c\bar{c}$ ,  $s\bar{s}$ ,  $b\bar{b}$ .

We apply lepton  $y_l$  and jet  $y_j$  rapidity cuts motivated by the geometrical acceptance of the ATLAS detector (by jet we mean here  $u$  or  $d$  quark of Eq.7.9 or gluon of Eq.7.11):

$$-2.47 < y_l < 2.47 \quad (7.12)$$

$$-2.47 < y_j < 2.47 \quad (7.13)$$

and lepton  $p_T(l)$  and jet  $p_T(j)$  transverse momentum cuts aimed at background suppression:

$$p_T(l) > 25 \text{ GeV} \quad (7.14)$$

$$15 \text{ GeV} < p_T(j) < 75 \text{ GeV} \quad (7.15)$$

The  $p_T(l)$  cut will be partially justified below by the  $p_T(l)$  distribution of Fig. 7.5. The  $p_T(j)$  cut is only applied when  $u$ ,  $d$  or gluon are present in the final state. The same cut was applied in our W boson searches.

Using cteq6l structure functions of the proton we obtain with CompHEP following total cross sections for the  $Z$  production processes of Eqs. 7.9-7.11

( $l = e$ ), respectively, at  $\sqrt{s} = 7$  TeV:

$$\sigma(Zu(d)) = 14(12) \text{ pb} \quad (7.16)$$

$$\sigma(Z) = 340 \text{ pb} \quad (7.17)$$

$$\sigma(Zg) = 28 \text{ pb} \quad (7.18)$$

### 7.2.1 Distributions in $m_{e^+e^-}$ and $p_T(e^+)$ . Z boson signatures in the electron and muon decay modes at LHC

Invariant mass  $m_{e^+e^-}$  and transverse momentum  $p_T(e^+)$  distributions for the dominant process  $pp \rightarrow Z \rightarrow e^+e^-$  are shown in Figs. 7.4 and 7.5.

Invariant mass distribution starts at  $m_{e^+e^-} = 50$  GeV as a consequence of the  $p_T(l) > 25$  GeV cut applied to both leptons. The Z peak is clear at  $M_Z = 91.1876$  GeV. The continuum is also easily seen in the logarithmic Y-scale (it would be hardly visible in the linear scale): e.g. at  $m_{e^+e^-} = 60$  GeV the cross section is much smaller than at the Z peak, nevertheless, it is nonzero. The continuum in this region is due to the photon Feynman diagram, see Fig. 7.2, which represents the so-called irreducible background (it is an intrinsic part of the whole signal process). Closer to the Z peak also the interference of the photon diagram with the Z diagram contributes. Reducible backgrounds (not included here), such as W boson production, top quark production, QCD jet production and Z decays to other than electron/muon modes will contribute to the continuum but will not threaten the Z peak which will remain clear above all backgrounds when the proper Z signatures criteria are applied.

The  $p_T(e^+)$  distribution (Fig. 7.5), cut off below 25 GeV, grows above 25 GeV and peaks at about 45 GeV which corresponds to  $M_Z/2$ , as could be expected from the Z boson produced with zero or almost zero  $p_T$ . Since below 25 GeV the cross section falls quickly (not shown), the choice  $p_T(l) > 25$  GeV seems reasonable: most signal events survive the cut which will remove much of the background events with typical  $p_T$  well below 25 GeV.

To summarize, we will look for the electron-positron or muon-antimuon pair, each lepton of the pair with high  $p_T$  ( $> 25$  GeV). High  $p_T$  daughter particle is the result of the decay of the high mass mother (Z). The leptons can be accompanied by a small or large number of hadrons from the final state quark or gluon. Missing transverse energy for the event is typically small ( $E_T^{miss} < 20 - 25$  GeV) since no neutrino is produced directly in the

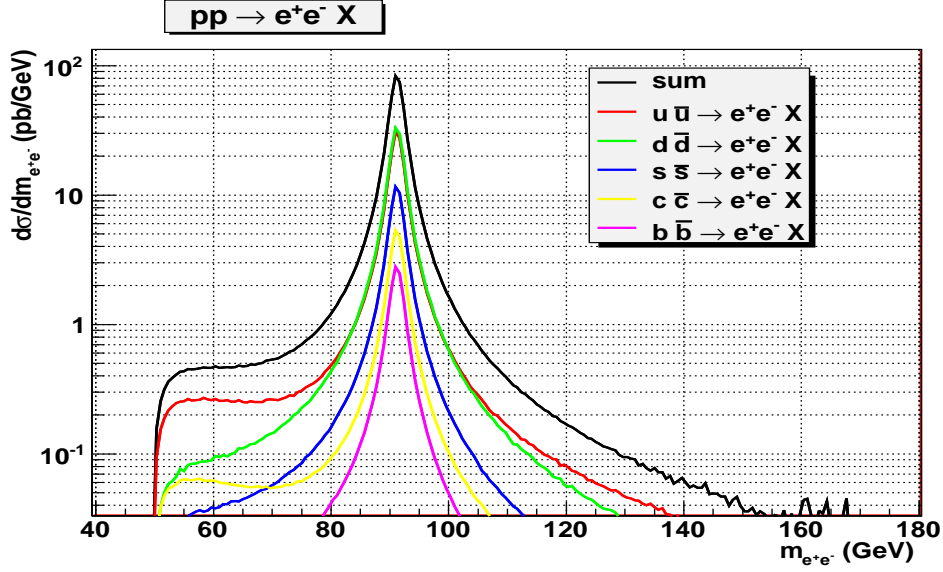


Figure 7.4: CompHEP calculation of the invariant mass ( $m_{e^+e^-}$ ) distribution for the process of  $pp \rightarrow q\bar{q} \rightarrow Z \rightarrow e^+e^-$ . All contributing subprocesses are included along with their sum (black).

collision (neutrinos can appear indirectly as a result of hadron decays in later stages but these have typically much smaller energies).

The most important signature is the invariant mass of the lepton pair,  $m_{ll}$ , which should be equal to the Z boson mass  $M_Z$  if the lepton pair indeed resulted from the Z boson decay, see Sec. 4.3. The background events typically give arbitrary values of  $m_{ll}$  and hence we expect the Z boson signal to show up as a peak at  $m_{ll} = M_Z$  above the continuum background in the  $m_{ll}$  distribution of events, Fig. 7.4. As noted before, this is the typical way new particles are discovered - as peaks in the invariant mass distributions.<sup>1</sup>

<sup>1</sup>Note that we could not have used this powerful invariant mass signature in the  $W$  boson ( $W^\pm \rightarrow l^\pm \nu_l$ ) searches since we did not know the 4-momentum of the (undetected) neutrino required along with the 4-momentum of the electron (muon) to find the invariant mass of the lepton pair  $l^\pm \nu_l$ . We could, however, have studied the peak at  $M_W/2$  in the  $p_T$  spectrum of the lepton into which the  $W$  boson had decayed.

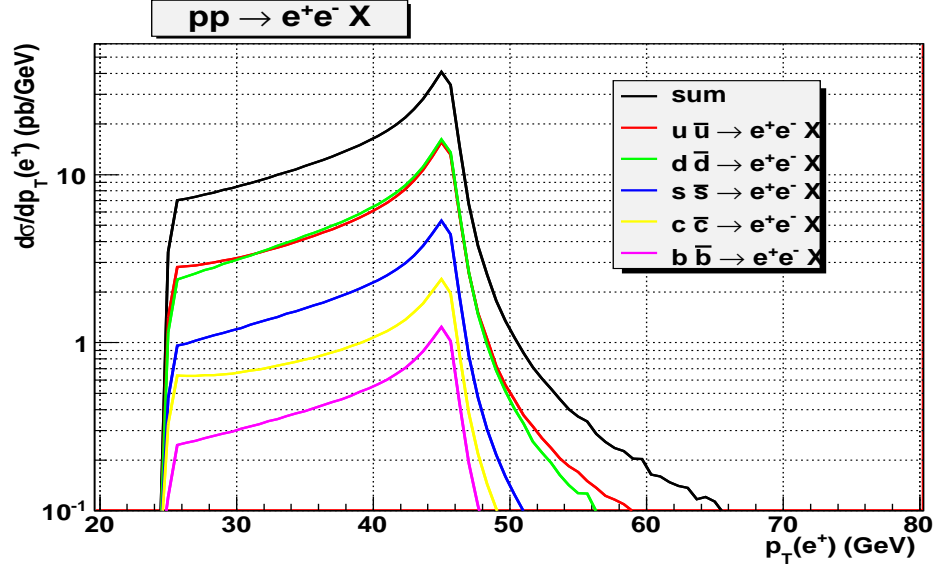


Figure 7.5: CompHEP calculation of the distribution of the transverse momentum of  $e^+$  for the process of  $pp \rightarrow q\bar{q} \rightarrow Z \rightarrow e^+e^-$ . All contributing subprocesses are included along with their sum (black).

### 7.3 Z boson events in Hypatia

Hypatia is a software tool very similar to Minerva since it is built upon the same Atlantis Event Display tool used by ATLAS physicists. It can be downloaded from its home page [21] or from the International Masterclasses ATLAS exercise page (follow the 'Z path - Get to work - Data samples and tools' links) [16]. From the latter page you can also download the data. Each package of 50 events is labeled by a letter.

Start Hypatia and load your 50 events through File - Read Event Locally functions in the Invariant Mass Window. The .zip file with events will be read by Hypatia as is (do not try to unzip it). A common bug of the versions that we have worked with is that Hypatia claims it cannot read events. If that happens, just click the Reset Canvas button in the right corner of the Track Momenta Window (expand the window if you do not see the Reset function). You can browse events with the Previous Event and Next Event functions in the Track Momenta Window.

The Canvas Window (Figs. 7.6 - 7.9) with the end view and side view

windows and the energy deposits in the calorimeters in the  $\eta - \Phi$  plane window looks very familiar to Minerva users. Minor changes can be noticed easily, such as  $p_T^{miss}$  (red dashed line in Minerva) depicted as a red arrow of the size proportional to the  $p_T^{miss}$ , muon detector hits (colored bright orange in Minerva) are not specifically marked in Hypatia with muons represented simply by a line crossing all four detector layers.  $E_T^{miss}$  information, having moved to the Track Momenta Window, is now missing in the  $\eta - \Phi$  plane window.

More differences can be found in the control windows (Figs. 7.7b,c and 7.9b,c). The Minerva GUI Window is replaced by three windows in Hypatia: i) Control Window (not shown here) with the Zoom/Move/Rotate functions and Index finger button available via Interaction and Window Control and Cuts functions available via Parameter Control; ii) Track Momenta Window used to browse events, display detailed track information and also to load the candidate tracks into the Invariant Mass Window; iii) Invariant Mass Window is used to load events into Hypatia, it further displays invariant masses of the candidate tracks and plots histograms in different variables.

### 7.3.1 Typical $Z \rightarrow e^+e^-$ event

A typical  $Z \rightarrow e^+e^-$  event is shown in Figs. 7.6 and 7.7. This event has tens of tracks with  $p_T > 1$  GeV but the cut  $p_T > 25$  GeV was applied leaving just four most energetic tracks (see the end view in Fig. 7.6). Two of them (one at 1:30 and the other at 8 o'clock) point to the large energy deposits in the electromagnetic calorimeter with no activity further down the line in the hadronic calorimeter and the muon detectors. These two tracks are therefore candidates for electrons/positrons. Note also that the two tracks are almost back to back (the angle between them is  $\sim 180$  degrees) in the end view which is typical for the  $Z \rightarrow l^+l^-$  events at LHC (note, however, that occasionally one encounters events where this angle can be much smaller than 180 degrees).

Another important criterion is verified in the Track Momenta Window in Fig. 7.7b - note that the tracks No. 5 and 10 which correspond to our two candidates have opposite electric charges (to relate the track in the tracker with the track number, click on the track in the Index finger regime and the track is highlighted in grey color in the Track Momenta Window). Also note their  $p_T$  values, azimuth angles  $\phi$  and polar angles  $\theta$ . A check of the missing energy yields  $E_T^{miss} = 6.684$  GeV, meaning no neutrino was produced and

reassuring us that we see a  $Z \rightarrow e^+e^-$  boson candidate.

It is instructive to examine energy deposits in the rolled out calorimeters in Fig. 7.7a. The two towers correspond to our candidate tracks No. 5 and 10, they are separated by 180 degrees in the azimuth angle  $\Phi$ , they both sit at pseudorapidity  $\eta \sim 1$  (corresponding to the polar angle  $\theta \sim 0.5 - 0.7 \text{ rad}$ ), and both towers dominate in the whole  $\eta - \Phi$  plane confirming that neither of the two leptons is the decay product of heavy hadrons inside jets (a jet can contain an electron/positron but the jet typically forms a cluster of several smaller towers).

Finally, after we insert the tracks No. 5 and 10 through the Insert electron button in the Track Momenta Window, the two tracks appear in the Invariant Mass Window (see Fig. 7.7c) with the calculated invariant mass of the electron-positron pair appearing as  $m_{ll} \equiv M(2l) = 90.512 \text{ GeV}$ . This is in good agreement with the known mass of the  $Z$  boson,  $M_Z = 91.1876 \text{ GeV}$ .

### 7.3.2 Typical $Z \rightarrow \mu^+\mu^-$ event

A typical  $Z \rightarrow \mu^+\mu^-$  event is shown in Figs. 7.8 and 7.9. This event has again tens of tracks with  $p_T > 1 \text{ GeV}$  but the cut  $p_T > 25 \text{ GeV}$  was applied leaving six most energetic tracks (see the end view in Fig. 7.8). Two tracks cross all four layers of detectors including the muon detectors, representing thus muons/antimuons candidates. The two tracks are back to back in the end view which is typical for the  $Z \rightarrow l^+l^-$  events at LHC (note again, however, that occasionally one encounters events where the angle between the two tracks can be much smaller than 180 degrees). The tracks have numbers 17 and 122 and a look at the Track Momenta Window (Fig. 7.9b) tells us that they have opposite electric charges and  $E_T^{miss} = 6.676 \text{ GeV}$  (no neutrino).

Energy deposits in the rolled out calorimeters in Fig. 7.9a show typical jet clusters without isolated dominant towers unlike the  $Z \rightarrow e^+e^-$  event discussed above. This is OK since the muons do not leave much energy in the calorimeters.

As a last step we insert the tracks No. 17 and 122 through the Insert muon button in the Track Momenta Window and find the calculated invariant mass of the muon-antimuon pair  $m_{ll} \equiv M(2l) = 90.427 \text{ GeV}$  in the Invariant Mass Window (see Fig. 7.9c). This is again in good agreement with the known mass of the  $Z$  boson,  $M_Z = 91.1876 \text{ GeV}$  and confirms that our event is most

likely the genuine  $Z \rightarrow \mu^+\mu^-$  event.

## 7.4 Search for Z bosons in the ATLAS data

### *Measurement*

This is the original International Masterclasses measurement described in [16] where you will also find the ATLAS data. To download the data follow the 'Z path - Get to work - Data samples and tools' links. Alternatively, you can find the same data on the Slovak Masterclasses page (follow the 'Fyzika' link) [17]. Each package of 50 events is labeled by a letter. You should analyze at least 50 events, working either on your own or, preferably, in a pair with your fellow student.

Start Hypatia and load you 50 events through File - Read Event Locally functions in the Invariant Mass Window. The .zip file with events will be read by Hypatia as is (do not try to unzip it). A common bug of the versions that we have worked with is that Hypatia claims it cannot read events. If that happens, just click the Reset Canvas button in the right corner of the Track Momenta Window (expand the window if you do not see the Reset function). Browse events with the Previous Event and Next Event functions in the Track Momenta Window.

Look for  $Z \rightarrow e^+e^-$  and  $Z \rightarrow \mu^+\mu^-$  candidate events which should meet the following criteria:

1. A pair of isolated leptons with opposite electric charge,  $l^+l^-$ , ( $l = e/\mu$ ).
2.  $p_T(l) > 25$  GeV for each lepton
3.  $E_T^{miss} < 25$  GeV
4. The two candidate tracks originate from the same collision (they come from a single point/vertex which means the difference in their  $z$  coordinates is not larger than 1 cm). You have to zoom in in the side view to check this one.

If the event meets ALL criteria, insert the two candidate tracks through Insert electron/muon buttons and check the invariant mass value. Do not be disturbed too much (assuming you did a good job) if it is not equal to  $M_Z$ . As we will see, it can be for a number of reasons. If the event does not meet the criteria (even if it is just one of the four) we conclude that it is

likely a background event. The most significant backgrounds are represented by W boson events (discussed in the previous chapter), top quark events, jet (QCD) events and also Z events with decay modes other than electron or muon. The level of these backgrounds had already been reduced significantly by the pre-selection cuts applied to ATLAS data.

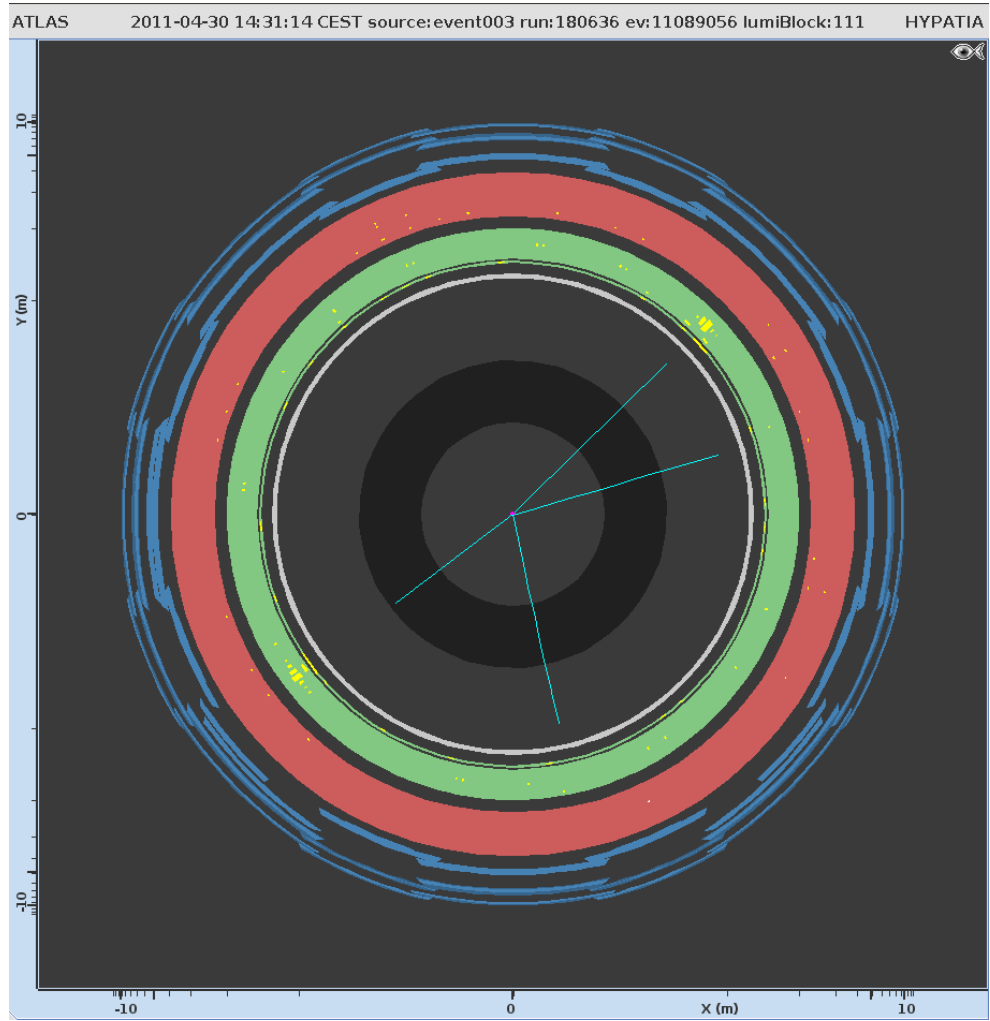
### *Results of measurement and discussion*

After you have analyzed at least 50 events and inserted all  $Z \rightarrow l^+l^-$  candidates, you can plot the histogram of  $m_{ll}$  through the Histograms button in the Invariant Mass Window. A possible result is in Fig. 7.10. There is one event at 3.0 GeV, two at 69 GeV, 24 at 90 GeV, one at 224 GeV and three at around 1000 GeV. The twenty-four are clearly Z boson candidates but what about the rest? We might be inclined to conclude that it is most likely background. It is true that we tried to eliminate background events through the cuts and indeed we rejected 19 events out of 50 which did not pass the cuts, however, this method is not 100 % efficient and inevitably some background events filtered in. While this interpretation is plausible, we cannot say anything definitive at this stage. It could also be signs of particles other than the Z boson - particles which decay into a pair of high  $p_T$  leptons just like the Z but their mass is different from  $m_Z$ . We need more data (better statistics) to resolve this problem.

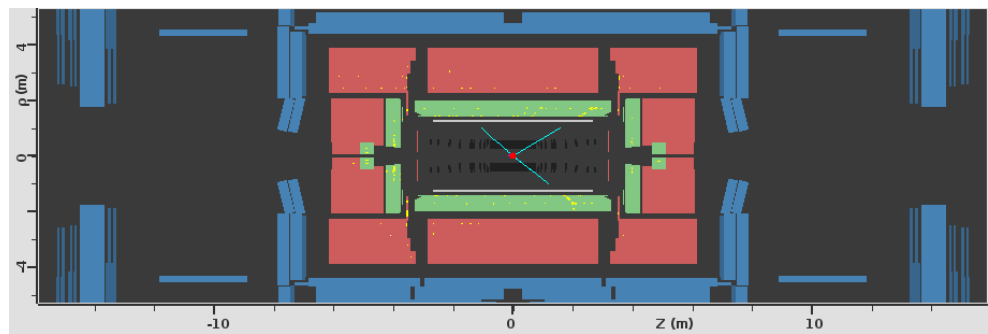
We show results of the combined analysis of high school students working for one day at four universities across Europe during International Master-classes in Fig. 7.11. Together they analyzed a much larger sample of data and found 2 308 candidate events. The Z peak maintains its dominance in the  $m_{ll}$  spectrum but three other peaks are shaping up at 3.0 GeV, at 9.8 GeV and 1 000 GeV. Since the continuum background between the peaks is almost zero, these peaks now look like they are due to particles decaying in the same way as the Z boson. In fact, the first peak corresponds to the  $J/\psi$  meson (composed of  $c\bar{c}$  quark pair) and the second peak corresponds to  $\Upsilon$  meson (composed of  $b\bar{b}$  quark pair). The third peak at 1 000 GeV represents so far hypothetical particle,  $Z'$  boson, predicted by many extensions of the Standard Model. Note that this is not the discovery of  $Z'$  since the corresponding events are just simulated ones - they were mixed in with the real ATLAS data ( $J/\psi$ ,  $\Upsilon$ , Z and backgrounds) to illustrate the discovery process of new particles.

Note that the peaks have finite widths, e.g., the Z peak has the width

$\Gamma_Z = 3.89$  GeV. This means that the true Z events can have invariant masses  $m_{ll}$  which can differ from the  $M_Z$  mass: with 66 % probability they will fall in the interval  $M_Z - \Gamma_Z < m_{ll} < M_Z + \Gamma_Z$ . In fact, the true width connected with the finite lifetime of Z is  $\Gamma_Z = 2.495$  GeV. The larger, 3.89 GeV value is due to statistical and systematical (detector is not perfect) errors.

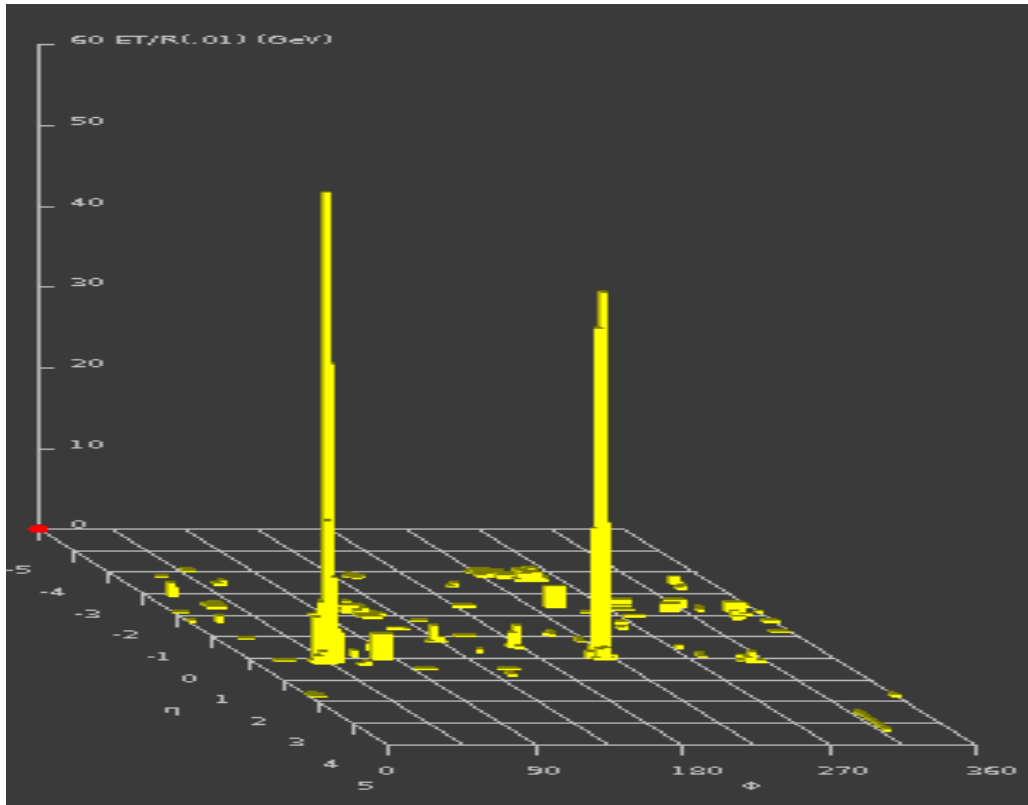


(a) End view



(b) Side view

Figure 7.6:  $Z \rightarrow e^+e^-$  event displayed in Hypatia



(a) Energy deposited in the calorimeters

**HYPATIA - Track Momenta Window**

File: Previous Event Next Event Insert Electron Insert Muon Delete Track Reset Canvas

ETHis: 6.684 GeV  $\varphi$ : -1.863 rad Collection: MET\_RefFinal

/home/melo/HYPATIA/events/groupD2012.zip/event003.xml

Reconstructed Tracks					
Track	+/-	P [GeV]	Pt [GeV]	$\varphi$	$\theta$
Tracks 5	-	87.31	46.89	0.769	0.567
<b>Tracks 10</b>	<b>+</b>	<b>67.83</b>	<b>43.32</b>	<b>-2.486</b>	<b>0.693</b>
Tracks 164	+	54.44	37.31	0.291	2.386
Tracks 167	-	42.30	27.19	-1.363	0.698

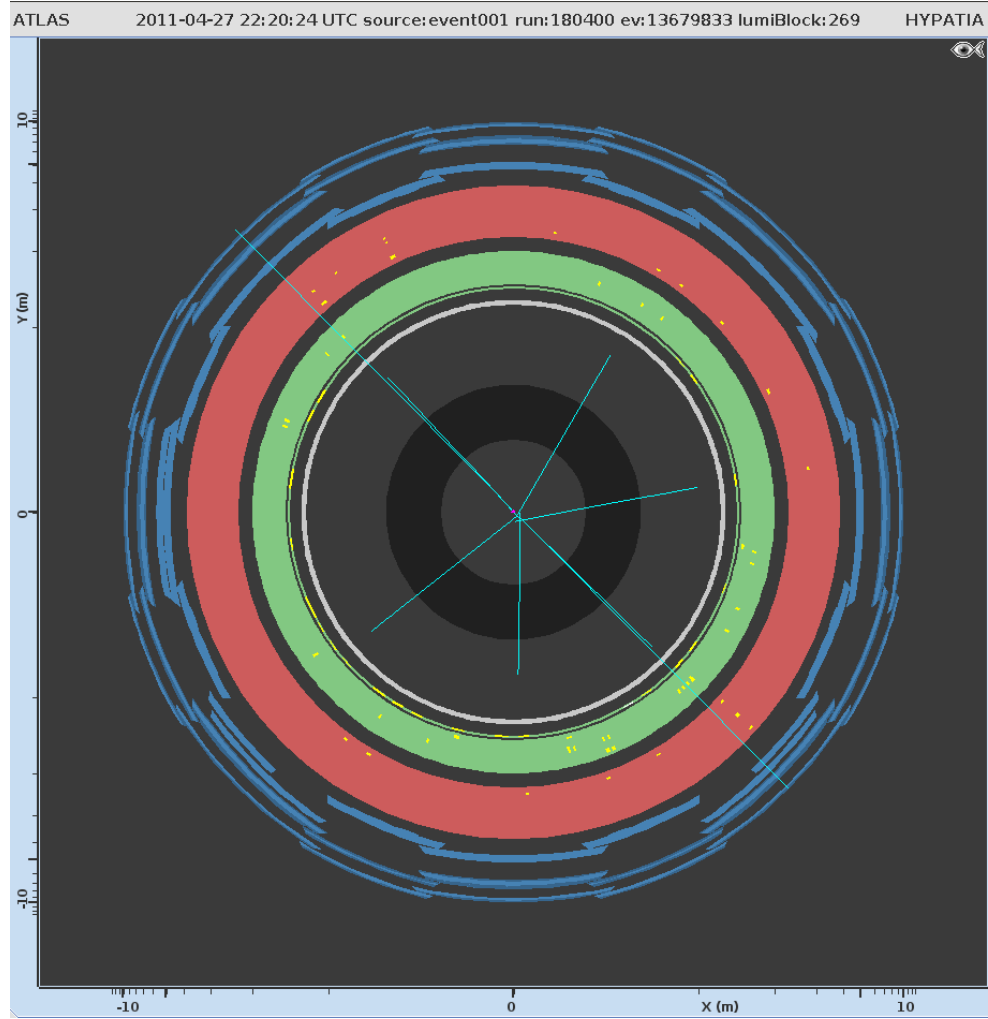
(b) Detailed track information (tracks 5 and 10)

**Hybrid pupils' analysis tool for interactions in ATLAS - version 6.0 - Invariant Mass Window**

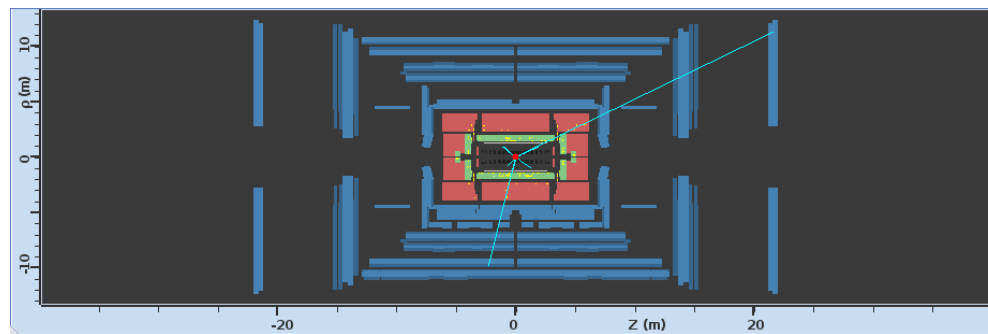
File View Histograms Preferences Help

File Name	ETMis [GeV]	Track	P [GeV]	+/-	Pt [GeV]	$\varphi$	$\eta$	M(2l) [GeV]
event003.xml	12.183	Tracks 5	87.3	-	46.9	0.769	1.233	90.512
		Tracks 10	67.8	+	43.3	-2.486	1.019	
event006.xml	4.687	Tracks 6	37.1	+	33.4	1.877	0.463	91.721
		Tracks 1	59.4	-	45.7	-0.851	-0.755	

(c)  $e^+e^-$  candidate invariant mass (tracks 5 and 10)Figure 7.7: Further info on the same  $Z \rightarrow e^+e^-$  event.

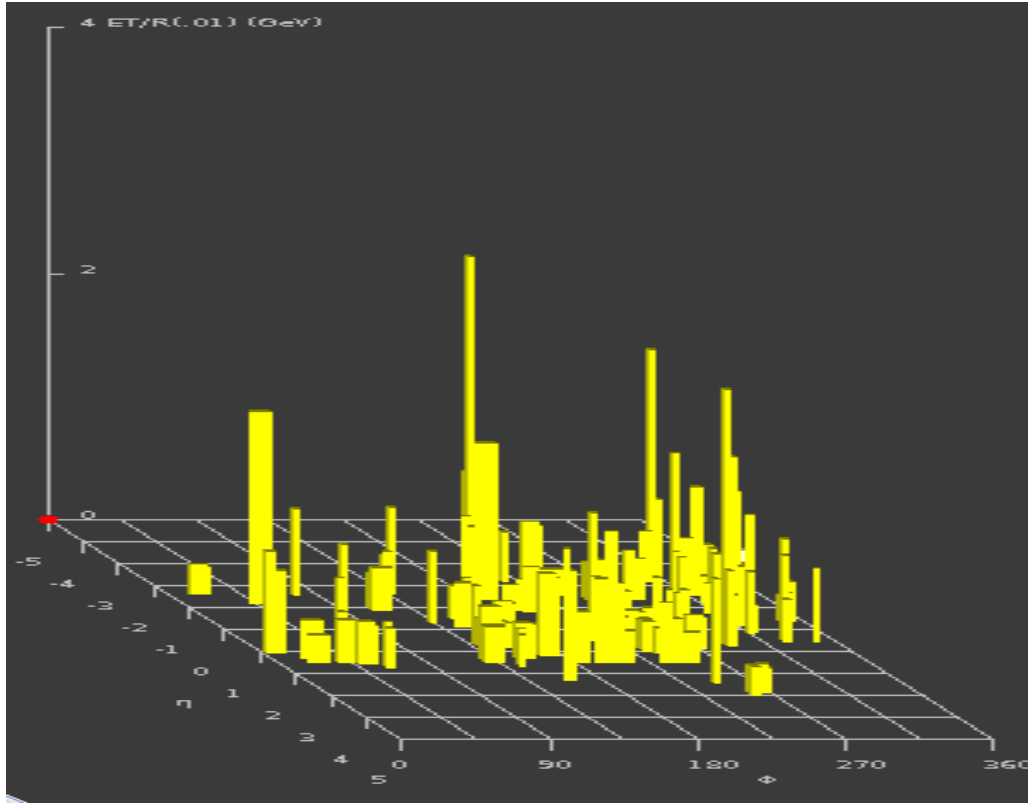


(a) End view



(b) Side view

Figure 7.8:  $Z \rightarrow \mu^+ \mu^-$  event displayed in Hypatia



(a) Energy deposited in the calorimeters

**HYPATIA - Track Momenta Window**

File: Previous Event Next Event Insert Electron Insert Muon Delete Track Reset Canvas

ETHis: 6.676 GeV  $\phi$ : 1.742 rad Collection: MET\_Reffinal

/home/melo/HYPATIA/events/groupD2012.zip/event001.xml

Track	+/-	P [GeV]	Pt [GeV]	$\phi$	$\theta$
Tracks 17	+	34.58	33.67	-0.763	1.800
Tracks 122	-	71.74	32.92	2.314	0.477
Tracks 129	+	260.43	168.33	1.036	2.439
Tracks 130	+	38.17	25.74	0.174	2.401
Tracks 131	+	61.00	45.75	-1.564	2.294
Tracks 151	+	842.93	516.98	-2.462	0.660

(b) Detailed track information (tracks 17 and 122)

**Hybrid pupils' analysis tool for interactions in ATLAS - version 6.0 - Invariant Mass Window**

File View Histograms Preferences Help

File Name	ETMis [GeV]	Track	P [GeV]	+/-	Pt [GeV]	$\phi$	$\eta$	M(2l) [GeV]
event003.xml	12.183	Tracks 5	87.3	-	46.9	0.769	1.233	90.512
		Tracks 10	67.8	+	43.3	-2.486	1.019	
event006.xml	4.687	Tracks 6	37.1	+	33.4	1.877	0.463	91.721
		Tracks 1	59.4	-	45.7	-0.851	-0.755	
event001.xml	4.103	Tracks 122	71.7	-	32.9	2.314	1.415	90.427
		Tracks 17	34.6	+	33.7	-0.763	-0.232	

(c)  $\mu^+\mu^-$  candidate invariant mass (tracks 17 and 122)Figure 7.9: Further info on the same  $Z \rightarrow \mu^+\mu^-$  event.

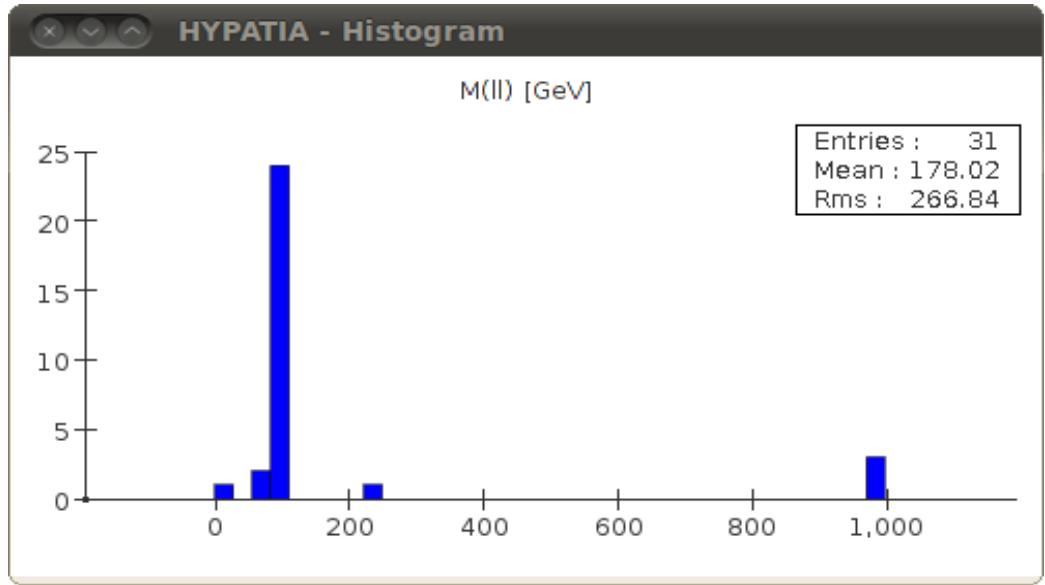


Figure 7.10: Histogram of events as a function of invariant mass  $m_{ll}$ . A possible result of an analysis of 50 events.

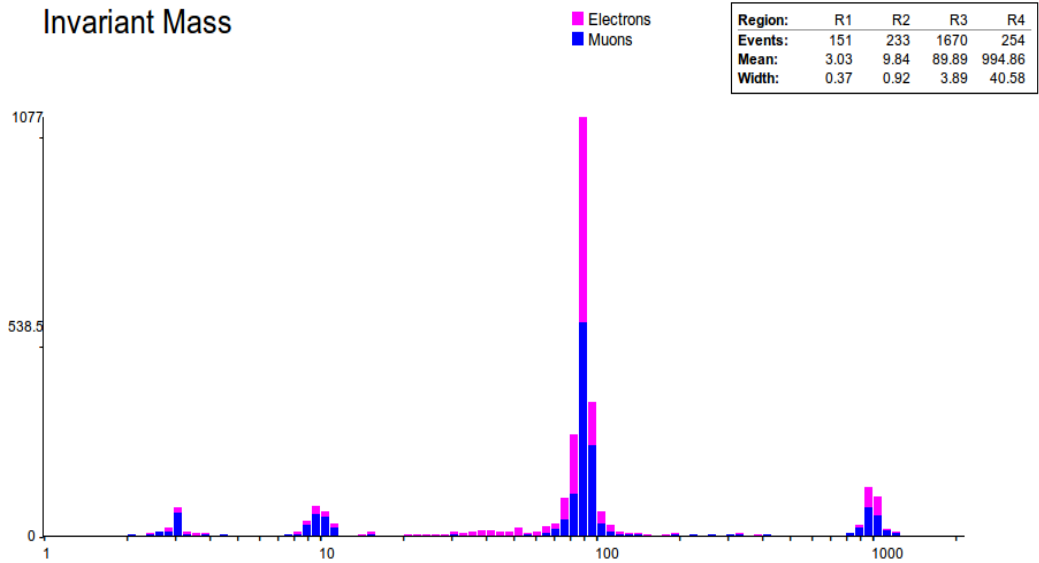


Figure 7.11: Histogram of events as a function of invariant mass  $m_{ll}$ . Combined work of high school students including those at University of Zilina during International Masterclasses on Mar 1, 2012.

# Chapter 8

## Cosmic Rays at SKALTA

### 8.1 Introduction to Cosmic Rays

Cosmic rays consist of high-energy particles coming to Earth from outer space (primary particles) and showers of secondary particles created in the earth atmosphere as a consequence of the interaction of primary particles with the atmosphere (fig. 8.1) <sup>1</sup>.

Cosmic rays were discovered by Austrian-American physicist Victor Francis Hess in 1912. During the first half of the 20th century the study of cosmic rays was the only way to discover new particles. Important discoveries using cosmic rays study include muons, pions, positron (the first antiparticle) and strange particles  $K^\pm, K^0$  and  $\Lambda$  (particles contain strange quarks). Recent cosmic rays physics involves studies of low energy cosmic rays coming from the Sun (e.g. solar wind study), galactic cosmic rays with energies up to  $10^{18}$ eV, or extragalactic cosmic rays with energy bigger than  $10^{18}$ eV, whose source still remains a mystery.

#### 8.1.1 Primary cosmic rays

The composition of charged primary particles varies with energy. However, about 86% of primary particles are protons, 11% alpha particles (helium nuclei), 1% heavier nuclei and 2% electrons [22]. Neutral primary particles are

---

<sup>1</sup>Sometimes in the literature the definition of secondary cosmic rays is more general; they are called secondary even if they come from interactions of primary particles with interstellar gas [8]. In that case, the primary cosmic particles come directly from the source.

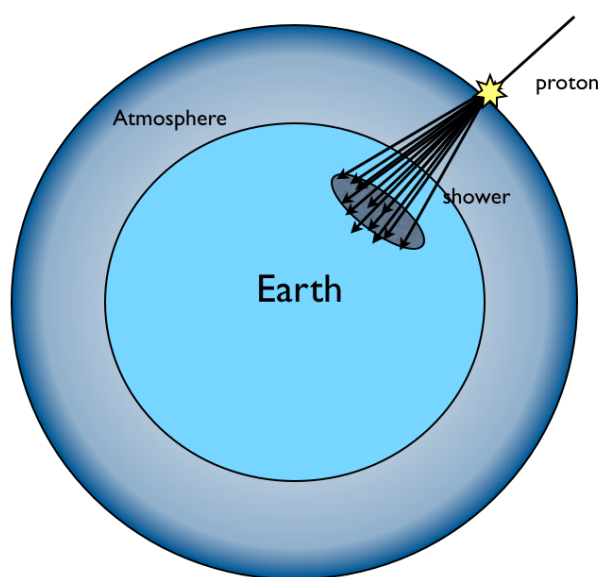


Figure 8.1: Diagram of primary (proton) and secondary cosmic rays (shower)

composed of photons, neutrinos and antineutrinos and for very high energies  $> 10^{15}\text{eV}$ , numbers of primary neutral particles are most likely negligible with respect to the charged ones (because the neutral particles cannot be accelerated).

The nuclear composition of cosmic rays is remarkably similar to the composition of the Solar system. This implies that sources of primary cosmic rays are stars. There are also traces of antiparticles in cosmic rays (antiprotons and positrons); however, it is generally assumed that they are created in interactions of primary particles with interstellar gas, for example in:

$$p + p \rightarrow p + p + p + \bar{p} \quad .$$

The different sources of primary cosmic rays can be derived from the energy spectrum of the primary cosmic rays (fig. 8.2). Low energy particles ( $< 10^9\text{eV}$ ) come from the Sun. Particles with approximately the same energy coming from other stars are shielded by the solar magnetic field <sup>2</sup>.

From the energy ( $> 10^9 - 10^{10}\text{eV}$ ) the magnetic field of the Sun can not redirect the charged primary particles and they start to cross the Solar system (the galactic band in the fig. 8.2).

There is a break in the spectrum around  $\sim 10^{15}\text{ eV}$  which is called the "knee". The spectrum below the break is steeper (i.e. the incoming particle rate is smaller than expected). The interpretations suggest that one of the acceleration mechanisms in the Galaxy reached its limit. For example, it is assumed that acceleration by supernovas ends at the same energy [8].

---

<sup>2</sup>Reminder: if a charged particle  $a$  enters magnetic field (we assume  $\mathbf{v} \perp \mathbf{B}$ ), then the centripetal Lorentz force bends its trajectory obeying the equation

$$\frac{m.v^2}{r} = Z.e.v.B$$

for singly charged particle we get

$$p = e.r.B$$

where  $p$  is particle momentum,  $e$  is electric charge,  $r$  is bending radius and  $B$  is magnetic field. We see that knowing the magnetic field  $B$  (solar, galactic, ...) and the particle charge and momentum, we can estimate the deflection of the particle trajectory when entering the magnetic field (by calculating the bending radius). The bigger the momentum of the particle the less it will be deflected by magnetic field. For example, extragalactic protons with momentum  $> 10^{18}\text{eV}/c$  are not deflected by the galactic magnetic field, and that is why we can use their trajectories for pointing to the source. On the other hand, any information about the source of galactic protons is completely lost, due to their circular movement inside the Galaxy.

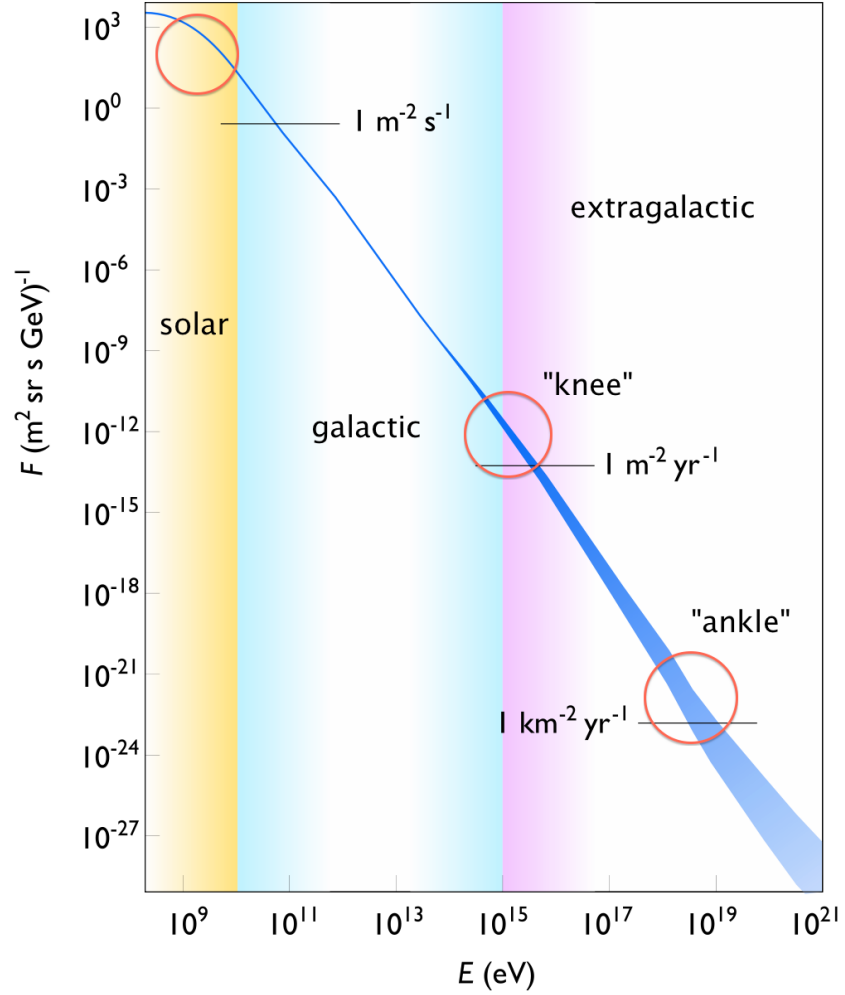


Figure 8.2: The flux of cosmic ray particles as a function of their energy. The flux for the lowest energies (yellow zone) is mainly attributed to solar cosmic rays, intermediate energies (blue) to galactic cosmic rays, and highest energies (purple) to extragalactic cosmic rays [23]. The sr is for steradian and it is the SI unit of solid angle. The values in the graph are normalized per steradian.

Another possible contribution to the steeper spectrum is that at this energy particles start to leak out of the Galaxy (i.e. the galactic magnetic field is not strong enough to keep them within the Galaxy) [24]. Charged particles with smaller energy are basically trapped inside our Galaxy for millions of years (on average 15 Myr [8] until they interact); they circulate inside the galactic field<sup>3</sup>. As was mentioned in the previous section, the similarities between the chemical composition of the Solar system and cosmic rays imply that the galactic cosmic rays come from stars.

The leaking out of galactic particles with energy more than  $\sim 10^{15}$  eV should also work the other way around: the extragalactic particles start to leak *into* the Galaxy above that energy, and with energy  $> 10^{18}$  eV they dominate the flux of the primary cosmic rays. That is why the spectrum below the "ankle" is flattened (note the log scale!), i.e. the incoming particle rate at this energy is higher than expected. The extragalactic particles above this energy start to cross our Galaxy in such a way that we can estimate their sources (i.e. they are basically not deflected by the galactic magnetic field). The sources are, however, still unknown. Some of the possible candidates could be supernovas or active galactic nuclei. The energy spectrum of cosmic rays reaches values between  $10^{20} - 10^{21}$  eV.

The acceleration mechanism for such energetic particles is an unsolved mystery. For comparison, the most powerful accelerator on the Earth - the Large Hadron Collider - can only accelerate particles up to  $4 \times 10^{12}$  eV.

There is a natural energy limit beyond which the particles cannot travel very long distances: it is called the GZK limit (after Greisen, Zatsepin and Kuzmin who first suggested it [25]). The idea is that if a particle, on its way through the Universe, somehow exceeds an energy  $6 \times 10^{19}$  eV [24] then it starts to interact with the photons in the cosmic microwave background<sup>4</sup> and pions are created (i.e., the collision energy is high enough to produce a

---

<sup>3</sup>The magnetic field of the Galaxy is approx.  $10^{-5}$  weaker than the geomagnetic field but acts on much longer distances - it has enough time to deflect much more energetic particles than the geomagnetic one.

<sup>4</sup>The cosmic microwave background (or cosmic blackbody radiation) is composed of photons originating from atom formation occurring about 400 000 years after Big Bang. The temperature of the radiation was about 3000K at that time. Due to the expansion of the Universe the background now has a temperature of only 2.7 K, which corresponds to average energy 1.1 meV of the photons. You can check that the proton with momentum  $6 \times 10^{19}$  eV/c has just enough energy to produce the pion in collision with the 1.1 meV photon (use chapter 1.6).

pion):

$$p + \gamma \rightarrow p + \pi^0$$

$$p + \gamma \rightarrow n + \pi^+$$

By creating the pion, the proton loses its energy under the GZK limit. Recent results from most experiments show that the limit most likely exists [8]: they see a drop at the very end of energy spectrum. The mean free path of protons with energy above the GZK limit is about  $10\text{Mpc}$ <sup>5</sup> [24]. There are also observations of particles with energy above  $6 \times 10^{19}\text{eV}$ . We know that our Galaxy cannot contain sources able to create and/or accelerate such particles (because their directions are seen isotropically from Earth, not from the galactic center and the galactic magnetic field is too weak to change their original trajectory.). The existence of particles with energies  $> 10^{20}\text{eV}$  means they must have an extragalactic origin, and they must have been created relatively close to our Galaxy ( $< 10\text{Mpc}$ ).

Fig. 8.2 provides also another important piece of information related to the absolute value of the flux. Particles coming from the interplay between solar and galactic part are frequent: on average every second there is one flying through one meter squared. The knee particles are much rarer: we have one per meter squared per year. And the most energetic particles (ankle part) are the rarest - if we count them over an area of 1 kilometer squared we would wait on average one year to see one. This limits the detectors usable for studying very high energy cosmic particles. Because of the very low rate we cannot use balloons or satellites. In order to collect reasonable statistics of those rare events we need to cover big enough areas on the earth's surface. This is done indirectly by using detectors on the ground which study showers of secondary cosmic particles (their lateral or longitudinal properties)<sup>6</sup>. Studying the showers in this way, the properties of the original primary particles can be estimated. Typical examples of experiments studying very high energy cosmic particles are the Pierre Auger laboratory, which can cover about  $3000\text{ km}^2$  [28], the Telescope Array [29] or the HiRes experiment [30].

---

<sup>5</sup>1 pc (parsec) is length unit in astronomy ( $\sim 3.26$  light-years).

<sup>6</sup>There is some progress in this field using the satellites too - for example the project JEM-EUSO [27], which would be a satellite covering about  $500\,000\text{ km}^2$ . Of course, it will not detect the primary particles - that would be impossible to cover, instead it will detect particles emitted upwards the shower.

### 8.1.2 Secondary cosmic rays

Most interactions of primary cosmic rays with the atmosphere take place at altitudes between 15 - 20 km. For example, the thickness of the atmosphere for protons is about 11 interaction lengths <sup>7</sup> [24], i.e. the probability that the proton will fly through the atmosphere untouched is negligible.

Secondary cosmic rays composition depends on the primary particle causing the shower - if the primary particle is a proton (or nucleus) then the particles in the shower (just after the interaction) are mostly hadrons (hadron shower). A pure electromagnetic shower is caused by photons, electrons or positrons.

Let us have a closer look at evolution of a typical proton shower (fig. 8.3):

The primary proton (usually) interacts with an atomic nucleus in the atmosphere (mostly nitrogen or oxygen). The momentum of the nucleus is very small in comparison to the proton's momentum so the momenta of all the particles created in such a collision have roughly the same direction as the original proton - we see it as a cone of particles (shower). Most particles created in that interaction are pions. Many of them decay immediately, but some of them (with high energy) interact with other nuclei and thus contribute with other newly created particles to the original shower. All of the pions created early decay (or vanish in inelastic interactions) before reaching the ground. Neutral pions (about 1/3 of all pions) decay very quickly ( $\sim 10^{-18}$ s in their rest frame) into 2 photons, which subsequently create cascades of electron-positron pairs and other photons, which continue the cascades, etc. This component of the shower is therefore called the soft component. During the shower evolution, when the number of created particles reaches maximum,  $e^+$  and  $e^-$  are the most abundant species. The charged pions decay a bit later ( $\sim 10^{-8}$ s), mostly into muons and muon neutrinos:

$$\pi^- \rightarrow \mu^- + \bar{\nu}_\mu ,$$

$$\pi^+ \rightarrow \mu^+ + \nu_\mu .$$

Muons easily penetrate the atmosphere because they do not interact by strong interaction and also they are quite heavy in comparison to electrons. On average, each muon loses about 2 GeV of its energy before hitting the

---

<sup>7</sup>The interaction length is the mean free path of a particle before undergoing an inelastic interaction in the medium.

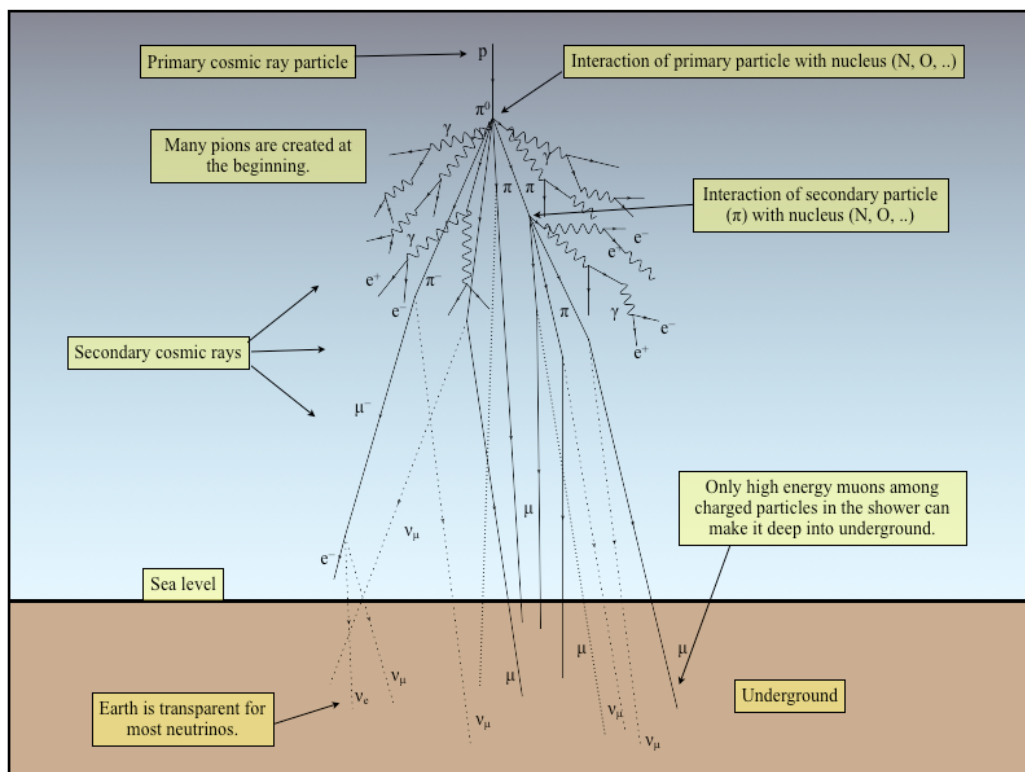


Figure 8.3: Diagram showing the development of a secondary cosmic rays shower

ground [8]. That means the most energetic ones ( $> 2 \text{ GeV}$ ) can end up underground. Due to their penetration, these are often called the hard component of the shower. At sea level, most particles left in the shower are muons. There are also electrons, positrons and photons originating from cascades started by neutral pions or from decays of other mesons, but the dominant source of electrons and positrons at sea level is from the muon decays

$$\mu^- \rightarrow e^- + \bar{\nu}_e + \nu_\mu ,$$

$$\mu^+ \rightarrow e^+ + \nu_e + \bar{\nu}_\mu .$$

Only muons and neutrinos (from pion and muon decays) remain among particles created in a shower when detecting underground. Neutrinos easily penetrate the whole Earth, charged muons with sufficiently large energy ( $> 10 \text{ TeV}$ ) can go several km further underground [8]. There is also a small fraction of protons at sea level from shower remnants, usually coming from neutron decays. For example, the number of protons with momentum  $1 \text{ GeV}/c$  is about 80 times smaller at sea level than the number of muons with the same momentum [8].

## 8.2 SKALTA experiment

The SKALTA experiment (SlovaKiAn Large-area Time coincidence Array) measures secondary cosmic rays originating from a primary particle with energy more than  $10^{14}$  eV. The experimental setup has similar architecture as the successful projects ALTA [31] and CZELTA [32] (fig. 8.4).

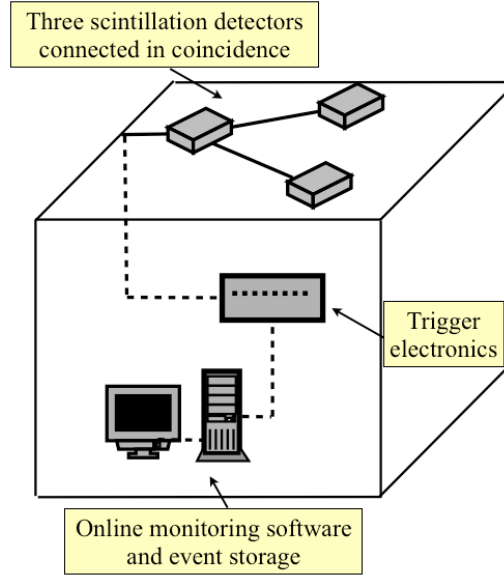


Figure 8.4: Basic architecture of the SKALTA experiment

The working station is composed of three scintillation detectors <sup>8</sup> each with the dimensions 60x60 cm. We can consider each of the detectors as a counter - one count corresponds to at least one particle crossing the detector. If at least 3 particles crossed all three detectors (one particle per one detector) at the same moment then we count it as a shower. The ionizing particle causing the signal in the detector is usually an energetic muon. All three detectors are connected in time coincidence, i.e. we say there is a shower detected when all three detectors are hit by a particle within some short time interval (120 ns in our case). The probability for the coincidence signal

<sup>8</sup>A short principle of the scintillator: it transforms energy losses of an ionizing particle into light which propagates to and is measured by a photodetector.

not being a shower is very close to 0. The detectors are arranged into a triangle with side length of 10 m. SKALTA uses a known property of the shower: the size of the area where the shower hits the ground is related to the energy of the original primary particle; The bigger the energy of the primary particle, the bigger the surface area the shower covers on the ground (fig. 8.5). Thus the area of the triangle in SKALTA architecture defines a minimal size of the shower and hence a minimal energy of the original primary particle ( $> 10^{14}$  eV), see figure 8.6.

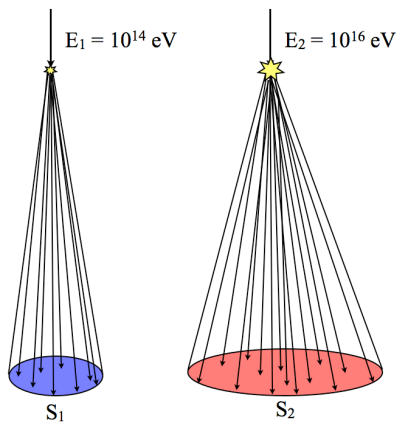


Figure 8.5: Two shower shapes related to two different energies of the primary particles (on Earth surface), if  $E_1 < E_2$  (for the same particle type) then  $S_1 < S_2$ .

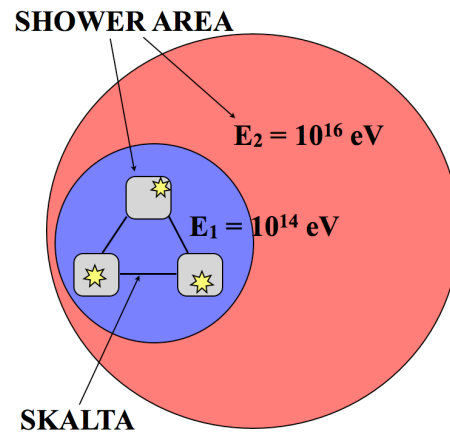


Figure 8.6: Two shower areas related to two different energies of the primary particles and the SKALTA detection area

In other words, SKALTA cannot measure the exact energy of the primary particle, it can only say: "The measured shower originates from primary particle with energy more than  $10^{14}$  eV". What SKALTA can measure (up to a certain resolution) is the point in the sky where the original particle came from. If we assume (see fig. 8.7):

1. the shower front is planar
2. the shower front is traveling at  $c$
3. the shower front is perpendicular to the shower axis

we get:

$$\cos\theta = \frac{c(t_1 - t_2)}{d} \quad (8.1)$$

i.e. using the time difference among the signals from the detectors the point in the sky can be localized in  $\phi$  and  $\theta$ . The resolution is about  $5^\circ$  in azimuthal angle ( $\phi$ ) and  $4^\circ/\sin\theta$  in  $\theta$  [26].

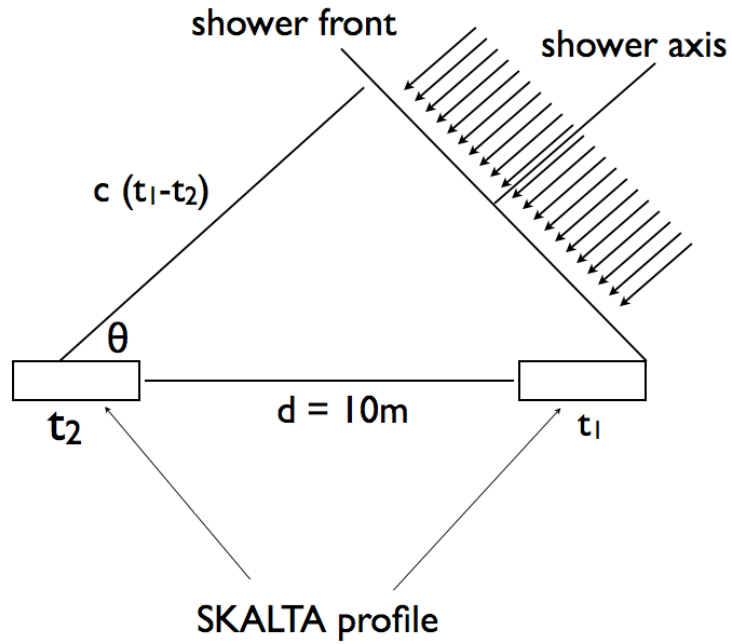


Figure 8.7: Shower front and SKALTA

By measuring the exact time by GPS (Global Positioning System) the data from other workstations (i.e. CZELTA) can be compared and long distance correlations can be studied.

The detectors of the SKALTA experiment are installed on the roof of the Institute of Physical Sciences at P. J. Šafárik University in Košice (fig. 8.8).

The read-out system is in the same building two levels lower (fig. 8.9). The experiment started to collect data at the end of June 2010.



Figure 8.8: Working station installed on the roof of the Institute of Physics, P. J. Šafárik University



Figure 8.9: Read-out system for the SKALTA experiment

Projects ALTA and CZELTA have also important pedagogical impact. Some of the workstations are installed on the roofs of secondary schools and the students have an opportunity to participate in a real scientific measurements. One of the future goals of the SKALTA project is the installation of workstations on the roofs of selected Slovak secondary schools, in order to make the education process more attractive and to stimulate interest in physics among the students.

## 8.3 Data analysis

The SKALTA data can be analysed in two ways:

1. by a web interface using a graph plotting program, or paper, pen and calculator. This is recommended for most users.
2. by raw data using some programming language (for example C/C++, Python, Pascal, etc.). This can be tried by skilled users.

### 8.3.1 How to use the web interface

The web interface for data analysis with SKALTA is at

`http://czelta.utef.cvut.cz`

The server is in IEAP (Institute of Experimental and Applied Physics) [33] at the CTU (Czech Technical University) in Prague, where you can find not only SKALTA but also all the stations in the Czech Republic (CZELTA), Romania, Canada (ALTA), US and UK. The username is *guest*, and the password is *czelta*. If you have logged in properly you should see a menu - fig. 8.10 (after changing to English language):

There are several options to try:

- **Site status** informs you about the general status of the site - basically, if it is working or not.
- **Site logs** should inform you about the power cuts at the site or other problems related to data acquisition.
- **Download data**: here you can download raw data for the requested time interval. The data description is in the next section.
- **Meteodata download**: some of the sites have their own meteo station and meteo data; not applicable for SKALTA though.
- **Preferences**: the account settings (presumably not applicable for account *guest*).
- **Event count**: most important for our analysis; description in the next section.

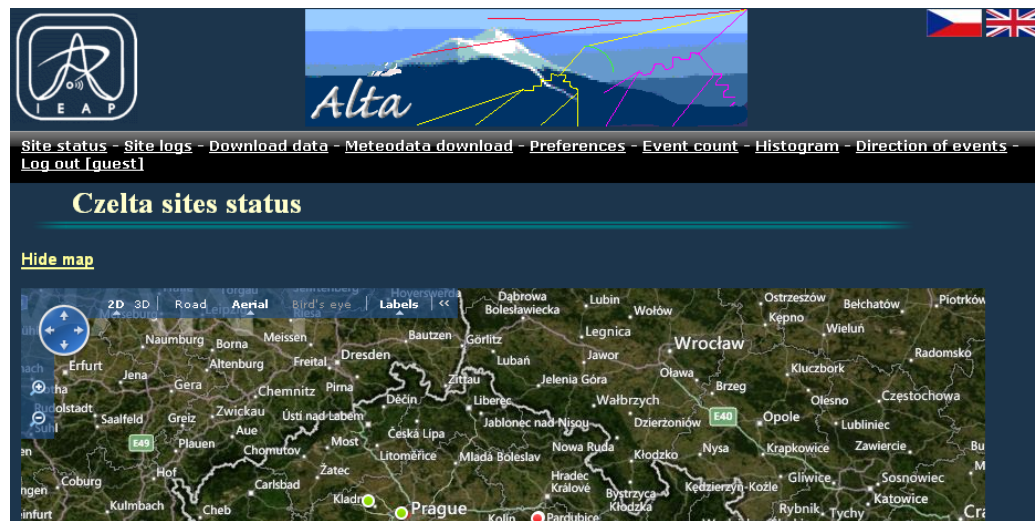


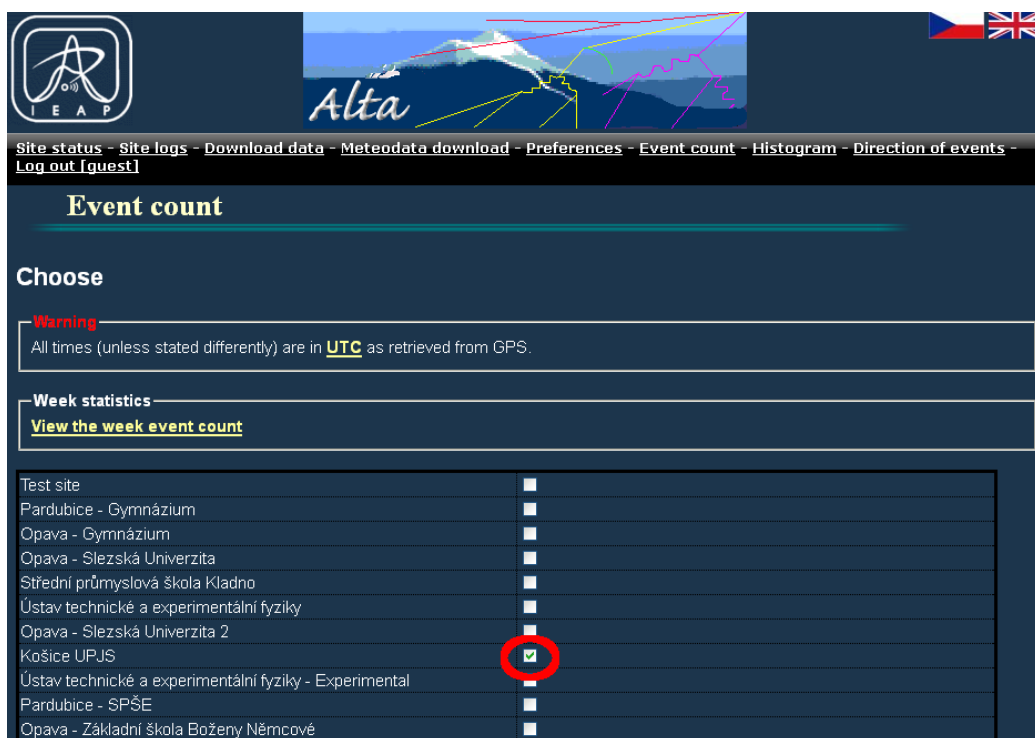
Figure 8.10: SKALTA web interface

- **Histogram:** graphical representation of some of the outputs of the detectors - raw data values...
- **Direction of events:** very nice representation (on-line sky map) of the most probable sky point where the original primary particles come from.
- **Log out:** Log out.

For now we will use the Event count option only. Example: Let us say we want to know how many showers were detected by SKALTA on 12.02.2012 from 9:00 till 11:00. We do this in this way: first we click on the **Event count**. Then we select Kosice UPJS (SKALTA) (fig. 8.11), scroll down and set plotting options (fig. 8.12).

We have again several options here:

- **From and To:** Time interval
- **Graph size px \* px:** graph size in pixels
- **Width of the float sum** must be a multiple of 5. min : it is a time step in which we want to know the shower number.



The screenshot shows the SKALTA web interface. At the top, there is a navigation bar with links: Site status, Site logs, Download data, Meteodata download, Preferences, Event count (selected), Histogram, and Direction of events. Below the navigation bar, the page title is "Event count". A "Choose" section contains a warning box stating: "Warning: All times (unless stated differently) are in UTC as retrieved from GPS." Below the warning, there is a "Week statistics" section with a link "View the week event count". The main part of the interface is a table with a list of test sites and checkboxes for selection. The site "Opava - Slezská Univerzita 2" is selected, indicated by a red circle around its checkbox.

Test site	
Pardubice - Gymnázium	<input type="checkbox"/>
Opava - Gymnázium	<input type="checkbox"/>
Opava - Slezská Univerzita	<input type="checkbox"/>
Střední průmyslová škola Kladno	<input type="checkbox"/>
Ústav technické a experimentální fyziky	<input type="checkbox"/>
Opava - Slezská Univerzita 2	<input checked="" type="checkbox"/>
Košice UPJS	<input type="checkbox"/>
Ústav technické a experimentální fyziky - Experimental	<input type="checkbox"/>
Pardubice - SPŠE	<input type="checkbox"/>
Opava - Základní škola Boženy Němcové	<input type="checkbox"/>

Figure 8.11: SKALTA web interface: Event count - selection of working station



The screenshot shows the SKALTA web interface for selecting a time interval. It includes a table with a list of test sites and checkboxes for selection. The site "Opava - Slezská Univerzita 2" is selected, indicated by a red circle around its checkbox. Below the table, there are input fields for "From" and "To" dates, a dropdown menu for "Without calibration events", and input fields for "Graph size" (width and height) and "Width of the float sum". There are also checkboxes for "Use JavaScript" and "Show value table", and a "Show" button.

Test site	
[UK] London - Highgate school	<input type="checkbox"/>
[RoLTA] Bucharest - Magurele	<input type="checkbox"/>
From	12.02.2012, 09:00:00
To	12.02.2012, 11:00:00
Without calibration events	<input type="checkbox"/>
Graph size	1000 px * 500 px
Width of the float sum. It must be multiple of 5.	60 min
Use JavaScript	<input checked="" type="checkbox"/>
Show value table	<input checked="" type="checkbox"/>
<input type="button" value="Show"/>	

This system has been written by [Jakub Čermák](#)

Figure 8.12: SKALTA web interface: selection of time interval for Event count

- **Use JavaScript:** use java script.
- **Show value table:** tick if you also want a table with absolute numbers of detected showers: necessary for our analysis.

We put from 12.02.2012, 9:00:00 to 12.02.2012, 11:00:00 with 60 minutes as a time step and click on show. What you get is a floating <sup>9</sup> (or moving) sum graph of showers between 9:00 and 11:00 on 12.02.2012 (fig. 8.13):

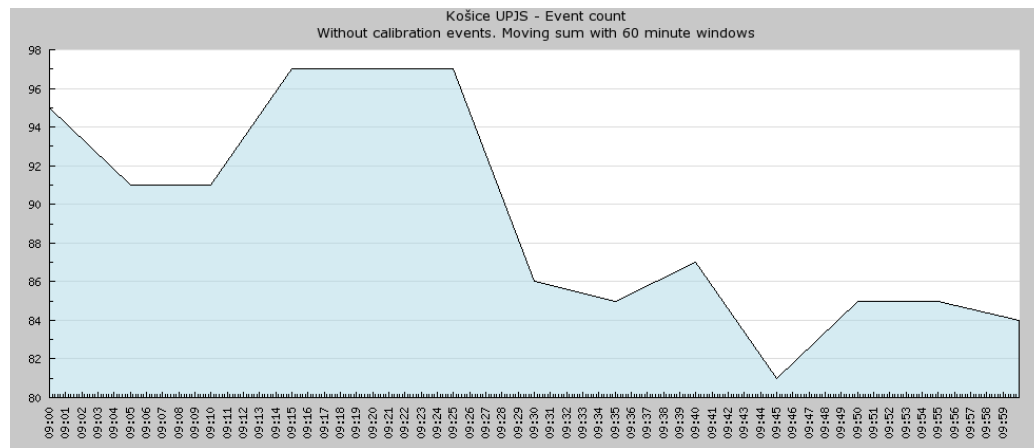


Figure 8.13: Floating sum graph for events measured in 9:00-11:00, 12.02.2012 with 5 minutes step

More important information lies below if you scroll the page down. There is a table with numbers (table 8.1). It shows values for the floating sum graph with a 5 minute step. We set as a width of the float sum 60 minutes and move those 60 minutes in time by 5 minutes. That means the first starting point is 9:00, the first ending point is +60 minute i.e. 10:00 and in the table we have number of showers in that interval (95). The second starting point is the first starting point + 5 minutes, i.e. 9:05 and the second ending point is the first ending point + 5 minutes, i.e. 10:05 (91 showers in that interval), and so on. On the graph the number of showers is plotted at the starting points, that is the reason why we miss whole second hour of the interval 9:00-11:00. If we want to plot only one value, e.g. how many showers hit the

<sup>9</sup>Floating window is useful when looking for aperiodic events, e.g. a burst of showers in certain time interval.

Table 8.1: Number of showers measured in 9:00-11:00, 12.02.2012 with 5 minutes step

Interval		Number of showers
From	To	
12.02.2012, 09:00:00	12.02.2012, 10:00:00	95
12.02.2012, 09:05:00	12.02.2012, 10:05:00	91
12.02.2012, 09:10:00	12.02.2012, 10:10:00	91
12.02.2012, 09:15:00	12.02.2012, 10:15:00	97
12.02.2012, 09:20:00	12.02.2012, 10:20:00	97
12.02.2012, 09:25:00	12.02.2012, 10:25:00	97
12.02.2012, 09:30:00	12.02.2012, 10:30:00	86
12.02.2012, 09:35:00	12.02.2012, 10:35:00	85
12.02.2012, 09:40:00	12.02.2012, 10:40:00	87
12.02.2012, 09:45:00	12.02.2012, 10:45:00	81
12.02.2012, 09:50:00	12.02.2012, 10:50:00	85
12.02.2012, 09:55:00	12.02.2012, 10:55:00	85
12.02.2012, 10:00:00	12.02.2012, 11:00:00	84

SKALTA in 9:00-10:00, then we put as a width of floating sum 60 minutes and time interval exactly 9:00-10:00, i.e. the width and the time interval must be same. The output is on figure 8.14.

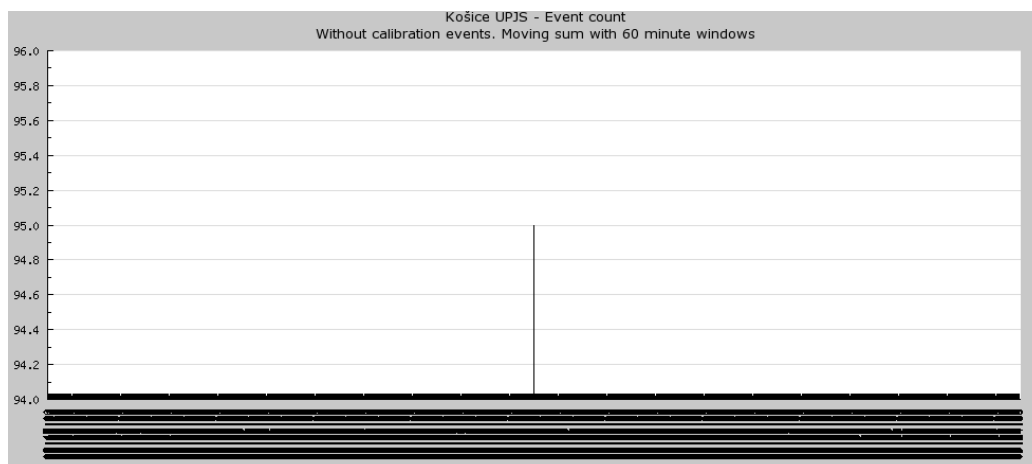


Figure 8.14: Floating sum graph for events measured in 9:00-10:00, 12.02.2012 with 60 minutes step

### 8.3.2 Analysis with raw data

To get the raw data, click on **Download data** in the web interface menu (fig. 8.15) and set the downloading options. Choose **Text format**, **Site** and **time** and **OS** where you want to analyze the data. For example fig. 8.16:

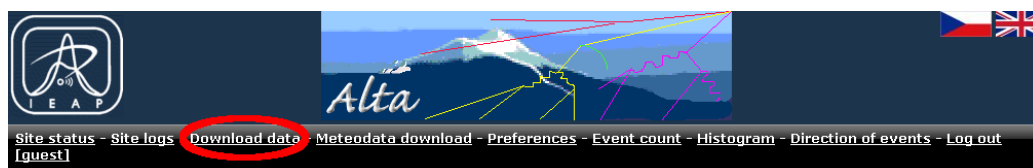


Figure 8.15: SKALTA web interface: Download data

Then click on download. The text file should be downloaded. Open it and you should see something like this:

Figure 8.16: SKALTA web interface

```

x 0 0 0 0 0 0 0.0 0 0 0 0 0 0 0.0 0.0 0.0
a 2011 03 24 15 05 45 645281133.9 2430 3164 4000 433 200 142 29.5 25.5 31.0 46.5
c 2011 03 24 15 05 51 673260.5 0 2322 3961 712 991 941 29.5 25.5 31.0 46.5
a 2011 03 24 15 05 55 854942857.6 1295 3119 4008 189 204 410 29.5 26.0 31.0 46.5
a 2011 03 24 15 05 56 657416869.7 1263 3118 4025 544 480 548 29.5 25.5 31.0 46.5
c 2011 03 24 15 06 51 674999.5 4095 2076 4017 776 1095 1006 29.5 25.5 31.0 46.5
a 2011 03 24 15 07 16 96301373.2 2140 3231 4007 576 213 125 29.5 25.5 30.5 46.5
a 2011 03 24 15 07 38 803003570.3 1634 3012 4000 1019 502 434 29.5 25.5 30.5
46.5
a 2011 03 24 15 07 44 893916939.4 2037 3279 4011 546 190 132 29.5 25.5 30.5 46.5
c 2011 03 24 15 07 51 674080.6 0 2082 3969 673 1062 1008 29.5 25.0 30.5 46.5
c 2011 03 24 15 08 51 670025.5 4095 2052 4012 793 1001 944 29.5 25.0 30.5 46.5
c 2011 03 24 15 09 51 670322.6 0 1908 3984 782 107 7 977 29.5 25.0 30.5 46.5

```

i.e. many rows and 18 columns. Each row represents 1 shower detected by SKALTA. The columns correspond to event properties, such as arrival time or detector signal size. The explanation of the columns is as follows:

- (1st column): character: a=*physics event*, c=*calibration event*, x=*new run*
- (2nd - 7th column): date in the format; *year month day hour minute second*
- (8th column) ns from the last second (resolution  $\sim 10$  ns)

- (9th - 11th): TDC0, TDC1, TDC2 - arrival times for each scintillator
- (12th - 14th): ADC0, ADC1, ADC2 - pulse heights from each scintillator
- (15th-18th): temperatures in  $^{\circ}\text{C}$  for scintillator 0, 1, 2 and in the electronics box

Note: students who want to work with raw data during the Masterclasses must be skilled in programming because of the short time for such analysis.

### 8.3.3 Caveats during analysis

There were many power cuts and some other detector failures with SKALTA during the early days. This should be taken into account in the analysis. Looking at the data, we might see suspiciously low rates on some days. Before we interpret this as some physical effect we should check if it is not a power cut. For example: if we look at a period of 10 days in September 2010 with a 1440 minutes step (1day), we see no suspicious behavior in the data (fig. 8.17). But when we look with a finer step (60 minutes), we clearly see

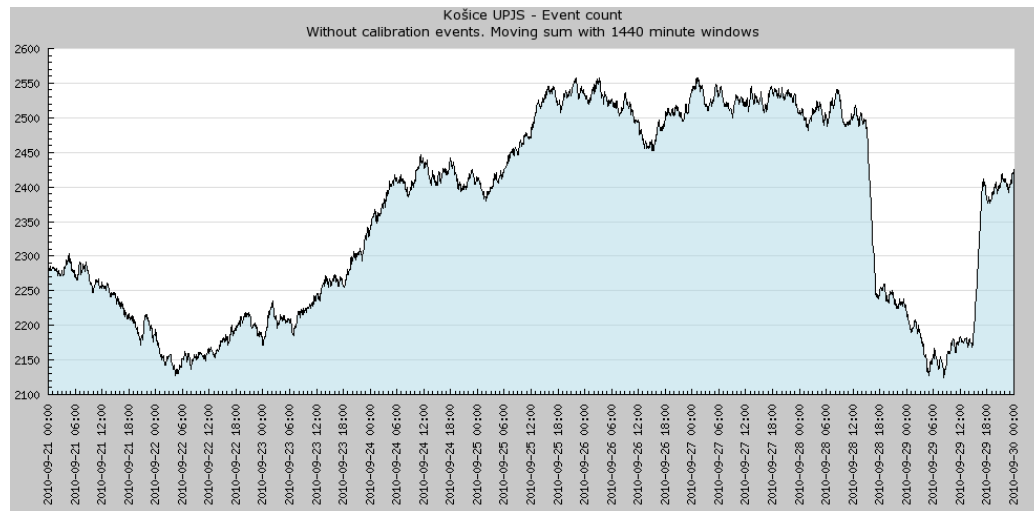


Figure 8.17: Floating sum graph for events measured in September 2010 with the 1440 minutes step

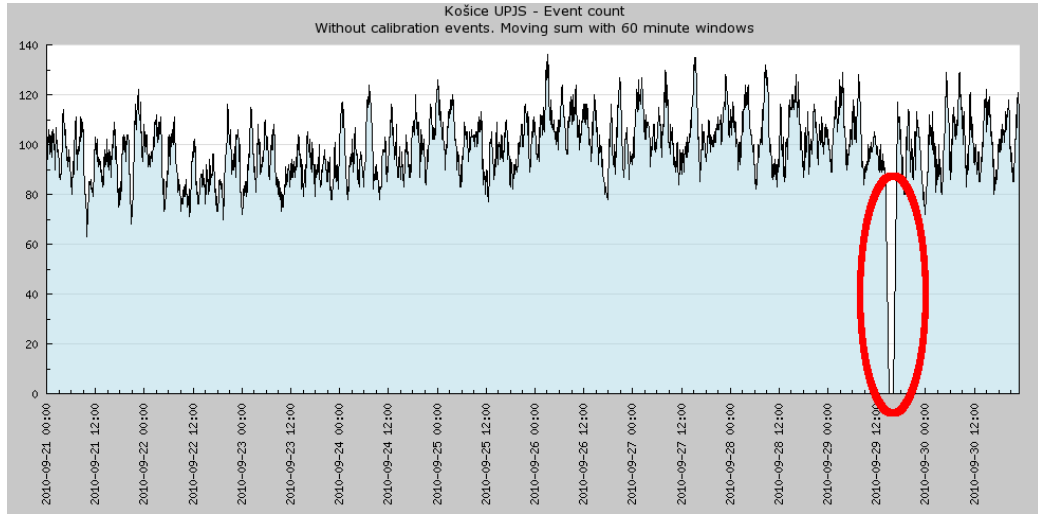


Figure 8.18: Floating sum graph for events measured in September 2010 with the 60 minutes step

that there was a power cut on September 29th (fig. 8.18). With an even finer step (5 minutes), obtained by zooming (28.9-30.9.), it is revealed that the power cut lasted two hours from 15:00 to 17:00 (fig. 8.19). We need to be very careful with the analysis. Power cuts can bias our interpretation of the results.

Other checks of the data are needed when dealing with raw data:

```
x 0 0 0 0 0 0 0.0 0 0 0 0 0 0 0.0 0.0 0.0 0.0
a 2011 03 24 15 05 45 645281133.9 2430 3164 4000 433 200 142 29.5 25.5 31.0 46.5
c 2011 03 24 15 05 51 673260.5 0 2322 3961 712 991 941 29.5 25.5 31.0 46.5
a 2011 03 24 15 05 55 854942857.6 1295 3119 4008 189 204 410 29.5 26.0 31.0 46.5
a 2011 03 24 15 05 56 657416869.7 1263 3118 4025 544 480 548 29.5 25.5 31.0 46.5
c 2011 03 24 15 06 51 674999.5 4095 2076 4017 776 1095 1006 29.5 25.5 31.0 46.5
a 2011 03 24 15 07 16 96301373.2 2140 3231 4007 576 213 125 29.5 25.5 30.5 46.5
a 2011 03 24 15 07 38 803003570.3 1634 3012 4000 1019 502 434 29.5 25.5 30.5
46.5
a 2011 03 24 15 07 44 893916939.4 2037 3279 4011 546 190 132 29.5 25.5 30.5 46.5
c 2011 03 24 15 07 51 674080.6 0 2082 3969 673 1062 1008 29.5 25.0 30.5 46.5
```

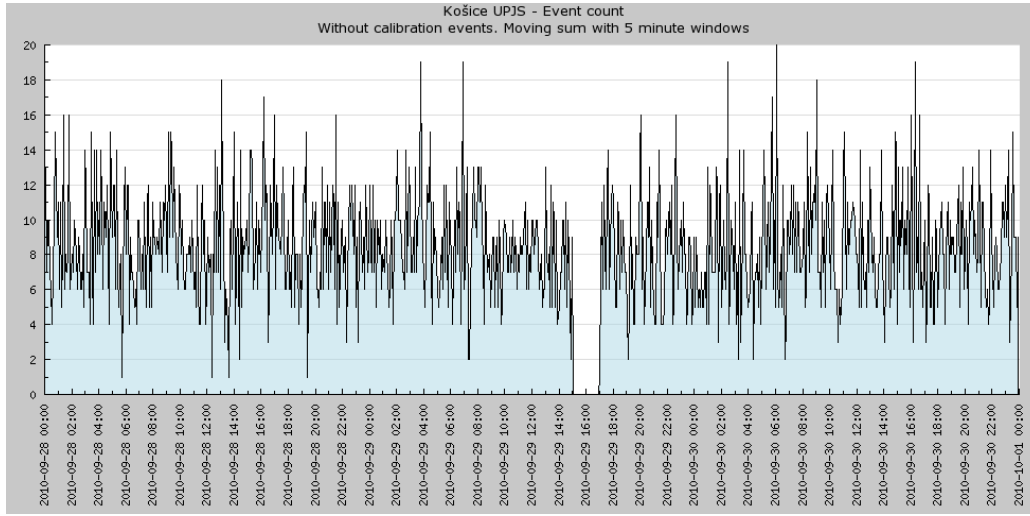


Figure 8.19: Floating sum graph for events measured in 28.9.-30.9. 2010 with the 5 minutes step

```
c 2011 03 24 15 08 51 670025.5 4095 2052 4012 793 1001 944 29.5 25.0 30.5 46.5
c 2011 03 24 15 09 51 670322.6 0 1908 3984 782 107 7 977 29.5 25.0 30.5 46.5
```

It is important to take into account only physics events, i.e. those lines which begin with the character "a".

Power cuts are also dangerous in the raw data analysis. We just need a reasonable definition of a power cut in our code. The shower rate behaves as a Poisson distribution with a mean of about 2000 events per day. A reasonable definition of a power cut in our code could be: no incoming showers within 15 minutes, because the probability that SKALTA does not detect any shower within 15 minutes is so small that it is most likely the power cut.

## 8.4 Exercises with SKALTA

Two exercises were prepared and tested, but feel free to make up new ones.

### 8.4.1 Exercise n. 1: Are the cosmic rays measured by SKALTA affected by the Sun?

The question can be changed depending on the audience. For example: Are the showers detected by SKALTA coming from the Sun? Or at least part of it? Or even better: is the source of the cosmic rays SKALTA detects inside or outside the Solar system? Or where is the origin of high energy cosmic rays detected by SKALTA? It is up to the instructor what question might sound more attractive for the audience.

#### A short introduction to the exercise

The sun is a source not only of light but also of the so-called solar wind. The solar wind is a stream of charged particles ejected from the upper atmosphere of the Sun. The energy of the most particles is in the MeV region [24]. It mostly consists of electrons and protons and it regularly affects the weather on Earth. It might be interesting to find out if the showers detected by SKALTA are somehow directly affected by the the solar wind (fig. 8.20).

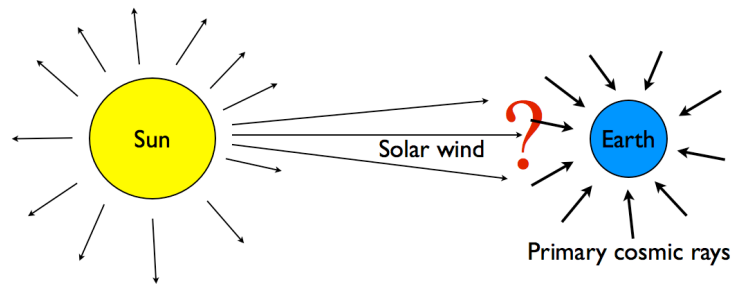


Figure 8.20: Solar wind and Earth

#### Proposed method of measurement

Compare numbers of events (showers of secondary cosmic rays) measured by SKALTA during the day and during the night, i.e. when SKALTA "sees" the Sun and when SKALTA looks towards the other side of the Solar system. For example: measurement for the day could be noon  $\pm$  3 hours (just to be sure the Sun was shining all that time) and night measurement could be midnight  $\pm$  3 hours. The outcome of the analysis should be a plot with (day and night) event number as a function of time (minimal time unit in the plot will be 24 hours). As we learned in the previous section, the data analysis can be performed using the web interface or by programming using raw data. The final graph could be drawn with some suitable graph plotting software application.

### 8.4.2 Exercise n. 2: What is the relation between secondary cosmic ray flux and atmospheric conditions (such as air temperature and density)?

#### A short introduction to the exercise

Most of the particles created in the shower are absorbed in the atmosphere. The atmosphere acts like a huge calorimeter with respect to the shower. Only a fraction of particles, mostly muons, survive the travel through the atmosphere. It would be interesting to find out if changing of atmospheric properties can change the propagation of the shower through the atmosphere (fig. 8.21).

#### Proposed method of the measurement

The outcome of the analysis should be 3 plots with SKALTA event numbers, air temperature and air density (or pressure) as a function of time (minimal time unit in the plot will be 24 hours). Make a comparison among them and try to interpret the result. The measurement of the air temperature and air pressure can be obtained from <sup>10</sup>

---

<sup>10</sup>The weather station is a common project of the Department of Cybernetics and Artificial Intelligence at The Technical University of Košice and the Slovak Organization for Space Activities [34].

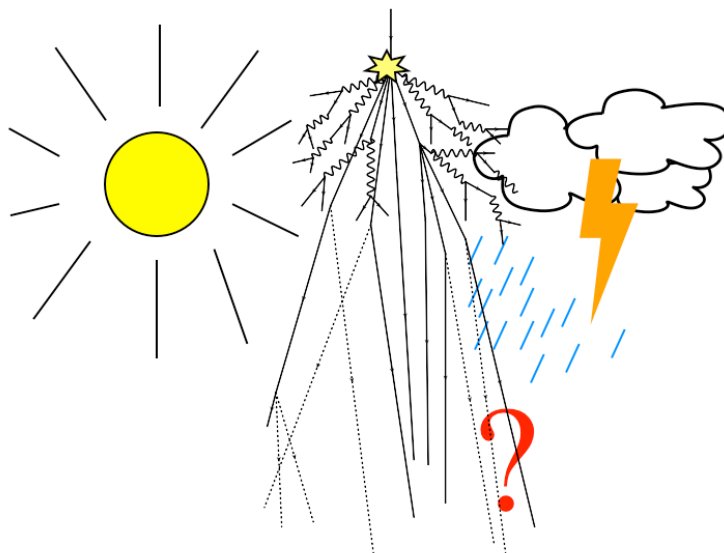


Figure 8.21: Weather and shower

<http://neuron.tuke.sk/adamcak/0/data/>

This weather station is located about 300 m from SKALTA. It is strongly recommended to transform the data to a more user-friendly format suitable for analysis using a spreadsheet application.

# Appendix A

## Physical constants

Table A.1: Physical constants.

name	symbol	value
speed of light in vacuum	$c$	$299\,792\,458\text{ m s}^{-1}$
Planck constant	$h$	$6.626\,069\,57 \times 10^{-34}\text{ J s}$
Planck constant, reduced	$\hbar$	$1.054\,571\,63 \times 10^{-34}\text{ J s}$ $6.582\,118\,99 \times 10^{-22}\text{ MeV s}$
electron charge magnitude	$e$	$1.602\,176\,487 \times 10^{-19}\text{ C}$
electron mass	$m_e$	$9.109\,382\,15 \times 10^{-31}\text{ kg}$ $0.510\,998\,910\text{ MeV/ c}^2$



# Bibliography

- [1] J. Pišút, L. Gomolčák, V. Černý, Úvod do kvantovej mechaniky, 2nd edition, Alfa Bratislava 1983.
- [2] D.J. Griffiths, Introduction to Quantum Mechanics, 1st edition, ISBN 0 13 124405 1.
- [3] T.M. Helliwell, Special Relativity, University Science Books (April 30, 2009), ISBN-10: 1891389610, ISBN-13: 978-1891389610.
- [4] David Griffiths, Introduction to Elementary Particles, ©2008 WILEY-VCH Verlag GmbH & Co.KGaA, Weinheim.
- [5] D.H. Perkins, Introduction to High Energy Physics, 4th edition, ISBN 0 521 62196 8.
- [6] The blog of Matt Strassler, *Of Particular Significance*, <http://profmattstrassler.com/>
- [7] Michael E. Peskin, Dan V. Schroeder, An Introduction To Quantum Field Theory, Westview Press; reprint edition (October 2, 1995), ISBN-10: 0201503972, ISBN-13: 978-0201503975.
- [8] J. Beringer et al. (Particle Data Group), J. Phys. D86, 010001 (2012). The on-line updated version of the data published in this reference can be found at <http://pdg.lbl.gov/>.
- [9] S. Chatrchyan et al. [CMS Collaboration], Phys. Lett. **B 716**, 30 (2012).
- [10] E.Boos et al, [CompHEP Collaboration], CompHEP 4.4: Automatic computations from Lagrangians to events, Nucl. Instrum. Meth. A534

- (2004) 250 (arXiv:hep-ph/0403113).  
 A.Pukhov et al, CompHEP - a package for evaluation of Feynman diagrams and integration over multi-particle phase space. User's manual for version 3.3, INP MSU report 98-41/542 (arXiv:hep-ph/9908288).  
 CompHEP home page: <http://comphep.sinp.msu.ru>
- [11] LanHEP home page: <http://theory.sinp.msu.ru/~semenov/lanhep.html>
- [12] T. Sjostrand, S. Mrenna, P. Skands, JHEP 05 (2006) 026 (LU TP 06-13, FERMILAB-PUB-06-052-CD-T, hep-ph/0603175).  
 Pythia home page: <http://home.thep.lu.se/~torbjorn/Pythia.html>
- [13] HERWIG 6.5, G. Corcella, I.G. Knowles, G. Marchesini, S. Moretti, K. Odagiri, P. Richardson, M.H. Seymour and B.R. Webber, JHEP 0101 (2001) 010 [hep-ph/0011363]; hep-ph/0210213.
- [14] The ATLAS Collaboration, JHEP 1012 (2010) 060.
- [15] MINERVA, T. McLaughlan, M. Stockton, P. Watkins (University of Birmingham), M. Wielers (Rutherford Appleton Laboratory), <http://atlas-minerva.web.cern.ch/atlas-minerva>
- [16] International Masterclasses ATLAS measurement web page: <http://atlas.physicsmasterclasses.org/en/index.htm>  
 W boson measurement (click W-Path); Authors: Michael Kobel, Konrad Jende, Uta Bilow, Julia Eckert, Constanze Hasterok, Christian Rudolph, Dresden Technical University.  
 Z boson measurement (click Z-Path); Authors: Farid Ould-Saada, Maiken Petersen, Eirik Gramstad, Magnar Bugge, Oslo University.
- [17] Slovak Masterclasses home page: <http://fyzika.uniza.sk/mc/>
- [18] HDECAY: a Program for Higgs Boson Decays in the Standard Model and its Supersymmetric Extension A. Djouadi, J. Kalinowski, M. Spira, Comput.Phys.Commun.108:56-74,1998.
- [19] *Observation of a new particle in the search for the Standard Model Higgs boson with the ATLAS detector at the LHC.* The ATLAS Collaboration (Georges Aad (Freiburg U.) et al.) Jul 31, 2012 24 pp. CERN-PH-EP-2012-218 e-Print: arXiv:1207.7214

- [20] The ATLAS Collaboration, Phys. Rev. D85, 072004 (2012).
- [21] HYPATIA, Ch. Kourkouvelis, D. Fassouliotis, S. Vourakis (University of Athens), D. Vudragovic (Institute of Physics, Belgrade), <http://hypatia.phys.uoa.gr>
- [22] D. Perkins: *Particle Astrophysics*, Oxford University Press, 2009, ISBN: 978-0199545452, p.229-272
- [23] [http://en.wikipedia.org/wiki/Cosmic\\_ray](http://en.wikipedia.org/wiki/Cosmic_ray)
- [24] C. Grupen: *Astroparticle Physics*, Springer-Verlag Berlin Heidelberg, 2005, ISBN: 978-3-540-25312-9, p.77-170
- [25] K. Greisen: End to the Cosmic-Ray Spectrum?, *Physical Review Letters* **16** (17), 748750. (1966)  
G.T. Zatsepin and V.A. Kuzmin, V. A: Upper Limit of the Spectrum of Cosmic Rays, *Journal of Experimental and Theoretical Physics Letters* **4**, (1966)
- [26] A. Hamilton: *ALTA: Alberta Large Area Time Coincidence Array*, MSc. thesis, University of Alberta, 2006
- [27] <http://jemeuso.riken.jp/en/index.html>
- [28] <http://www.auger.org/>
- [29] <http://www.telescopearray.org/>
- [30] <http://www.cosmic-ray.org/>
- [31] <http://csr.phys.ualberta.ca/~alta/>
- [32] <http://www.utef.cvut.cz/czelta/czelta-en>
- [33] <http://www.utef.cvut.cz/en/>
- [34] <http://meteo.sosa.sk>